Modeling and assessing the impact of nocturnal NO_x chemistry on air quality

By

Alicia Hoffman

A dissertation submitted in partial fulfillment of
the requirements for the degree of

Doctor of Philosophy

(Atmospheric and Oceanic Sciences)

at the

UNIVERSITY OF WISCONSIN-MADISON

2024

Date of final oral examination: 1/22/2024

This dissertation is approved by the following members of the Final Oral Committee:
Tracey Holloway, Professor, Atmospheric and Oceanic Sciences
Timothy Bertram, Professor, Chemistry
Ankur R. Desai, Professor, Atmospheric and Oceanic Sciences
Elizabeth Maroon, Assistant Professor, Atmospheric and Oceanic Sciences
R. Bradley Pierce, Professor, Atmospheric and Oceanic Sciences

Abstract

Nitrogen oxides ($NO_x \equiv NO + NO_2$) are air pollutants in the United States because they have direct human health impacts and play a central role in the production of secondary pollutants like ozone and particle pollution. Air quality models are a powerful tool to understand the complex chemistry that affects NO_x, but model representations of nocturnal NO_x chemical mechanisms cannot capture the full variability seen in observations because of simplifying assumptions. My dissertation assesses the impact of these assumptions on nighttime NO_x chemistry and daytime air quality in models.

First, I updated the nocturnal heterogeneous chemical mechanisms for N_2O_5 uptake and $ClNO_2$ yield in the EPA Community Multiscale Air Quality (CMAQ) model. The new mechanisms are more representative of the chemistry of real particles because they account for the role of particulate organic matter in regulating N_2O_5 uptake and the role of reactive solutes in suppressing $ClNO_2$ production. Following the implementation of the two updated heterogeneous chemistry mechanisms, I calculate the contribution of different nocturnal loss pathways to the NO_x budget. Nocturnal loss pathways of NO_x reservoir species impact daytime concentrations of NO_2, so it is important to understand the role of nocturnal loss pathways, such as N_2O_5 uptake, in local air quality. By changing the model representation of heterogeneous N_2O_5 uptake, early morning NO_2 concentrations fluctuated by 7.3% in January.

Finally, I assessed the sensitivity of CMAQ to representations of sea spray particle emissions to highlighting the impact these particles have on heterogeneous chemistry. Although sea spray aerosol particles affect heterogeneous chemistry, their emission in chemical transport

models excludes the smallest particle sizes. By changing the sea spray emissions in CMAQ, I increased particle surface area over 200% in the smallest particle size. The changes to modal surface area resulted in a similar impact to heterogeneous loss of N_2O_5 to the particle phase.

This dissertation highlights the interconnected nature of nocturnal NO_x chemistry and the complex impact on daytime air quality. It contributes to the efforts to improve the CMAQ model and its representations of NO_x chemistry. Through my dissertation, I show that updating chemical and emission mechanisms in the CMAQ model have implications for nocturnal heterogeneous loss and therefore daytime air quality.

Acknowledgements

A thesis is not possible alone, and I have so many people to thank. First and foremost, a huge thank you to my advisor, Tracey Holloway. I would not be the person I am today – professionally or personally – without Tracey. Not only does she give the best advice, but she also loves to share it. She is the type of mentor I hope to be one day. Second, I must thank Monica Harkey for her endless patience answering my CMAQ questions. She has a wealth of knowledge, and I would not have been able to build the model, let alone run it, without her help.

Thank you to my committee members, Tim Bertram, Ankur Desai, Liz Maroon, and Brad Pierce. I am grateful for the advice you've all provided, and I am most grateful for the fact that you all choose to support me and my research path, unconventional though I wanted it to be. I don't know how many people would have been willing to have a pedagogy chapter be part of a dissertation, but you all went for it (although it never ended up happening).

A huge thank you to everyone in AOS and SAGE who has supported me over my time in Madison. Gesang, you're the best group member I could have asked for, and it was so strange to have to write a dissertation without you around. Chen Nuo, thank you for putting up with me and Tank for three years. I can say, hands down, you were the best roommate I've ever had. Thank you to my many AOS friends, especially Vijit, Jerrold, and Steph. Thank you to Pete Pokrandt, Christi Balas Levenson, Dee VanRuyven, Carolyn Lipke, and Laurel Fletcher: you are the friendliest, most helpful people on the planet.

Finally, thank you to Abby Letak and the Wednesday morning writing group. I'm a procrastinator when it comes to writing, but you kept me on track. Abby, your words of wisdom

kept me sane through this dissertation, and I can't say enough how much I appreciate your efforts in leading a writing group. I think it is only fitting that one of the last things I write in my dissertation is a quote that has come to define my approach to writing:

> *Finish each day and be done with it. You have done what you could. Some blunders and absurdities no doubt crept in; forget them as soon as you can. Tomorrow is a new day. You shall begin it serenely and with too high a spirit to be encumbered with your old nonsense.*
>
> — Ralph Waldo Emerson

This research in this dissertation was developed under Assistance Agreement No. R840006 awarded by the U.S. Environmental Protection Agency to The University of Wisconsin-Madison. It has not been formally reviewed by EPA. The views expressed in this document are solely those of the authors and do not necessarily reflect those of the Agency. EPA does not endorse any products or commercial services mentioned in this publication. The authors acknowledge that this research has been supported by a grant from the U.S. Environmental Protection Agency's Science to Achieve Results (STAR) program.

There are several scientists and developers at the EPA who deserve recognition for their support in this work as well. Thank you to Kristen Foley, Todd Plessel, and the EPA EQUATES team. Thank you to Havala Pye, Golam Sarwar, and Ben Murphy for providing feedback on the work presented in Chapter 3. Thank you also to AnnMarie Carlton for her initial inputs on this work.

Table of Contents

Chapter 1 Introduction

1.1 Overview of nitrogen oxide air pollution

One common group of ambient air quality pollutants in the United States are nitrogen oxides ($NO_x \equiv NO + NO_2$) which are emitted from human sources such as vehicles or smokestacks and from biogenic sources such as lightning and soils (U.S. EPA, 2011; U.S. EPA, 2016; Zhang et al., 2003). NO_x have negative effects on human health and wellbeing by irritating airways, exacerbating pre-existing conditions like asthma, and increasing susceptibility to respiratory infections (American Lung Association, 2023; César et al., 2015). NO_x also play a central role in the production of secondary pollutants like ozone (O3) and particulate matter (PM), which have further air quality and climate concerns (Jacob et al., 1996; Pandis et al., 1992). NO_x are regulated to reduce their direct health effects and production of secondary pollutants.

In the US, outdoor air quality is regulated by the EPA's National Ambient Air Quality Standards, or NAAQS. The longer-lived component of NO_x, nitrogen dioxide (NO_2), is one of the six criteria pollutants regulated under the NAAQS (U.S. EPA, 2014). The NAAQS standards are responsible for large improvements in national air quality: since 1990, 1-hr NO_x concentrations have decreased 54% on average across the US (U.S. EPA, 2021).

Although on average NO_x air pollution has improved, annual changes in NO_x are not consistent year-to-year and not all regions show the same trends in improvement (Buckley & Mitchell, 2010; Lamsal et al., 2015). There are regional and local differences in emissions, meteorology, and climate which impact the transport and chemistry of NO_x and therefore air quality improvements (He et al., 2020). It is important to understand these differences on local,

regional, and national levels to improve ambient NO_x air quality, but assessment at multiple scales is difficult or impractical with field studies and surface monitors alone.

To aid in air quality regulation and prediction, the EPA developed the Community Multiscale Air Quality (CMAQ) model (Appel et al., 2021; Byun & Schere, 2006). Air quality models answer air quality and atmospheric chemistry questions at multiple spatial and temporal scales and fill in gaps that surface monitors or satellite data cannot address. This dissertation will assess chemistry and air quality predictions using the CMAQ model, with a focus on heterogeneous (gas-particle) chemistry impacting NO_x and associated gas-phase species. This work is guided by three questions relevant to NO_x -particle interactions.

Question 1: How do parameterizations of nocturnal heterogeneous chemistry affect model predictions of the NO_x reservoir species N_2O_5 and $ClNO_2$?

Question 2: What is the spatial and seasonal impact of the updated parameterizations on the NO_x budget and air quality?

Question 3: How do representations of sea spray aerosol emissions affect particle size distributions and the loss of N_2O_5?

1.2 Assessment of air quality on multiple scales

The CMAQ model is a useful tool to understand the atmospheric chemistry and physics affecting air quality. It is a three-dimensional, gridded, chemical transport model that uses parameterizations of first principles of chemistry, air-surface exchange, and atmospheric dynamics to predict air quality in the troposphere (Appel et al., 2021). Model users define the horizontal resolution and spatial coverage, vertical extent and resolution, and temporal range

and data output frequency (U.S. EPA, 2017). The CMAQ model is used in a regulatory and policy-making capacity, and by researchers, developers, and air-quality forecasters, each of whom are interested in air quality at various scales (U.S. EPA, 2017).

The CMAQ model is a powerful tool to understand the chemistry that impacts NO_x air quality. However, many of the underlying assumptions in the model mean that CMAQ does not capture the variability of heterogeneous NO_x chemistry (Brown et al., 2009; Chang et al., 2016; McDuffie et al., 2018) or sea spray aerosol emissions (Grythe et al., 2014; Neumann et al., 2016). The CMAQ mechanisms are based on the best understanding of atmospheric physics and chemistry relevant to air quality, yet the complexity of the model and abundance of new laboratory and field data mean that updating CMAQ can be a slow process. Throughout this dissertation, I assess several mechanisms in the CMAQ model that impact heterogeneous processes affecting NO_x.

1.3 Processes affecting **NO_x** air quality in CMAQ

While accurate treatment of NO_x in chemical transport models is essential to predictions of air quality, the representations of nocturnal heterogeneous NO_x chemistry in models is simplified and does not capture the variability seen in observations (Chang et al., 2011; Chang et al., 2016; McDuffie et al., 2018; Staudt et al., 2019). This nighttime chemistry regulates the loss pathways (sinks) and unreacted storage (reservoirs) of NO_x (Figure 1) (Brown et al., 2006; Richards, 1983). At night, the absence of sunlight to drive photochemical reactions allows reservoir species such as nitrate radical (NO_3), dinitrogen pentoxide (N_2O_5), and nitryl chloride ($ClNO_2$) to build up (Atkinson et al., 1986; Platt et al., 1984; Simpson et al., 2015). At sunrise, NO_3,

N_2O_5, and $ClNO_2$ photolyze to form NO_2 (Riedel et al., 2013; Simpson et al., 2015; Wayne et al., 1991). It is important for ozone modeling that regional air quality models include up-to-date parameterizations of heterogeneous NO_x chemistry so that predictions of early-morning NO_2 concentrations are accurate.

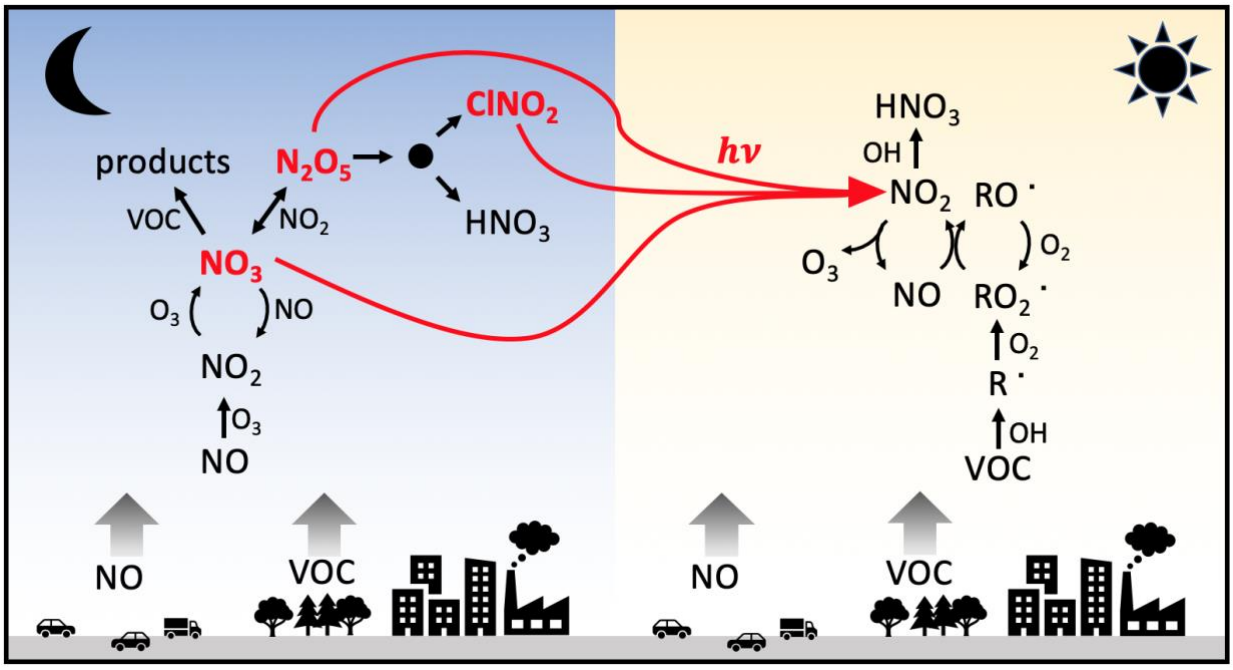

Figure 1 Simplified chemical reactions involving NO_x during the day (right side, yellow) and night (left side, blue). Thick grey arrows represent emission of NO and VOCs. Thin black arrows indicate reaction pathways. Red species are nocturnal reservoirs of NO_x, and the red arrows show how these species will dissociate with sunlight to form NO_2.

In Chapter 3, I focus on two heterogeneous reactions that help regulate the nocturnal reservoir species: uptake of N_2O_5 to particles and the yield of $ClNO_2$ from particles. The uptake of N_2O_5 occurs when gas-phase N_2O_5 diffuses through the particle surface and is incorporated into the bulk particle volume (Chang et al., 2011). Several factors impact uptake including particle surface area and composition (Folkers et al., 2003; Griffiths et al., 2009; Wagner et al., 2013). The yield of $ClNO_2$ occurs when $ClNO_2$ is produced in an aqueous particle and then evaporates to the gas phase (Finlayson-Pitts et al., 1989). The total production of $ClNO_2$ depends on particle

composition (Roberts et al., 2009). There are several new insights into the chemistry affecting uptake and yield mechanisms which have yet to be included in chemical transport models (Anttila et al., 2006; Gaston et al., 2014; Staudt et al., 2019). In Chapter 3 of this dissertation, I will implement two parameterizations of heterogeneous NO_x chemistry into CMAQ and assess how these mechanisms impact concentrations of reservoir species N_2O_5 and $ClNO_2$.

Following my assessment of the impact of heterogeneous parameterizations on reservoir species concentrations, I will examine how these mechanisms contribute to nighttime NO_x loss and daytime NO_x air quality. The extent of the impact of heterogeneous chemistry on daytime air quality varies spatially and temporally depending on factors such as relative humidity and nocturnal boundary layer height, particle concentration, size, and composition, and ambient gas-phase concentrations (Aldener et al., 2006; Allan et al., 1999; Brown et al., 2006; Sindelarova et al., 2014; Warneke et al., 2004). In Chapter 4, I explore these factors seasonally across the US to determine where nocturnal chemistry plays a dominant role in early morning NO_x formation.

Although comparison of different heterogeneous schemes can show where and how nocturnal chemistry dominates daytime NO_2 formation, these mechanisms rely on accurate representations of particles (Chang et al., 2011). There are several parameterizations of sea spray formation mechanisms, each impacting the size distribution of the emitted particles (Grythe et al., 2014). CMAQ produces sea spray particles via one mechanism, which focuses on larger particles and does not include emissions in the smallest particle mode (Gantt et al., 2015; Gong, 2003). Smaller sea spray particles contribute a significant fraction to total particle surface area and have a different composition than larger particles (Jayarathne et al., 2016; Keene et al., 2007;

Wang et al., 2015). In Chapter 5, I assess how the formation of sea spray aerosol impacts particle number and surface area concentrations, thus impacting N_2O_5 uptake.

1.4 Summary

Throughout my dissertation, I use the CMAQ model to investigate the complex chemistry affecting NO_x air quality. In Chapter 2, I outline the CMAQ experiments design and flow, as well as describe the specifics of the aerosol, heterogeneous chemistry, and sea spray emission modules. In Chapter 3, I present the updated N_2O_5 and $ClNO_2$ parameterization updates and resulting changes to the model predictions. In Chapter 4, I explore how the updates implemented in Chapter 3 affect the nocturnal NO_x budget, daytime NO_2 air quality, and particle nitrate concentrations. In Chapter 5, I describe the sensitivity of the CMAQ model to different representations of sea spray aerosol emissions and the resulting impact on heterogeneous chemistry.

References

Aldener, M., Brown, S. S., Stark, H., Williams, E. J., Lerner, B. M., Kuster, W. C., et al. (2006). Reactivity and loss mechanisms of NO3 and N2O5 in a polluted marine environment: Results from in situ measurements during New England Air Quality Study 2002. *Journal of Geophysical Research: Atmospheres*, *111*(D23). https://doi.org/10.1029/2006JD007252

Allan, B. J., Carslaw, N., Coe, H., Burgess, R. A., & Plane, J. M. C. (1999). Observations of the Nitrate Radical in the Marine Boundary Layer. *Journal of Atmospheric Chemistry*, *33*(2), 129–154. https://doi.org/10.1023/A:1005917203307

American Lung Association. (2023). Nitrogen Dioxide. Retrieved August 8, 2023, from https://www.lung.org/clean-air/outdoors/what-makes-air-unhealthy/nitrogen-dioxide

Anttila, T., Kiendler-Scharr, A., Tillmann, R., & Mentel, T. F. (2006). On the Reactive Uptake of Gaseous Compounds by Organic-Coated Aqueous Aerosols: Theoretical Analysis and Application to the Heterogeneous Hydrolysis of N2O5. *Journal of Physical Chemistry A*, *110*(35), 10435–10443. https://doi.org/10.1021/JP062403C

Appel, K. W., Bash, J. O., Fahey, K. M., Foley, K. M., Gilliam, R. C., Hogrefe, C., et al. (2021). The Community Multiscale Air Quality (CMAQ) model versions 5.3 and 5.3.1: system updates and evaluation. *Geoscientific Model Development*, *14*(5), 2867–2897. https://doi.org/10.5194/gmd-14-2867-2021

Atkinson, R., Winer, A. M., & Pitts, J. N. (1986). Estimation of Night-time N2O5 Concentrations from Ambient NO2 and NO3 Radical Concentrations and the Role of N2O5 in Night-time Chemistry. *Atmospheric Environment*, *20*(2), 331–339. https://doi.org/10.1016/0004-6981(86)90035-1

Brown, S. S., Ryerson, T. B., Wollny, A. G., Brock, C. A., Peltier, R., Sullivan, A. P., et al. (2006). Variability in Nocturnal Nitrogen Oxide Processing and Its Role in Regional Air Quality. *Science*, *311*, 76–70.

Brown, S. S., Dubé, W. P., Fuchs, H., Ryerson, T. B., Wollny, A. G., Brock, C. A., et al. (2009). Reactive uptake coefficients for N_2O_5 determined from aircraft measurements during the Second Texas Air Quality Study: Comparison to current model parameterizations. *Journal of Geophysical Research*, *114*, D00F10. https://doi.org/10.1029/2008JD011679

Buckley, S. M., & Mitchell, M. J. (2010). Improvements in Urban Air Quality: Case Studies from New York State, USA. *Water, Air, & Soil Pollution*, *214*, 93–106. https://doi.org/10.1007/s11270-010-0407-z

Byun, D., & Schere, K. L. (2006). Review of the Governing Equations, Computational Algorithms, and Other Components of the Models-3 Community Multiscale Air Quality (CMAQ) Modeling System. *Applied Mechanics Reviews*, *59*(2). https://doi.org/10.1115/1.2128636

César, A. C. G., Carvalho Jr., J. A., & Nascimento, L. F. C. (2015). Association between NOx exposure and deaths caused by respiratory diseases in a medium-sized Brazilian city. *Brazilian Journal of Medical and Biological Research*, *48*(12), 1130–1135. https://doi.org/10.1590/1414-431x20154396

Chang, W. L., Bhave, P. V., Brown, S. S., Riemer, N., Stutz, J., & Dabdub, D. (2011). Heterogeneous Atmospheric Chemistry, Ambient Measurements, and Model Calculations of N2O5: A Review. *Aerosol Science and Technology*, *45*(6), 665–695. https://doi.org/10.1080/02786826.2010.551672

Chang, W. L., Brown, S. S., Stutz, J., Middlebrook, A. M., Bahreini, R., Wagner, N. L., et al. (2016). Evaluating N2O5 heterogeneous hydrolysis parameterizations for CalNex 2010. *Journal of Geophysical Research: Atmospheres*, *121*(9), 5051–5070. https://doi.org/10.1002/2015JD024737

Finlayson-Pitts, B. J., Ezell, M. J., & Pitts Jr., J. N. (1989). Formation of chemically active chlorine compounds by reactions of atmospheric NaCl particles with gaseous N2O5 and ClONO2. *Nature*, *337*, 241–244.

Folkers, M., Mentel, Th. F., & Wahner, A. (2003). Influence of an organic coating on the reactivity of aqueous aerosols probed by the heterogeneous hydrolysis of N2O5. *Geophysical Research Letters*, *30*(12), 1644. https://doi.org/10.1029/2003GL017168

Gantt, B., Kelly, J. T., & Bash, J. O. (2015). Updating sea spray aerosol emissions in the Community Multiscale Air Quality (CMAQ) model version 5.0.2. *Geoscientific Model Development*, *8*(11), 3733–3746. https://doi.org/10.5194/GMD-8-3733-2015

Gaston, C. J., Thornton, J. A., & Ng, N. L. (2014). Reactive uptake of N2O5 to internally mixed inorganic and organic particles: The role of organic carbon oxidation state and inferred organic phase separations. *Atmospheric Chemistry and Physics*, *14*(11), 5693–5707. https://doi.org/10.5194/ACP-14-5693-2014

Gong, S. L. (2003). A parameterization of sea-salt aerosol source function for sub- and super-micron particles. *Global Biogeochemical Cycles*, *17*(4), 1097. https://doi.org/10.1029/2003GB002079

Griffiths, P. T., Badger, C. L., Cox, R. A., Folkers, M., Henk, H. H., & Mentel, T. F. (2009). Reactive uptake of N2O5 by aerosols containing dicarboxylic acids. Effect of particle phase, composition, and nitrate content. *Journal of Physical Chemistry A*, *113*(17), 5082–5090. https://doi.org/10.1021/JP8096814/ASSET/IMAGES/JP-2008-096814_M023.GIF

Grythe, H., Ström, J., Krejci, R., Quinn, P., & Stohl, A. (2014). A review of sea-spray aerosol source functions using a large global set of sea salt aerosol concentration measurements. *Atmospheric Chemistry and Physics*, *14*(3), 1277–1297. https://doi.org/10.5194/acp-14-1277-2014

He, H., Liang, X. Z., Sun, C., Tao, Z., & Tong, D. Q. (2020). The long-term trend and production sensitivity change in the US ozone pollution from observations and model simulations. *Atmospheric Chemistry and Physics*, *20*(5), 3191–3208. https://doi.org/10.5194/ACP-20-3191-2020

Jacob, D. J., Heikes, E. G., Fan, S.-M., Logan, J. A., Mauzerall, D. L., Bradshaw, J. D., et al. (1996). Origin of ozone and NO_x in the tropical troposphere: A photochemical analysis of aircraft observations over the South Atlantic basin. *Journal of Geophysical Research: Atmospheres*, *101*(D19), 24235–24250. https://doi.org/10.1029/96JD00336

Jayarathne, T., Sultana, C. M., Lee, C., Malfatti, F., Cox, J. L., Pendergraft, M. A., et al. (2016). Enrichment of Saccharides and Divalent Cations in Sea Spray Aerosol During Two Phytoplankton Blooms. *Environmental Science & Technology*, *50*(21), 11511–11520. https://doi.org/10.1021/acs.est.6b02988

Keene, W. C., Maring, H., Maben, J. R., Kieber, D. J., Pszenny, A. A. P., Dahl, E. E., et al. (2007). Chemical and physical characteristics of nascent aerosols produced by bursting bubbles at a model air-sea interface. *Journal of Geophysical Research*, *112*(D21), D21202. https://doi.org/10.1029/2007JD008464

Lamsal, L. N., Duncan, B. N., Yoshida, Y., Krotkov, N. A., Pickering, K. E., Streets, D. G., & Lu, Z. (2015). U.S. NO2 trends (2005–2013): EPA Air Quality System (AQS) data versus improved observations from the Ozone Monitoring Instrument (OMI). *Atmospheric Environment*, *110*, 130–143. https://doi.org/10.1016/J.ATMOSENV.2015.03.055

McDuffie, E. E., Fibiger, D. L., Dubé, W. P., Lopez-Hilfiker, F., Lee, B. H., Thornton, J. A., et al. (2018). Heterogeneous N2O5 Uptake During Winter: Aircraft Measurements During the 2015 WINTER Campaign and Critical Evaluation of Current Parameterizations. *Journal of Geophysical Research: Atmospheres*, *123*(8), 4345–4372. https://doi.org/10.1002/2018JD028336

Neumann, D., Matthias, V., Bieser, J., Aulinger, A., & Quante, M. (2016). Sensitivity of modeled atmospheric nitrogen species and nitrogen deposition to variations in sea salt emissions in the North Sea and Baltic Sea regions. *Atmospheric Chemistry and Physics*, *16*(5), 2921–2942. https://doi.org/10.5194/acp-16-2921-2016

Pandis, S. N., Harley, R. A., Cass, G. R., & Seinfeld, J. H. (1992). Secondary organic aerosol formation and transport. *Atmospheric Environment. Part A. General Topics*, *26*(13), 2269–2282. https://doi.org/10.1016/0960-1686(92)90358-R

Platt, U. F., Winer, A. M., Biermann, H. W., Atkinson, R., & Pitts, J. N. (1984). Measurement of Nitrate Radical Concentrations in Continental Air. *Environ. Sci. Technol*, *18*(5), 365–369. https://doi.org/10.1021/ES00123A015

Richards, L. W. (1983). Comments on the oxidation of NO2 to nitrate—day and night. *Atmospheric Environment (1967)*, *17*(2), 397–402. https://doi.org/10.1016/0004-6981(83)90057-4

Riedel, T. P., Wagner, N. L., Dubé, W. P., Middlebrook, A. M., Young, C. J., Öztürk, F., et al. (2013). Chlorine activation within urban or power plant plumes: Vertically resolved ClNO2 and Cl2 measurements from a tall tower in a polluted continental setting. *Journal of Geophysical Research: Atmospheres*, *118*(15), 8702–8715. https://doi.org/10.1002/jgrd.50637

Roberts, J. M., Osthoff, H. D., Brown, S. S., Ravishankara, A. R., Coffman, D., Quinn, P., & Bates, T. (2009). Laboratory studies of products of N2O5 uptake on Cl- containing substrates. *Geophysical Research Letters*, *36*(20). https://doi.org/10.1029/2009GL040448

Simpson, W. R., Brown, S. S., Saiz-Lopez, A., Thornton, J. A., & Von Glasow, R. (2015). Tropospheric Halogen Chemistry: Sources, Cycling, and Impacts. *Chemical Reviews*, *115*(10), 4035–4062. https://doi.org/10.1021/cr5006638

Sindelarova, K., Granier, C., Bouarar, I., Guenther, A., Tilmes, S., Stavrakou, T., et al. (2014). Global data set of biogenic VOC emissions calculated by the MEGAN model over the last 30 years. *Atmos. Chem. Phys*, *14*, 9317–9341. https://doi.org/10.5194/acp-14-9317-2014

Staudt, S., Gord, J. R., Karimova, N. V., Mcduffie, E. E., Brown, S. S., Gerber, R. B., et al. (2019). Sulfate and Carboxylate Suppress the Formation of ClNO2 at Atmospheric Interfaces. *ACS Earth Space Chem*, *3*(9). https://doi.org/10.1021/acsearthspacechem.9b00177

U.S. EPA. (2011). Nitrogen Oxides Control Regulations [Overviews & Factsheets,]. Retrieved November 15, 2023, from https://www3.epa.gov/region1/airquality/nox.html

U.S. EPA. (2014, April 9). Criteria Air Pollutants [Other Policies and Guidance]. Retrieved August 8, 2023, from https://www.epa.gov/criteria-air-pollutants

U.S. EPA. (2016, July 6). Basic Information about NO2 [Overviews and Factsheets]. Retrieved August 8, 2023, from https://www.epa.gov/no2-pollution/basic-information-about-no2

U.S. EPA. (2017, July 24). CMAQ's Purpose [Overviews and Factsheets]. Retrieved November 15, 2023, from https://www.epa.gov/cmaq/cmaqs-purpose

U.S. EPA. (2021). Our Nation's Air: Trends through 2021. Retrieved from https://gispub.epa.gov/air/trendsreport/2022/

Wagner, N. L., Riedel, T. P., Young, C. J., Bahreini, R., Brock, C. A., Dubé, W. P., et al. (2013). N_2O_5 uptake coefficients and nocturnal NO_2 removal rates determined from ambient wintertime measurements. *Journal of Geophysical Research: Atmospheres*, *118*(16), 9331–9350. https://doi.org/10.1002/jgrd.50653

Wang, D., Gouhier, T. C., Menge, B. A., & Ganguly, A. R. (2015). Intensification and spatial homogenization of coastal upwelling under climate change. *Nature*, *518*(7539), 390–394. https://doi.org/10.1038/nature14235

Warneke, C., de Gouw, J. A., Goldan, P. D., Kuster, W. C., Williams, E. J., Lerner, B. M., et al. (2004). Comparison of daytime and nighttime oxidation of biogenic and anthropogenic VOCs along the New England coast in summer during New England Air Quality Study 2002. *Journal of Geophysical Research: Atmospheres*, *109*(D10). https://doi.org/10.1029/2003JD004424

Wayne, R. P., Barnes, I., Biggs, P., Burrows, J. P., Canosa-Mas, C. E., Hjorth, J., et al. (1991). The nitrate radical: Physics, chemistry, and the atmosphere. *Atmospheric Environment. Part A. General Topics*, *25*(1), 1–203. https://doi.org/10.1016/0960-1686(91)90192-A

Zhang, R., Tie, X., & Bond, D. W. (2003). Impacts of anthropogenic and natural NOx sources over the U.S. on tropospheric chemistry. *Proceedings of the National Academy of Sciences*, *100*(4), 1505–1509. https://doi.org/10.1073/pnas.252763799

Chapter 2 Data and Methodology

Highlights

- The EPA Community Multiscale Air Quality (CMAQ) model is a collection of Fortran-based source code that I use to predict the chemistry impacting NO_x air quality over the Continental US
- User-defined inputs, study domain, and chemical mechanisms can have large impacts on the model outputs
- Heterogeneous chemistry is modified in the AEROSOL_CHEMISTRY module and sea spray emissions are modified in the SSEMIS module in CMAQ
- Observational data is necessary to validate model performance

2.1 About the CMAQ Model

The CMAQ model is a combination of programs that work together to predict air quality (Figure 1). The core of CMAQ is the CMAQ Chemistry Transport Model (CCTM). This core program relies on inputs of meteorology, primary pollution emission rates and composition, and surface properties to predict air quality conditions in time and space across a three-dimensional gridded domain using parameterized chemical mechanisms. However, all the green boxes in Figure 1 are part of the CMAQ model source code. These components include the Meteorology-Chemistry Interface Processor (MCIP), which prepares meteorological inputs for use; the initial condition (ICON) processor; and the boundary condition (BCON) processor. The ICON provides an input file of all chemical species concentrations at the start of the simulation period while BCON provides

an input file of the chemistry for each grid cell at the horizontal boundaries of the model domain. These two inputs constrain the chemistry within each CMAQ run, so the BCON and ICON must be defined before running the CCTM. Together, the ICON, BCON, MCIP, and CCTM components make up the entire CMAQ model.

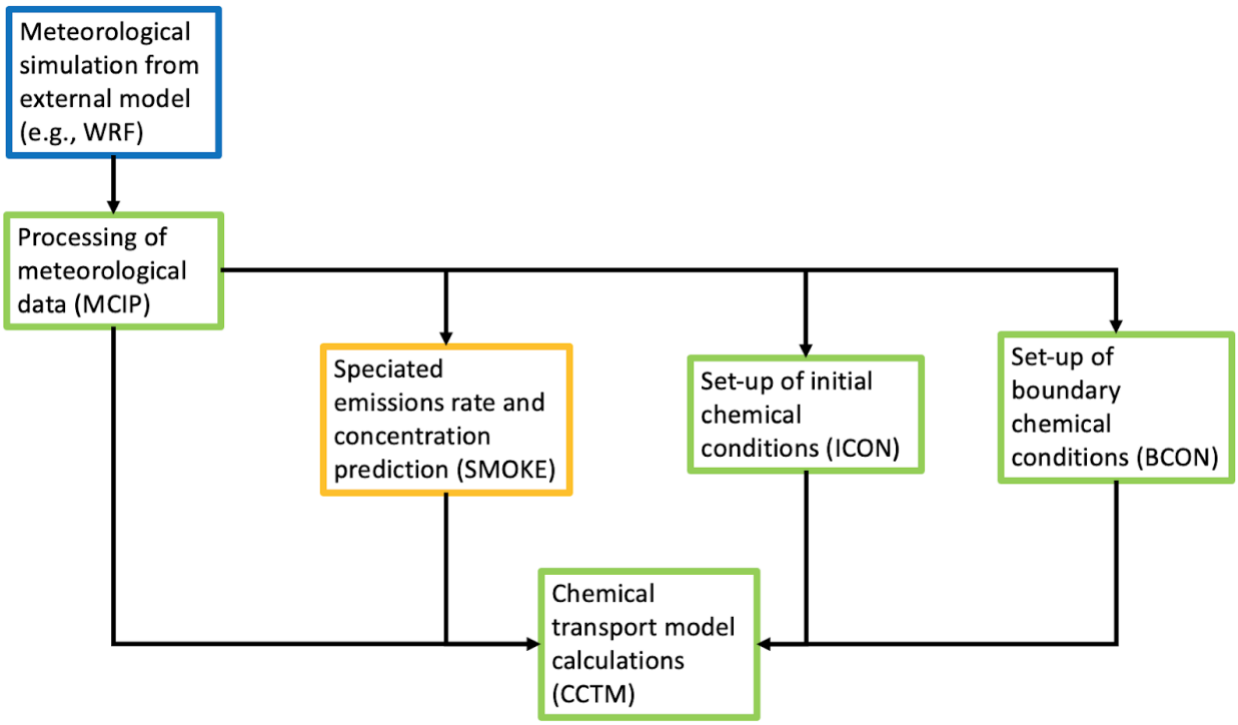

Figure 1. Flow of programs in the CMAQ model. Green boxes are part of the CMAQ package, downloaded together from the CMAQ repository, including MCIP, ICON, BCON, and CCTM. The blue box is the meteorological inputs, and the yellow box is the emission inputs. The models or inventories used for these external inputs can vary, which has impacts on the CMAQ output.

2.1.1 CMAQ Inputs

There are two components in Figure 1 that are not part of the CMAQ source code: the meteorological inputs (blue) and the speciated emissions processor (yellow). Meteorological conditions come from external regional-scale numerical weather models, such as the Weather Research and Forecasting (WRF) model. These meteorological inputs are prepared for use by MCIP. Gridded and speciated emissions can come from the Sparse Matrix Operator Kernel

Emissions (SMOKE) modelling system (https://www.cmascenter.org/smoke/), which calculates speciated emissions data for the entire CMAQ run in space and time. SMOKE defines area, point-source, and mobile anthropogenic emissions as well as biogenic emissions, including biomass burning, for the CMAQ grid. Some emissions are first calculated by source-specific models such as MEGAN, which predicts biogenic emissions based on meteorology and land cover (Guenther et al., 2012). The use of separate emission models and inputs is determined by the user and can have impacts on the final CCTM predictions.

Because CMAQ relies on inputs of emission inventories and the outputs of other models, results vary depending on the modelled inputs used (Appel et al., 2017; Gilliam et al., 2015; Travis et al., 2016). Deviations in wind speed and direction can cause differences of 100-200 km in downwind transport locations, while 8-hour maximum ozone concentrations can vary by 15-20% given differences in planetary boundary layer height, wind, cloud cover, and solar radiation (Gilliam et al., 2015). The type of spatial proxies used to allocate gridded emissions from regional totals also affects CCTM predictions, especially when moving to a smaller spatial resolution (Zheng et al., 2017). CMAQ relies on accurate inputs to produce reliable outputs.

2.1.2 Output data from CMAQ

The outputs from CMAQ include a range of gas and particle phase information, including concentrations of various gases, concentrations of particle components, total number of particles, and particle-phase information such as geometric mean diameter, geometric mean standard deviation, and some heterogeneous reaction rates. Gas phase concentrations are a

straightforward sum of the total number of gas molecules within a grid cell. However, particle concentrations are separated into categories based on which size particle is being measured.

Within CMAQ, three particle sizes are defined that make up the entire particle size distribution. These are the Aitken, accumulation, and coarse modes. Each of these modes is defined by the geometric mean diameter and standard deviation of particles in the mode. The Aitken mode is the smallest size, and particles typically have a diameter smaller than 0.1 µm; the accumulation mode is the next size and particles have a diameter between 0.1 to 2.5 µm; the coarse mode is the largest size with particles having a diameter greater than 0.3 µm (Bergin et al., 2022; Binkowski & Roselle, 2003). The Aitken and accumulation modes are together referred to as "fine" mode. All three modes overlap with each other, and the mean diameter and standard deviation of each mode will fluctuate during model runs. CMAQ tracks the particle composition within each mode, so that Aitken mode particles can have a different composition from accumulation mode particles, which can have a different composition from coarse mode particles.

2.1.3 Structure of the CCTM

The CCTM has a fixed grid in three dimensions (x, y, z) and calculates the change in mass of air pollutants over time by tracking each term in Eq. 1 within each grid cell (Byun & Schere, 2006). These processes include advection, diffusion, cloud processing, dry and wet deposition, emissions, and chemical transformations and removal processes such as cloud processing and gas-phase and multiphase (aerosol) reactions for each species i. Each C_i term is a concentration affected by transport or processing, R_i are gas-phase reactions, and E_i are emission terms.

$$\frac{\partial C_i}{\partial t} = \left(\frac{\partial C_i}{\partial t}\right)_{adv} + \left(\frac{\partial C_i}{\partial t}\right)_{diff} + \left(\frac{\partial C_i}{\partial t}\right)_{cloud} + \left(\frac{\partial C_i}{\partial t}\right)_{dep} + \left(\frac{\partial C_i}{\partial t}\right)_{aero} + R_{gas,i} + E_i \quad \text{Eq. 1}$$

There are several modules within the CCTM that assess each of the processes listed in Eq. 1. Because the CMAQ code is modular, it is relatively straightforward to focus on a code modification for one specific aspect of the model. The two modules of interest that have been modified in this dissertation are the AEROSOL_CHEMISTRY module for heterogeneous NO_x chemistry and SSEMIS module for sea spray emissions.

2.1.4 The aerosol chemistry module

The AEROSOL_CHEMISTRY module deals with heterogeneous and particle-phase reactions and this information is then used in the AERO_DRIVER module to calculate the changes to particle composition (Figure 2). Within AEROSOL_CHEMISTRY, CMAQ calculates heterogeneous reaction rates for several species, including N_2O_5 and $ClNO_2$, but the species available for reactions depends on the model reaction scheme used. The CMAQ model has multiple libraries of gas-phase and multiphase reaction schemes, which impacts the chemical species that affect heterogeneous reactions (Appel et al., 2021; Shareef et al., 2022). Throughout my dissertation, I use the Carbon Bond 6 revision 3 mechanism with aqueous aero7 aerosol chemistry (cb6r3_aero7_aq) (Cao et al., 2021; Emery et al., 2015, Pye et al., 2017). A high degree of variation in model prediction can be attributed to differences in mechanism choice, especially

for pollution in urban areas (Faraji et al., 2008; Jimenez, 2003; Luecken et al., 2008; Sarwar et al., 2013; Shareef et al., 2022).

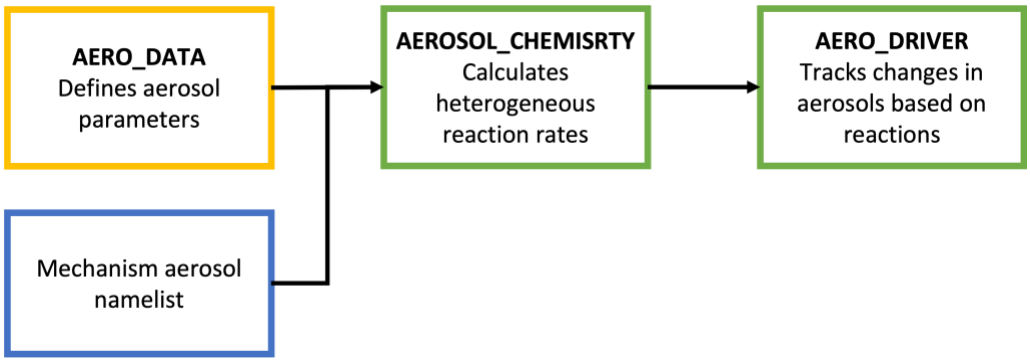

Figure 2. Flow of information for the calculation of heterogeneous mechanisms. The namelist input file is blue, modules that define labels and parameters for particle composition are yellow, and modules that calculate and track particle chemistry are green.

Each mechanism in CMAQ has unique treatment of chemical species as either explicit or lumped, where explicit species are individual chemical compounds and lumped species are combinations of chemicals with similar structure, reaction rates, and behavior such that they can be combined into one lumped species and tracked together in the model (Stockwell et al., 2020). The number and type of heterogeneous reactions depends on the explicit and lumped species included in the mechanism (Stockwell et al., 2020; Yarwood et al., 2010). The CB6 mechanism was developed using a lumped structure (Carter & Atkinson, 1996; Gery et al., 1989; Luecken et al., 2008; Whitten et al., 2010) but updates have increased the number of explicit species over time (Whitten et al., 2010; Yarwood et al., 2010) or have splits lumped species into multiple groups (Cao et al., 2021; Emery et al., 2015). The CB6r3 version of this mechanism includes interactions between organic aerosol and oxidized nitrogen species, split organic nitrates into two groups (monofunctional and multifunctional), and allows organic nitrates to contribute to total organic aerosol (Cao et al., 2021; Emery et al., 2015). These updates are important for the predictions of heterogeneous NO_x chemistry and the NO_x budget.

The aero7 aerosol chemistry mechanism affects particle phase reactions and gas-particle reactions, as well as the number of aerosol species. The aero7 mechanism is updated compared to the aero6 mechanism by adding or changing reaction pathways affecting secondary organic aerosol and by reorganizing particle components (Appel et al., 2021; Xu et al., 2018). In aero7, particle species are lumped together based on volatility and oxidation pathway, rather than being lumped by VOC precursor species (Xu et al., 2018). There are updates to the oxidation of VOCs to secondary organic aerosol, including the addition of NO_x-oxidizing reactions (Pye et al., 2015).

2.1.5 The sea spray emissions module

The SSEMIS module deals only with the calculation of sea spray particle number, surface area, volume, and mass emission rates. The number, surface area, and volume fluxes are calculated in-line using meteorological inputs and static grid definition files (Figure 3). Wind speed, relative humidity, and temperature variables are required from the meteorological data inputs. Open ocean and surf-zone fractions are defined by static grid definition files. To calculate mass emission rates and speciate the particle composition, the SSEMIS module calls the sea spray density variable and composition information from the AERO_DATA module. The emission rates calculated in SSEMIS are then passed into AERO_EMIS to add to the total emission in each time step. However, emission inputs are organized in the EMIS_DEFN module and changes to emissions – adding or omitting an emission source – must be tracked in EMIS_DEFN. In addition, the allocation of fine mode emissions is tracked in the AERO_DATA module, so changes to the

fraction of fine mode emissions that go to the Aitken mode versus the accumulation mode must be recorded in this module as well.

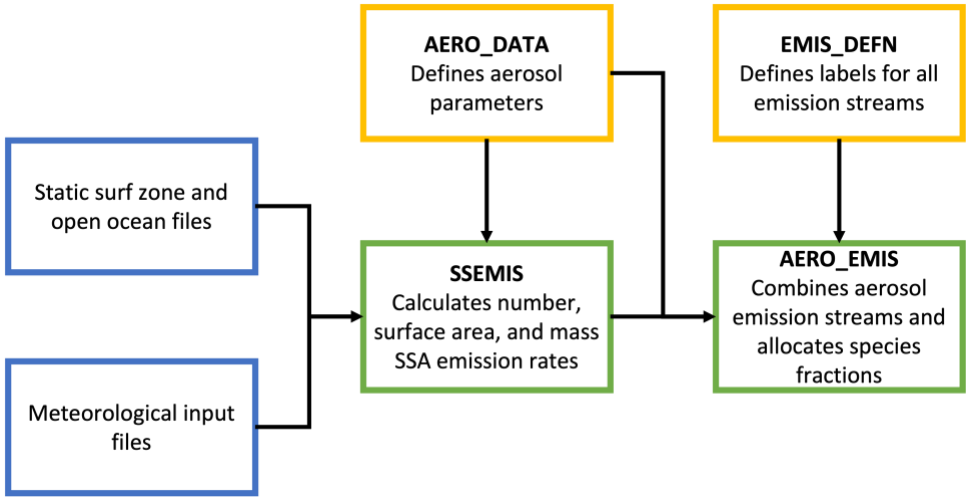

Figure 3. Information flow for the SSEMIS module. Input files are blue, modules that define labels and parameters for sea spray emissions are yellow, and modules that calculate and allocate SSA emissions are green.

2.2 Observational Data for CMAQ Evaluation

2.2.1 Wintertime Investigation of Transport, Emission, and Reactivity field campaign

To assess the impact of adjusting nocturnal heterogeneous uptake and yield parameterizations in the CMAQ model, I compared model results against data collected during the 2015 Wintertime Investigation of Transport, Emission, and Reactivity (WINTER) field campaign (Jaeglé et al., 2018; Schroder et al., 2018). The campaign was based out of NASA Langley in Hampton, VA. Thirteen research flights onboard the National Center for Atmospheric Research (NCAR) C-130 were conducted over the eastern US between 1 February and 15 March 2015. The objectives of the campaign were to characterize wintertime chemistry, with an equal focus on nocturnal and daytime processes, and to assess dominant aerosol formation and reaction pathways (https://www.eol.ucar.edu/field_projects/winter). As such, the campaign had

flights during both the day and night. Because of the importance of sampling nocturnal chemistry within the nocturnal residual layer, 85% of measurements were made within 2 km of the surface (Jaeglé et al., 2018). I compared modelled results with N_2O_5, $ClNO_2$, oxygen to carbon ratio, and particle nitrate measurements during the field campaign (Guo et al., 2016; Jaeglé et al., 2018; Lee et al., 2018).

In addition to comparison with concentrations measured during the field campaign, I compared CMAQ N_2O_5 uptake ($\gamma(N_2O_5)$) and $ClNO_2$ yield ($\Phi(ClNO_2)$) values with box model calculations made using the WINTER data (McDuffie et al., 2018b; McDuffie et al., 2018a). An iterative box model was used to calculate $\gamma(N_2O_5)$ and $\Phi(ClNO_2)$ from airborne measurements of relevant gas and particle phase species, particle surface area, and actinic flux (McDuffie et al., 2018b; McDuffie et al., 2018a). These box model results are presented in McDuffie et al. (2018a; 2018b), and the data was shared with me by Erin McDuffie.

2.2.2 Air Quality System monitors

The EPA coordinates several networks of monitors to measure ambient air pollution and reports the air quality data through the Air Quality System (AQS) (U.S. EPA, 2013). The AQS combines monitor data from all EPA networks that measure each air pollutant; for example, five monitor networks are associated with NO_2 measurements in 2019 (U.S. EPA, 2023). Depending on the network, these monitors are placed to both enable enforcement of the ambient air quality standards and provide data for studying air pollution (Muller & Ruud, 2018). Hourly NO_2 data was downloaded from the AQS website https://aqs.epa.gov/aqsweb/airdata/download_files.html.

For verification of model results in Chapter 4, I compare model NO_2 to monitor data from AQS. Over the entire United States in 2019, there were 491 operational NO_2 monitors, four of

which were in Alaska, Hawaii, and Puerto Rico (U.S. EPA, 2023). Some of these monitors were deployed as short-term special purpose monitors.

2.2.3 Model-observation comparisons

Because models work on a fixed grid while observational data is often a point location, CMAQ model results must be aligned with the location of each observational data point. The resolution of the CMAQ model runs (12 km by 12 km grid, 1 hr output frequency, 35 vertical layers) means that for observational data that are temporally or spatially close together (i.e., within the same grid cell or 1 hr output time range) may not have unique CMAQ values. Additionally, CMAQ outputs are either instantaneous on the hour or hourly averages, which impacts how temporally similar the model and observed values are. Within the model, changes in concentration are tracked in 1 s timesteps, but this information is output either as an instantaneous value (the second on the hour) or as an hourly average. I used hourly averages to compare against AQS data because the monitors report data as hourly averages, and I used instantaneous values for WINTER flight data to better align with the instantaneous measurements made during the campaign.

2.3 Advantages and disadvantages to air quality models

There are numerous advantages to using CMAQ to understand the chemistry that impacts NO_x air quality. However, there are also disadvantages to air quality models such as CMAQ, including the reliance on simplifying assumptions and input data.

Some of the advantages of CMAQ are the continuous spatial and temporal coverage and the ability of the model to answer questions of different “what if” scenarios. Unlike AQS surface

monitors, which make *in situ* measurements with an irregular spatial coverage, the CMAQ model will calculate pollutant concentrations continuously over the user-defined spatial grid. And unlike most satellites, CMAQ will continuously model pollutant concentrations during the user-defined period and output the data at a user-defined frequency. The Tropospheric Emissions: Monitoring of Pollution (TEMPO) satellite, launched in April 2023, is the first geostationary satellite over the US to provide hourly data of many pollutants and thus can compliment CMAQ in the temporal frequency and spatial coverage (NASA, 2023). However, CMAQ and other air quality models can also answer "what if" questions, such as what might happen with different emission scenarios or policy interventions. I use the ability to compare different scenarios throughout my dissertation to compare chemical mechanisms and assess the impacts.

One of the largest disadvantages to air quality models is that they are representations of the physical world based on assumptions and the best scientific understanding of physical and chemical processes. These assumptions mean that model outputs may not be accurate, and verification is required to assess model performance (Simon et al., 2012). For example, the most recent versions of CMAQ often overpredict peak ozone concentration and underpredict NO_2 concentration (Gilliland et al., 2008; Toro et al., 2021). The CMAQ model also has large requirements for both the data inputs such as meteorology, emissions, and surface type and the computing power needed to run the model. Finally, CMAQ is complex and learning to run the model requires a steep learning curve.

References

Appel, K. W., Napelenok, S. L., Foley, K. M., Pye, H. O. T., Hogrefe, C., Luecken, D. J., et al. (2017). Description and evaluation of the Community Multiscale Air Quality (CMAQ)

modeling system version 5.1. *Geoscientific Model Development*, *10*(4), 1703–1732. https://doi.org/10.5194/gmd-10-1703-2017

Appel, K. W., Bash, J. O., Fahey, K. M., Foley, K. M., Gilliam, R. C., Hogrefe, C., et al. (2021). The Community Multiscale Air Quality (CMAQ) model versions 5.3 and 5.3.1: system updates and evaluation. *Geoscientific Model Development*, *14*(5), 2867–2897. https://doi.org/10.5194/gmd-14-2867-2021

Bergin, R. A., Harkey, M., Hoffman, A., Moore, R. H., Anderson, B., Beyersdorf, A., et al. (2022). Observation-based constraints on modeled aerosol surface area: implications for heterogeneous chemistry. *Atmos. Chem. Phys*, *22*, 15449–15468. https://doi.org/10.5194/acp-22-15449-2022

Binkowski, F. S., & Roselle, S. J. (2003). Models-3 Community Multiscale Air Quality (CMAQ) model aerosol component 1. Model description. *Journal of Geophysical Research D: Atmospheres*, *108*(6). https://doi.org/10.1029/2001jd001409

Byun, D., & Schere, K. L. (2006). Review of the Governing Equations, Computational Algorithms, and Other Components of the Models-3 Community Multiscale Air Quality (CMAQ) Modeling System. *Applied Mechanics Reviews*, *59*(2). https://doi.org/10.1115/1.2128636

Cao, L., Li, S., & Sun, L. (2021). Study of different Carbon Bond 6 (CB6) mechanisms by using a concentration sensitivity analysis. *Atmospheric Chemistry and Physics*, *21*(16), 12687–12714. https://doi.org/10.5194/acp-21-12687-2021

Carter, W. P. L., & Atkinson, R. (1996). Development and evaluation of a detailed mechanism for the atmospheric reactions of isoprene and NOx. *International Journal of Chemical Kinetics*, *28*(7), 497–530. https://doi.org/10.1002/(SICI)1097-4601(1996)28:7<497::AID-KIN4>3.0.CO;2-Q

Emery, C., Jung, J., Koo, B., & Yarwood, G. (2015). *Improvements to CAMx Snow Cover Treatments and Carbon Bond Chemical Mechanism for Winter Ozone. Final Report*. Salt Lake City, UT: Ramboll Environ. Retrieved from http://www.deq.utah.gov/locations/U/uintahbasin/docs/2014/03Mar

Faraji, M., Kimura, Y., McDonald-Buller, E., & Allen, D. (2008). Comparison of the carbon bond and SAPRC photochemical mechanisms under conditions relevant to southeast Texas. *Atmospheric Environment*, *42*(23), 5821–5836. https://doi.org/10.1016/j.atmosenv.2007.07.048

Gery, M. W., Whitten, G. Z., Killus, J. P., & Dodge, M. C. (1989). A photochemical kinetics mechanism for urban and regional scale computer modeling. *Journal of Geophysical Research: Atmospheres*, *94*(D10), 12925–12956. https://doi.org/10.1029/JD094iD10p12925

Gilliam, R. C., Hogrefe, C., Godowitch, J. M., Napelenok, S., Mathur, R., & Rao, S. T. (2015). Impact of inherent meteorology uncertainty on air quality model predictions. *Journal of Geophysical Research: Atmospheres*, *120*(23), 12,259-12,280. https://doi.org/10.1002/2015JD023674

Gilliland, A. B., Hogrefe, C., Pinder, R. W., Godowitch, J. M., Foley, K. L., & Rao, S. T. (2008). Dynamic evaluation of regional air quality models: Assessing changes in O3 stemming from changes in emissions and meteorology. *Atmospheric Environment*, *42*(20), 5110–5123. https://doi.org/10.1016/j.atmosenv.2008.02.018

Guenther, A. B., Jiang, X., Heald, C. L., Sakulyanontvittaya, T., Duhl, T., Emmons, L. K., & Wang, X. (2012). The model of emissions of gases and aerosols from nature version 2.1 (MEGAN2.1): An extended and updated framework for modeling biogenic emissions. *Geoscientific Model Development*, *5*(6), 1471–1492. https://doi.org/10.5194/GMD-5-1471-2012

Guo, H., Sullivan, A. P., Campuzano-Jost, P., Schroder, J. C., Lopez-Hilfiker, F. D., Dibb, J. E., et al. (2016). Fine particle pH and the partitioning of nitric acid during winter in the northeastern United States. *Journal of Geophysical Research: Atmospheres*, *121*(17), 10,355-10,376. https://doi.org/10.1002/2016JD025311

Jaeglé, L., Shah, V., Thornton, J. A., Lopez-Hilfiker, F. D., Lee, B. H., McDuffie, E. E., et al. (2018). Nitrogen Oxides Emissions, Chemistry, Deposition, and Export Over the Northeast United States During the WINTER Aircraft Campaign. *Journal of Geophysical Research: Atmospheres*, *123*(21), 12,368-12,393. https://doi.org/10.1029/2018JD029133

Jimenez, P. (2003). Comparison of photochemical mechanisms for air quality modeling. *Atmospheric Environment*, *37*(30), 4179–4194. https://doi.org/10.1016/S1352-2310(03)00567-3

Lee, B. H., Lopez-Hilfiker, F. D., Veres, P. R., McDuffie, E. E., Fibiger, D. L., Sparks, T. L., et al. (2018). Flight Deployment of a High-Resolution Time-of-Flight Chemical Ionization Mass Spectrometer: Observations of Reactive Halogen and Nitrogen Oxide Species. *Journal of Geophysical Research: Atmospheres*, *123*(14), 7670–7686. https://doi.org/10.1029/2017JD028082

Luecken, D. J., Phillips, S., Sarwar, G., & Jang, C. (2008). Effects of using the CB05 vs. SAPRC99 vs. CB4 chemical mechanism on model predictions: Ozone and gas-phase photochemical precursor concentrations. *Atmospheric Environment*, *42*(23), 5805–5820. https://doi.org/10.1016/j.atmosenv.2007.08.056

McDuffie, E. E., Fibiger, D. L., Dubé, W. P., Lopez Hilfiker, F., Lee, B. H., Jaeglé, L., et al. (2018a). ClNO 2 Yields From Aircraft Measurements During the 2015 WINTER Campaign and Critical Evaluation of the Current Parameterization. *Journal of Geophysical Research: Atmospheres*, *123*(22), 12,994-13,015. https://doi.org/10.1029/2018JD029358

McDuffie, E. E., Fibiger, D. L., Dubé, W. P., Lopez-Hilfiker, F., Lee, B. H., Thornton, J. A., et al. (2018b). Heterogeneous N2O5 Uptake During Winter: Aircraft Measurements During the 2015 WINTER Campaign and Critical Evaluation of Current Parameterizations. *Journal of Geophysical Research: Atmospheres*, *123*(8), 4345–4372. https://doi.org/10.1002/2018JD028336

Muller, N. Z., & Ruud, P. A. (2018). What Forces Dictate the Design of Pollution Monitoring Networks? *Environmental Modeling & Assessment*, *23*(1), 1–14. https://doi.org/10.1007/s10666-017-9553-7

NASA. (2023, November). TEMPO: Tropospheric Emissions: Monitoring of POllution. Retrieved from https://science.nasa.gov/mission/tempo/

Pye, H. O. T., Luecken, D. J., Xu, L., Boyd, C. M., Ng, N. L., Baker, K. R., et al. (2015). Modeling the Current and Future Roles of Particulate Organic Nitrates in the Southeastern United States. *Environmental Science & Technology*, *49*(24), 14195–14203. https://doi.org/10.1021/acs.est.5b03738

Pye, H. O. T., Murphy, B. N., Xu, L., Ng, N. L., Carlton, A. G., Guo, H., et al. (2017). On the implications of aerosol liquid water and phase separation for organic aerosol mass. *Atmos. Chem. Phys*, *17*, 343–369. https://doi.org/10.5194/acp-17-343-2017

Sarwar, G., Godowitch, J., Henderson, B. H., Fahey, K., Pouliot, G., Hutzell, W. T., et al. (2013). A comparison of atmospheric composition using the Carbon Bond and Regional Atmospheric Chemistry Mechanisms. *Atmospheric Chemistry and Physics*, *13*(19), 9695–9712. https://doi.org/10.5194/acp-13-9695-2013

Schroder, J. C., Campuzano-Jost, P., Day, D. A., Shah, V., Larson, K., Sommers, J. M., et al. (2018). Sources and Secondary Production of Organic Aerosols in the Northeastern United States during WINTER. *Journal of Geophysical Research: Atmospheres*, *123*(14), 7771–7796. https://doi.org/10.1029/2018JD028475

Shareef, M., Cho, S., Lyder, D., Zelensky, M., & Heckbert, S. (2022). Evaluation of Different Chemical Mechanisms on O3 and PM2.5 Predictions in Alberta, Canada. *Applied Sciences*, *12*(17), 8576. https://doi.org/10.3390/app12178576

Simon, H., Baker, K. R., & Phillips, S. (2012). Compilation and interpretation of photochemical model performance statistics published between 2006 and 2012. *Atmospheric Environment*, *61*, 124–139. https://doi.org/10.1016/j.atmosenv.2012.07.012

Stockwell, W. R., Saunders, E., Goliff, W. S., & Fitzgerald, R. M. (2020). A perspective on the development of gas-phase chemical mechanisms for Eulerian air quality models. *Journal of the Air & Waste Management Association*, *70*(1), 44–70. https://doi.org/10.1080/10962247.2019.1694605

Toro, C., Foley, K., Simon, H., Henderson, B., Baker, K. R., Eyth, A., et al. (2021). Evaluation of 15 years of modeled atmospheric oxidized nitrogen compounds across the contiguous United States. *Elementa: Science of the Anthropocene*, *9*(1), 00158. https://doi.org/10.1525/elementa.2020.00158

Travis, K. R., Jacob, D. J., Fisher, J. A., Kim, P. S., Marais, E. A., Zhu, L., et al. (2016). Why do models overestimate surface ozone in the Southeast United States? *Atmospheric Chemistry and Physics*, *16*(21), 13561–13577. https://doi.org/10.5194/acp-16-13561-2016

U.S. EPA. (2013, August 1). Air Quality System (AQS) [Data and Tools]. Retrieved January 5, 2024, from https://www.epa.gov/aqs

U.S. EPA. (2023). *Overview of Nitrogen Dioxide (NO2) Air Quality in the United States*. Washington, D.C.: U.S. Environmental Protection Agency. Retrieved from https://www.epa.gov/system/files/documents/2022-08/NO2_2021.pdf

Whitten, G. Z., Heo, G., Kimura, Y., McDonald-Buller, E., Allen, D. T., Carter, W. P. L., & Yarwood, G. (2010). A new condensed toluene mechanism for Carbon Bond: CB05-TU. *Atmospheric Environment*, *44*(40), 5346–5355. https://doi.org/10.1016/j.atmosenv.2009.12.029

Xu, L., Pye, H. O. T., He, J., Chen, Y., Murphy, B. N., & Ng, N. L. (2018). Experimental and model estimates of the contributions from biogenic monoterpenes and sesquiterpenes to secondary organic aerosol in the southeastern United States. *Atmospheric Chemistry and Physics*, *18*(17), 12613–12637. https://doi.org/10.5194/ACP-18-12613-2018

Yarwood, G., Jung, J., Whitten, G. Z., Heo, G., Mellberg, J., & Estes, M. (2010). Updates to the Carbon Bond Mechanism for Version 6 (CB6). Presented at the 9th Annual CMAQ Conference, Chapel Hill, NC.

Zheng, B., Zhang, Q., Tong, D., Chen, C., Hong, C., Li, M., et al. (2017). Resolution dependence of uncertainties in gridded emission inventories: a case study in Hebei, China. *Atmospheric Chemistry and Physics*, *17*(2), 921–933. https://doi.org/10.5194/acp-17-921-2017

Chapter 3 Assessment of nocturnal NO_x heterogeneous reaction mechanisms in the Community Multiscale Air Quality (CMAQ) model

Highlights

- Accounting for organic coatings on particles reduces the amount of N_2O_5 that enters the particle phase.
- The addition of the competitive effect of sulfate inhibits $ClNO_2$ yield.
- Composition of fine and coarse mode particles in the CMAQ model is different, resulting in a disparate influence on uptake and yield.

Abstract

Nitrogen oxides have adverse human health impacts and play a central role in the production of ozone and $PM_{2.5}$. While day-time NO_x cycling depends on gas-phase photolytic reactions, night-time heterogeneous chemistry regulates the nocturnal reservoirs and sinks of NO_x. However, existing parameterizations of nocturnal NO_x heterogeneous chemistry in air quality models do not capture the variability in observed N_2O_5 removal or $ClNO_2$ production. Here, I implemented new N_2O_5 uptake ($\gamma(N_2O_5)$) and $ClNO_2$ yield ($\Phi(ClNO_2)$) parameterizations in the Community Multiscale Air Quality model that account for the role of particulate organic matter in regulating N_2O_5 uptake and the role of reactive solutes in suppressing $ClNO_2$ production. I compared the performance against existing model parameterizations and field measurements. With the new parameterizations, the coarse mode particles contributed modestly to N_2O_5 loss (17.2%) but significantly to $ClNO_2$ production (60.3%), highlighting the impact of coarse mode chemistry. The new $\gamma(N_2O_5)$ parameterization in the fine mode increased agreement between modeled N_2O_5

concentration and observations ($RMSE_{new} = 0.37\ ppb$) compared to the model default ($RMSE_{default} = 0.43\ ppb$). The new $\gamma(N_2O_5)$ parameterization was overall biased low due to underestimates in modelled particle oxygen to carbon ratio (O:C). The new $\Phi(ClNO_2)$ parameterization resulted in further underestimation ($NMB_{new} = -73.7\%$) compared to the model default ($NMB_{default} = -37.9\%$) because of underestimation of fine mode particle chloride concentration. I expect that the new parameterizations will more accurately capture the mean state and variability in $\gamma(N_2O_5)$ and $\Phi(ClNO_2)$ under conditions where model particulate O:C and chloride are better represented.

3.1 Introduction

Nitrogen oxides ($NO_x \equiv NO + NO_2$) play a central role in the photochemical production of tropospheric ozone (O_3) and significantly impact the production rate of aerosol mass (Jacob, 2000; Lei & Wang, 2014; Spicer, 1983). Accurate treatment of the nocturnal NO_x chemistry in chemical transport models is essential to predicting air quality because night-time nitrogen oxide chemistry limits the NO_x lifetime, particularly during winter (Brown et al., 2006; Richards, 1983). However, nocturnal heterogeneous processes that affect NO_x are simplified in most atmospheric chemical transport models (Chang et al., 2011).

Nocturnal heterogeneous reactions impact early morning NO_2 concentrations by regulating NO_x reservoir species such as NO_3 and N_2O_5 (Brown et al., 2006; Chang et al., 2011; Richards, 1983). Nitrate radical (NO_3) loss through photolysis is negligible at night, such that production through the reaction of NO_2 and O_3 results in sustained concentrations of NO_3 (R1). Nitrate radicals reach equilibrium with dinitrogen pentoxide (N_2O_5) through (R2). In the

daytime, NO_3 can be depleted through reactions with NO (R5), but this is negligible at night. Thus, the lifetime of nocturnal nitrogen oxides (NO_3 + N_2O_5) is a function of volatile organic compound (VOC) concentration and speciation (R3) and aerosol surface area and composition (R4). When NO_3 gas-phase reactions (R3) are slow, the heterogeneous reaction of N_2O_5 with aerosol particles (R4) – known as the uptake of N_2O_5 ($\gamma(N_2O_5)$) – dictates the nocturnal lifetime of NO_x (Bertram et al., 2009; Chang et al., 2011).

$$NO_2 + O_3 \rightarrow NO_3 + O_2 \quad \text{(R1)}$$

$$NO_2 + NO_3 + M \rightleftharpoons N_2O_5 + M \quad \text{(R2)}$$

$$NO_3 + VOC \rightarrow products \quad \text{(R3)}$$

$$N_2O_5(g) + aerosol \rightarrow N_2O_5(aq) \quad \text{(R4)}$$

$$NO_3 + NO \rightarrow 2NO_2 \quad \text{(R5)}$$

Global estimates indicate that N_2O_5-aerosol reactions may account for up to 50% of the total NO_x loss, depending on location and season (Alexander et al., 2009; Evans & Jacob, 2005; Holmes et al., 2019) and can impact the global budgets of OH and O_3 by as much as 15% (Bauer et al., 2004; MacIntyre & Evans, 2010). Once in the particle phase, N_2O_5 can dissociate and react with particle water to form HNO_3 (R6-8) (Bertram & Thornton, 2009; Griffiths et al., 2009).

$$N_2O_5(aq) \rightleftharpoons NO_3^-(aq) + NO_2^+(aq) \quad \text{(R6)}$$

$$NO_3^-(aq) + H^+(aq) \rightleftharpoons HNO_3(aq) \quad \text{(R7)}$$

$$NO_2^+(aq) + H_2O \rightarrow H^+(aq) + HNO_3(aq) \quad \text{(R8)}$$

Laboratory measurements demonstrated that N_2O_5 uptake into chloride-containing particles can lead to the production and evaporation of nitryl chloride ($ClNO_2$) (R9), which will subsequently photo-dissociate to form gaseous Cl and NO_2 (R10) (Behnke et al., 1997; Finlayson-

Pitts et al., 1989; Roberts et al., 2009; Thornton & Abbatt, 2005). Heterogeneous production of $ClNO_2$ can cause large increases in O_3 episodes (>10 ppb) (Sarwar et al., 2012). Together, N_2O_5 and $ClNO_2$ chemistry has large impacts on particle nitrate concentration (Bertram & Thornton, 2009; Prabhakar et al., 2017; Riemer et al., 2003). Because of their influence on global NO_x, OH, O_3, and nitrate aerosol budgets, improved parameterizations of heterogeneous N_2O_5 and $ClNO_2$ chemistry offer the potential to improve atmospheric chemistry models.

$$NO_2^+(aq) + Cl^-(aq) \rightarrow ClNO_2 \quad \text{(R9)}$$

$$ClNO_2 + h\nu \rightarrow Cl\cdot + NO_2 \quad \text{(R10)}$$

Measurements of uptake of N_2O_5 onto particles ($\gamma(N_2O_5)$) span more than three orders of magnitude depending on the chemical and physical properties of atmospheric aerosol and the location and season of the measurements (Chang et al., 2011). Uptake is a complex function of factors including: i) aerosol liquid water content which increases uptake by promoting N_2O_5 dissolution (Bertram et al., 2009; Thornton et al., 2003), ii) particle nitrate which decreases uptake by pushing the equilibrium in (R6) towards aqueous N_2O_5 (Griffiths et al., 2009; Mentel et al., 1999), and iii) organic coatings that either suppress N_2O_5 mass accommodation or decrease water availability at the surface (Anttila et al., 2006; Folkers et al., 2003; Gaston et al., 2014). This particle phase separation demonstrates how internal mixing of the particles is important for determining $\gamma(N_2O_5)$ to individual particles (Ryder et al., 2014).

Chemical transport models have mechanisms for heterogeneous reactions that include some of the factors affecting $\gamma(N_2O_5)$ (see Table 2 of Chang et al. (2011) or Table S8 of McDuffie et al. (2018b) for reviews of existing parameterizations of N_2O_5 uptake). However, there has been limited comparison of chemical transport model predictions against measurement-based

calculations of $\gamma(N_2O_5)$. Chang et al. (2016) compared WRF-Chem predictions of $\gamma(N_2O_5)$ against calculations derived from field measurements made during the CalNex2010 field campaign. Organic coatings improved model performance by decreasing the model overestimates of $\gamma(N_2O_5)$ (Chang et al., 2016). Brown et al. (2009) calculated $\gamma(N_2O_5)$ during the TexAQS II flight campaign and compared against several parameterizations of $\gamma(N_2O_5)$, using flight data to drive the parameterized $\gamma(N_2O_5)$ calculations. Uptake derived from each of the parameterizations was significantly larger than steady-state calculations of uptake, potentially due to missing impacts of organic aerosol in model parameterizations (Brown et al., 2009). McDuffie et al. (2018b) implemented a box model using aircraft observations made during the WINTER 2015 field campaign to derive $\gamma(N_2O_5)$ with 14 different parameterizations, not all of which have been previously used in a chemical transport model. None of the parameterizations captured the range of the steady state box model $\gamma(N_2O_5)$ values (McDuffie et al., 2018b).

In addition to N_2O_5 uptake, the production and subsequent evaporation of $ClNO_2$, i.e., the yield of $ClNO_2$ ($\Phi(ClNO_2)$) is overpredicted in calculations for both coastal and continental airmasses (McDuffie et al., 2018a; Osthoff et al., 2008; Thornton et al., 2010; Wang et al., 2017). It has been suggested that chloride is not evenly distributed throughout the aerosol population, resulting in a subset of aerosol particles having higher chloride concentration, and higher values of $\Phi(ClNO_2)$ (McNamara et al., 2020). With few exceptions, chemical transport models assume that the chemical composition of individual aerosol particles within a given size mode are identical (i.e., that the aerosol population is internally mixed) and are thus blind to particle-to-particle variability in $\Phi(ClNO_2)$. Staudt et al. (2019) showed that anions such as sulfate can significantly suppress the formation of $ClNO_2$. The effect of sulfate suppression of $\Phi(ClNO_2)$ is

not currently accounted for in any chemical transport model.

Despite the central role of nocturnal nitrogen oxide chemistry in limiting NO_x lifetimes, existing chemical transport model parametrizations of the key heterogeneous mechanisms $\gamma(N_2O_5)$ and $\Phi(ClNO_2)$ use simplified chemical mechanisms that do not capture the variability seen in field measurements. Current parameterizations of N_2O_5 uptake in the Community Multiscale Air Quality (CMAQ) model (Appel et al., 2021; Byun & Schere, 2006) ignore the effects of organics on uptake and assume that particles are internally mixed (i.e., all particles within a mode have the same chemical composition), and the current CMAQ parameterization of $ClNO_2$ yield only includes the effects of particle chloride and water. Here, I implement two chemically representative parameterizations in CMAQ: a N_2O_5 uptake parameterization based on Gaston, et al. (2014) and a $ClNO_2$ yield parameterization based on Staudt, et al. (2019). The primary objective of this chapter is the assessment of the Gaston and Staudt parameterizations for the first time in a regional chemical transport model by comparison with measurements, with a specific focus on the role of aerosol chemical composition.

3.2 Model parameterization development and implementation

3.2.1 Uptake of N_2O_5 to particles

In the CMAQ versions 5.1 and later, there are five parameterizations of $\gamma(N_2O_5)$ that can be selected by the user, some of which are specific to a particle size mode. The current default uses the parameterization developed by Davis, et al. (2008) for fine mode particles and the method developed by Bertram and Thornton (2009) for coarse mode particles (Sarwar et al., 2012). None of the existing CMAQ parameterizations include the effects of organics on uptake, and all assume that particles are internally mixed.

I implemented a new parameterization for $\gamma(N_2O_5)$ from Gaston et al. (2014) which includes the effects of particle phase separation, based on the resistor model devised by Anttila et al. (2006) shown in Figure 1. This $\gamma(N_2O_5)$ schematic contains resistance terms for gas-phase diffusion (Γ_{diff}), mass accommodation (Γ_{α}), and bulk-phase processes (Γ_{bulk}). Bulk-phase processes include diffusion and chemical reactions in both the organic coating of thickness l and the aqueous core with radius r_{aq}. Gaston et al. (2014) found that presence of an organic coating consistently suppressed uptake, but to varying degrees depending on particle oxygen to carbon ratio (O:C). The O:C ratio is a measure of how oxidized the organic phase is, where higher O:C means more oxidized, and, therefore, more polar organic composition. A more polar organic phase is less repulsive to N_2O_5 molecules, thus allowing uptake to increase (Gaston et al., 2014). Relative humidity also impacted $\gamma(N_2O_5)$ where reactive uptake increased with increasing RH.

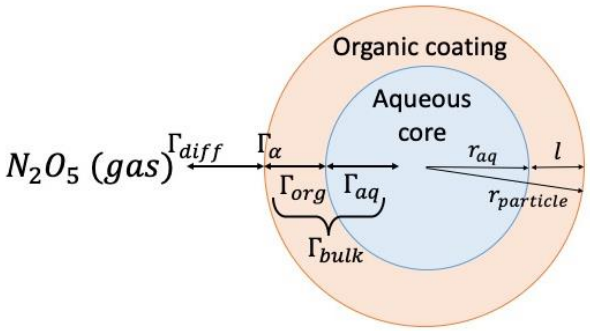

Figure 1. Schematic of the resistor model of N_2O_5 uptake to particles. Each step in the uptake of the gas into a particle is modelled as a resistance Γ: gas-phase diffusion to the surface (Γ_{diff}), mass accommodation (Γ_{α}), and bulk-phase processes (Γ_{bulk}) such as reactions, dissolution, and diffusion in the organic coating and the aqueous core. Here, l is the organic coating thickness and r_{aq} is the radius of the aqueous core.

I implemented four modal combinations of the $\gamma(N_2O_5)$ parameterizations, listed in Table 1, in the CMAQ model. These include the i) the Davis et al. (2008) parameterization (hereafter Davis) for both fine and coarse modes; ii) Bertram and Thornton (2009) parameterization

(hereafter referred to as B+T) for both fine and coarse modes; iii) the Gaston et al. (2014) parameterization (hereafter Gaston) for both fine and coarse modes; and iv) the current default parameterization in CMAQ v5.3.2 (hereafter default), which is a combination of the Davis parameterization for fine mode and the B+T parameterization for coarse mode (Sarwar et al., 2012).

Table 1: Parameterization equations of $\gamma(N_2O_5)$ incorporated in the CMAQ model

Parameterization	Parameterization Equations
Davis (Davis et al., 2008) Fine and coarse mode	$\gamma_i = \frac{1}{1+e^{-\lambda_i}}$ $x_3 = \frac{n_{NO_3^-}}{n_{NO_3^-}+n_{SO_4^{2-}}}$ $x_2 = \max\left(0, min\left(1-x_3, \frac{n_{NH_4^+}}{n_{NO_3^-}+n_{SO_4^{2-}}}-1\right)\right)$ $x_1 = 1-(x_2+x_3)$ $\lambda_3 = -8.10774 + 4.902RH$ $\gamma_3^* = \min(\gamma_3, 0.0154)$ $\lambda_1 = \lambda_2 + 0.97579 - 0.20427 \cdot \max(0, T-291)$ $\lambda_2 = -3.64849 + 9.553 \cdot \min(0, RH-0.46)$ Aqueous particles: $\gamma_1^* = \min(\gamma_1, 0.08585)$ $\gamma_2^* = \min(\gamma_2, 0.053)$ $\gamma_{aq} = \sum_{i=1}^{3} x_i\gamma_i^*$ Dry particles: $\lambda_{dry} = -6.13376 + 3.592RH - 0.19688 \cdot \max(0, T-293)$ $\gamma_{dry}^* = \min(\gamma_{dry}, 0.0124)$ $\gamma_{dry} = (x_1+x_2)\gamma_{dry}^* + x_3 \cdot \min(\gamma_{dry}^*, \gamma_3^*)$ Ice particles: $\gamma_{ice} = 0.02$
B+T (Bertram and Thornton, 2009) Fine and coarse mode	$\gamma(N_2O_5) = Ak'_{2f}\left[1 - \frac{1}{\left(\frac{k_3[H_2O(l)]}{k_{2b}[NO_3^-]}\right)+1+\left(\frac{k_4[Cl^-]}{k_{2b}[NO_3^-]}\right)}\right]$ $A = \frac{4VK_H}{\omega S_a} = 3.2\times10^{-8}\ (s)$ $k'_{2f} = \beta - \beta e^{(-\delta[H_2O(l)])}$ $\beta = 1.15\times10^{6}\ (s^{-1})$ $\delta = 1.3\times10^{-1}\ (M^{-1})$ $\frac{k_3}{k_{2b}} = 6.0\times10^{-2}$, $\frac{k_4}{k_{2b}} = 29.0$

Gaston (Gaston et al., 2014) Fine and coarse mode	$$\gamma(N_2O_5) = \frac{1}{\frac{\omega r_{particle}}{4D_{gas}} + \frac{1}{\alpha_{org}} + \frac{\omega r_{particle}}{4RTH_{org}D_{org}(q_{org}F - 1)}}$$ $$F = \frac{\coth(q_{org}) + h(q_{aq}, q^*_{org})}{1 + \coth(q_{aq})h(q_{aq}, q^*_{org})}$$ $$h(q_{aq}, q^*_{org}) = -\tanh(q^*_{org})\frac{\frac{H_{aq}D_{aq}}{H_{org}D_{org}}(q_{aq}\coth(q_{aq}) - 1) - (q^*_{org}\coth(q^*_{org}) - 1)}{\frac{H_{aq}D_{aq}}{H_{org}D_{org}}(q_{aq}\coth(q_{aq}) - 1) - (q^*_{org}\tanh(q^*_{org}) - 1)}$$ $$q_{org} = r_{particle}\sqrt{\frac{k_{org}}{D_{org}}},\ q^*_{org} = q_{org}\frac{r_{core}}{r_{particle}},\ q_{aq} = r_{core}\sqrt{\frac{k_{aq}}{D_{aq}}}$$ $$r_{core} = r_{particle} - \ell$$ $k_{aq} = k'_{2f}$ see B+T above If $RH \leq 0.3$ and $O{:}C < 0.7$: $D_{org} = 8 \times 10^{-12}$, $k_{org} = 1.23 \times 10^4$, $H_{org} = \frac{0.6H_{aq}D_{aq}}{D_{org}}$ If $RH \leq 0.3$ and $O{:}C \geq 0.7$: $D_{org} = 6 \times 10^{-11}$, $k_{org} = 7 \times 10^4$, $H_{org} = \frac{0.6H_{aq}D_{aq}}{D_{org}}$ If $0.3 < RH \leq 0.7$ and $O{:}C < 0.7$: $D_{org} = 5 \times 10^{-11}$, $k_{org} = 3.5 \times 10^4$, $H_{org} = \frac{0.5H_{aq}D_{aq}}{D_{org}}$ If $0.3 < RH \leq 0.7$ and $O{:}C \geq 0.7$: $D_{org} = 5 \times 10^{-10}$, $k_{org} = 2 \times 10^5$, $H_{org} = \frac{0.3H_{aq}D_{aq}}{D_{org}}$ If $0.7 < RH$ and $O{:}C < 0.7$: $D_{org} = 1 \times 10^{-9}$, $k_{org} = 5.6 \times 10^4$, $H_{org} = \frac{0.8H_{aq}D_{aq}}{D_{org}}$ If $0.7 < RH$ and $O{:}C \geq 0.7$: $D_{org} = 1 \times 10^{-9}$, $k_{org} = 3.2 \times 10^5$, $H_{org} = \frac{1.0H_{aq}D_{aq}}{D_{org}}$
Default Davis fine mode, B+T coarse mode	See Davis and B+T above

Implementation of the parameterizations in Table 1 required modification of the CMAQ source code in the AEROSOL_CHEMISTRY module. Prior to this study, no coarse mode Davis parameterization existed. I added a second Davis parameterization specific to coarse mode particles, which included duplicating the crystalized subroutine for particle mode. For the Gaston parameterization, I added the necessary equations listed in Table 1 to the N2O5_GAMMA function.

The implementation of the Gaston parameterization in this work also required the calculation of two new variables: O:C of the particle organic phase and volume ratio (β). Version 5.4 and later of CMAQ includes the O:C of the entire particle phase mixture, but I used CMAQ v5.3.2. Here, O:C was calculated according to (E1) (Canagaratna et al., 2015) using individual O:C values, the mole fraction of each species (n_i), and the number of carbon atoms in that species (x_i) (Li et al., 2021; Murphy et al., 2017; Pye et al., 2017; Xu et al., 2018). I used the same individual O:C values from CMAQ v5.4 for each organic component in our O:C calculations. The species included are listed in Table A2, along with a more detailed description of the O:C calculation. This calculation was added to the CMAQ model in the AEROSOL_CHEMISTRY module as a function called CALC_OC.

$$O{:}\,C_{mix} = \frac{\sum_i O{:}\,C_i n_i x_i}{\sum_i n_i x_i} \quad (1)$$

To represent the phase-separation of the particle, I calculated organic layer thickness (l) (E2) from the relative volumes of inorganic (V_{inorg}) and organic components (V_{org}) (E3) (Riemer et al., 2009). The volume ratio β of the inorganic particle components relative to the sum of organic and inorganic particle components was added to the AEROSOL_CHEMISTRY module in a new function called CALC_VOLUMES. Of the 110 species currently included in the aerosol species list in CMAQ v5.3.2, I included 91 total species in the calculation of volume ratio (Table A1).

$$l = r_{particle}\left(1 - \beta^{\frac{1}{3}}\right) \quad (2)$$

$$\beta = \frac{V_{inorg}}{V_{inorg} + V_{org}} \quad (3)$$

As particle radius increases, both the denominator and numerator of F (in Table 1) approach zero (Anttila et al., 2006). To avoid this, I set a maximum radius for each range of

volume ratio, aqueous-phase reaction rate, O:C, and RH where F would be 1 above this maximum. Rather than a smooth progression to 1 at all combinations of O:C, RH, k_{aq}, and $r_{particle}$, some F functions perform a step-function to avoid non-physical behavior at large radii. Refer Appendix Text A1, Figure A1, and Table A3 for more detail on the implementation of these limits to the Gaston parameterization in the CMAQ model.

I calculated Gaston $\gamma(N_2O_5)$ for each aero7 aerosol mode in CMAQ: Aitken, accumulation, and coarse. The CMAQ model only uses a coarse mode and a combined fine mode $\gamma(N_2O_5)$. I used modal surface area to weight the individual Aitken and accumulation mode $\gamma(N_2O_5)$ and use the sum of these weighted $\gamma(N_2O_5)$ values to find fine mode Gaston $\gamma(N_2O_5)$.

3.2.2 Yield of $ClNO_2$

The current version of CMAQ has a single parameterization for the yield of $ClNO_2$, which depends only on the water and Cl^- concentration in the particle, as shown in (E4) (Bertram & Thornton, 2009). Staudt, et al. (2019) measured the dependence of $\Phi(ClNO_2)$ on the concentration of sulfate to evaluate the role of spectator ions in suppressing $ClNO_2$ production. Sulfate reduced $\Phi(ClNO_2)$ because of a reaction between SO_4^{2-} and N_2O_5 that catalysed the hydrolysis reaction at the expense of $ClNO_2$ formation. The authors derived a new equation for $\Phi(ClNO_2)$ that included the effects of sulfate (E6), but the reaction rates varied for field versus laboratory measurements. In implementing this new parameterization in the CMAQ model, I used a value of $\frac{k_4}{k_2} = 0.5$ based on the laboratory measurements (E5) (Staudt et al., 2019). Following analysis of $\gamma(N_2O_5)$ parameterizations, I tested the new parameterization of $\Phi(ClNO_2)$ with both the default and Gaston $\gamma(N_2O_5)$ parameterizations as listed in Table 2.

$$\Phi(ClNO_2) = \frac{1}{1 + \frac{[H_2O]}{483[Cl^-]}} \quad (4)$$

$$\Phi(ClNO_2) = \frac{1}{1 + \frac{[H_2O]}{483[Cl^-]} + 0.5\frac{[SO_4^{2-}]}{[Cl^-]}} \quad (5)$$

Table 2: Combinations of $\gamma(N_2O_5)$ and $\Phi(ClNO_2)$ parameterizations tested

Model combination	$\gamma(N_2O_5)$ parameterization	$\Phi(ClNO_2)$ parameterization
Davis-Sarwar	CMAQ default (Davis et al., 2008)	CMAQ default (Sarwar et al., 2012)
Davis-Staudt	CMAQ default (Davis et al., 2008)	(Staudt et al., 2019)
Gaston-Sarwar	(Gaston et al., 2014)	CMAQ default (Sarwar et al., 2012)
Gaston-Staudt	(Gaston et al., 2014)	(Staudt et al., 2019)

3.2.3 Model configuration

I tested the parameterizations and configurations listed in Tables 1 and 2 in CMAQ version 5.3.2 with aero7 aerosol chemistry (Appel et al., 2021), the Carbon Bond 6 chemical mechanism (Emery et al., 2015; Luecken et al., 2019), and in-line photolysis. CMAQ was run with 35 vertical layers with a top of approximately 100 hPa and a 12 km by 12 km horizontal resolution over the contiguous U.S. (396 by 246 grid points). The CMAQ simulations employ lateral boundary conditions from a larger 12 km by 12 km simulation from the EPA Air QUAlity Time Series (EQUATES) project (Foley et al., 2023). CMAQ was run from 21 January 2015 to 12 March 2015 to allow for a 12-day spin-up period. Meteorological inputs came from the Weather Research and Forecasting model (WRF) version 3.8 (Skamarock et al., 2008), configured with analysis nudging of temperature, humidity, and horizontal wind to the North American Regional Reanalysis (Mesinger et al., 2006) per (Harkey et al., 2021; Harkey & Holloway, 2013). Anthropogenic emissions were taken from the 2016 National Emissions Inventory Collaborative,

version 1 (National Emissions Inventory Collaborative, 2019). Fire emissions were taken from the EPA EQUATES dataset (Pouliot et al., 2020). Biogenic emissions were calculated inline using the Biogenic Emission Inventory System (BEIS) version 3.6.1 with the Biogenic Emissions Landuse Database version 5 (Appel et al., 2021).

3.2.4 Comparison with measurements

I compared model results against data collected during the 2015 Wintertime Investigation of Transport, Emission, and Reactivity (WINTER) field campaign (Jaeglé et al., 2018; Schroder et al., 2018). The campaign was based out of NASA Langley in Hampton, VA. Thirteen research flights onboard the National Center for Atmospheric Research (NCAR) C-130 were conducted over the eastern US between 1 February and 15 March 2015. I compared modelled results with cavity ring-down spectroscopy N_2O_5 measurements, chemical ionization mass spectrometry $ClNO_2$ measurements, aerosol mass spectrometry measurements of O:C, and particle nitrate measurements made by Particle Into Liquid Sampler-coupled to Ion Chromatography (Guo et al., 2016; Jaeglé et al., 2018; Lee et al., 2018).

I compared modelled $\gamma(N_2O_5)$ and $\Phi(ClNO_2)$ with box model calculations made using the WINTER data (McDuffie et al., 2018b; McDuffie et al., 2018a). For detailed information on the box model performance and results, refer to sections 2.2 and 3 of (McDuffie et al., 2018b) and sections 2 and 3 of (McDuffie et al., 2018a). Briefly, an iterative box model was used to calculate $\gamma(N_2O_5)$ and $\Phi(ClNO_2)$ from airborne measurements of relevant gas and particle phase species, particle surface area, and actinic flux. There are 2876 $\gamma(N_2O_5)$ values calculated from this box model approach and 3425 $\Phi(ClNO_2)$ values. These box model results are presented in McDuffie et al. (2018a; 2018b), and the data was shared with me by Erin McDuffie.

Model results are aligned with the flight data and box model values at each time, latitude, longitude, and altitude. The resolution of the CMAQ model runs (12 km by 12 km grid, 1 hr output frequency, 35 vertical layers) means that for flight data that are temporally and spatially close together (i.e., within the same grid cell or output hour), the aligned CMAQ values are not unique. Rather than remove instances of non-unique CMAQ $\gamma(N_2O_5)$ from the dataset, I maintain all 2876 $\gamma(N_2O_5)$ and 3425 $\Phi(ClNO_2)$ data points. I used instantaneous values for each hour, which is the calculated value on the hour, rather than the hourly average to better compare with measurements.

3.3 Results

3.3.1 Uptake of N_2O_5 to particles

The CMAQ model contains three particle size modes: Aitken, accumulation, and coarse (Bergin et al., 2022; Binkowski & Roselle, 2003). While three particle modes exist for surface area calculations, the calculation of $\gamma(N_2O_5)$ is combined for the fine mode (Aitken + accumulation). The box model calculations of uptake (McDuffie et al., 2018b) did not include measurements of particles with dry diameters greater than 3 μm. This roughly aligns with the CMAQ accumulation mode (appendix Figure A2). The coarse mode in the CMAQ model runs contributes 7% on average to the total surface area during the WINTER 2015 period. Therefore, for the initial comparison of CMAQ model results to the box model calculations, I focus on the fine mode under the assumption that the small fraction of surface area in the coarse mode will not contribute significantly to heterogeneous chemistry. I evaluate this assumption in section 3.3.5.

The four combinations of modal parameterizations contain only three different fine-mode uptake methods. The default CMAQ case used the Davis parameterization in the fine mode

but B+T for coarse mode, whereas the Davis case uses the Davis parameterization for both fine and coarse modes. The uptake coefficient calculated in the default case in the fine mode is statistically similar to the Davis case as it fails to reject the null hypothesis of the Student's T-test ($t = 0.053, p = 0.96$), though the relationship is not perfectly one-to-one ($slope = 0.999, R^2 = 0.999$). Because of the similarity between the default and Davis parameterizations, I consider only the Davis parameterization further, not the default case.

I compared the three fine-mode $\gamma(N_2O_5)$ outputs with data from the WINTER aircraft campaign. Descriptive statistics and model performance metrics are listed in Table 3. Figure 2 shows the distributions of the flight $\gamma(N_2O_5)$ data and the three CMAQ model outputs. The flight data had a large range in $\gamma(N_2O_5)$ values, spanning four orders of magnitude. None of the model parameterizations were able to replicate this range. The Gaston parameterization tends toward underestimation compared to the flight data. It had the lowest maximum uptake of the three parameterizations ($\gamma(N_2O_5) = 2.00 \times 10^{-2}$), about a factor of 10 smaller than the flight data maximum, as well as the smallest mean. The negative normalized mean bias ($NMB = -87.4\%$) means that the Gaston parameterization tends to underestimate $\gamma(N_2O_5)$. The normalized mean error is the largest of the three parameterizations, though all parameterizations have NME greater than 50%, indicating that, on average, all three parameterizations are not able to capture each individual uptake value accurately.

Table 3: Descriptive statistics of $\gamma(N_2O_5)$ data and model performance metrics

$\gamma(N_2O_5)$	Maximum	Minimum	Mean ($\pm 1\sigma$)	NMB (%)	NME (%)
Flight data	0.175	2.09×10^{-5}	$1.90 \times 10^{-2} (1.82 \times 10^{-2})$		

Gaston	2.00×10^{-2}	3.21×10^{-4}	2.39×10^{-3} (1.86×10^{-3})	-87.4%	88.0%
B+T	3.65×10^{-2}	2.50×10^{-3}	1.86×10^{-2} (8.41×10^{-3})	-1.80%	59.6%
Davis	6.46×10^{-2}	2.47×10^{-3}	2.23×10^{-2} (1.05×10^{-2})	17.4%	63.1%

In comparison to the Gaston parameterization, the Davis and B+T parameterizations were better at modelling the larger $\gamma(N_2O_5)$ values. The Davis parameterization had a positive NMB (17.4%) which indicates that the Davis parameterization is generally biased high compared to field measurements and is the most likely to overestimate $\gamma(N_2O_5)$ of the three parameterizations tested. The B+T parameterization was not able to capture either the maximum or minimum values of $\gamma(N_2O_5)$, but the B+T parameterization demonstrated the smallest bias and error ($NMB = -1.8\%, NME = 59.6\%$), indicating it was the most accurate at modelling $\gamma(N_2O_5)$ during the WINTER flights.

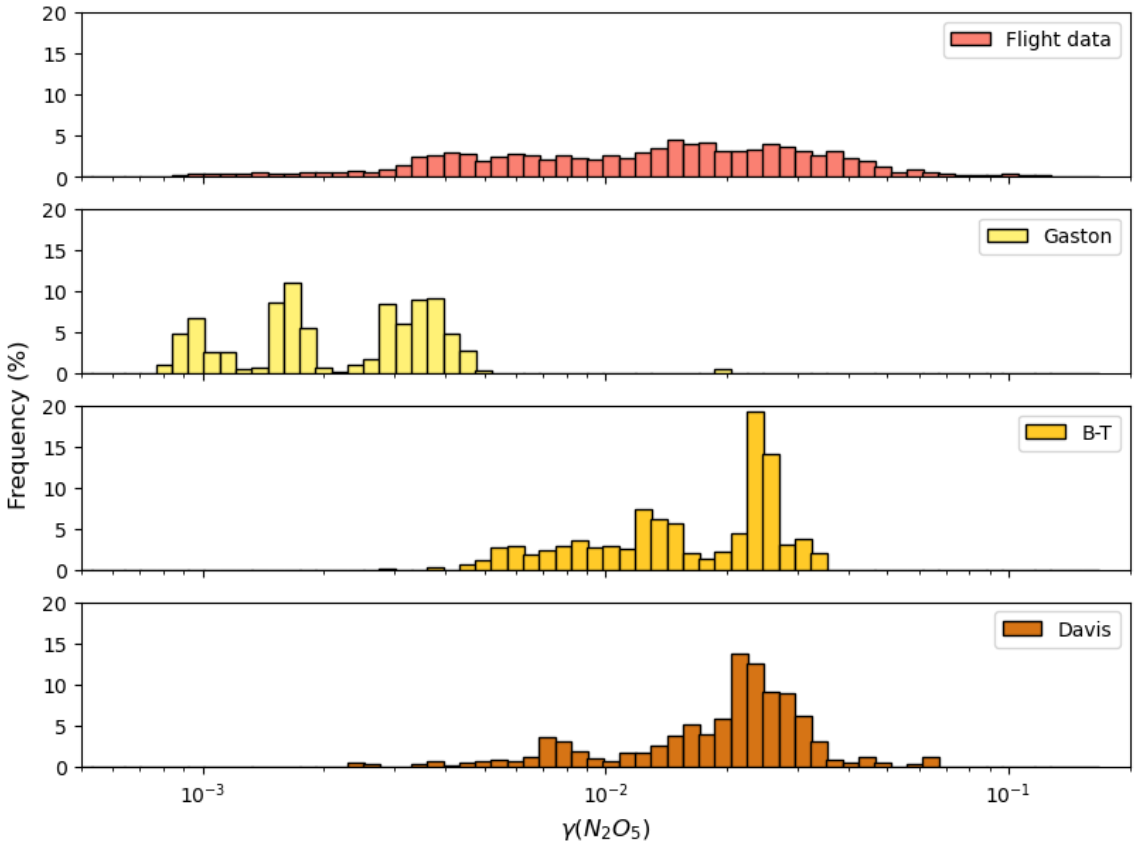

Figure 2. Frequency distributions of flight and CMAQ modeled $\gamma(N_2O_5)$. Histograms show the normalized frequency of occurrence of $\gamma(N_2O_5)$ values. The full range of flight data (minimum

$= 2 \times 10^{-5}$) is excluded to highlight the distribution of the model parameterizations between 10^{-3} and 10^{-1}.

The skill of the B+T parameterization at modelling the WINTER flight data compared to the other two parameterizations can also be seen in Figure 3. The B+T parameterization is the most centered around the 1:1 line, with over 47% of the B+T values within a factor of two greater or less than this 1:1 line (1354 data points). In comparison, 43% of the Davis parameterization is within this ± x2 area (1250 points), and only 4% of the Gaston parameterization falls within the ± x2 area (116 points). All parameterizations predict most data points within the ± x10 area (B+T = 97%, Davis = 95%, and Gaston = 60%). The median point of the B+T data is also closest to the 1:1 line. Both the B+T and Davis parameterizations have median values greater than the 1:1 line in Figure 3, indicating that they tend to overestimate $\gamma(N_2O_5)$ compared to the flight data. The Gaston parameterization has a median well below the 1:1 line, again showing that this parameterization tends to underpredict $\gamma(N_2O_5)$ compared to the flight data.

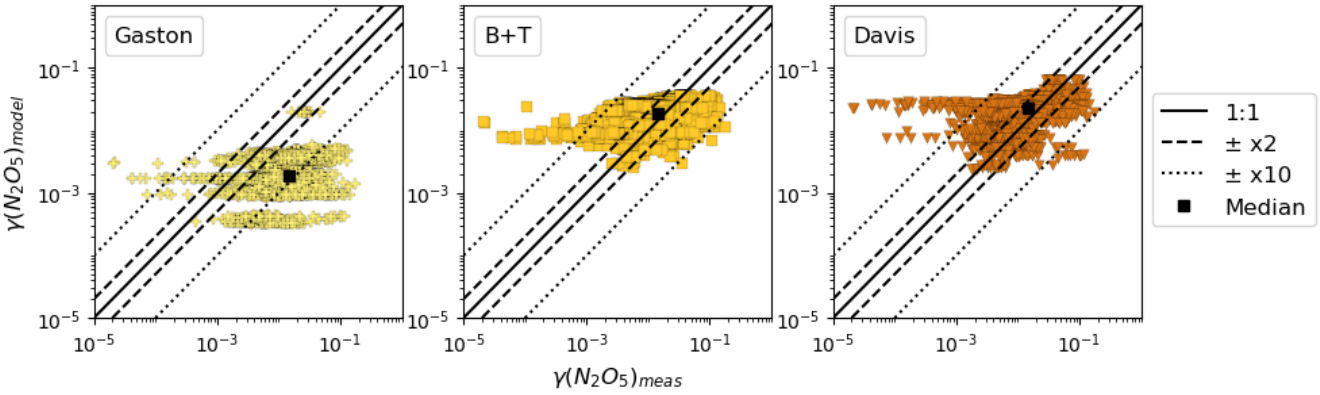

Figure 3. Scatterplots of CMAQ $\gamma(N_2O_5)$ versus the corresponding flight value, aligned within CMAQ grid and timestep. The dashed black line marks where values are a factor of two greater or less than 1:1, and the dotted black line marks where values are a factor of ten greater or less than 1:1. The black squares are the CMAQ median versus flight median. A median point above the 1:1 black line means most of the CMAQ uptake values are greater than the corresponding flight values; a median point below the 1:1 line means most of the CMAQ values are less than the corresponding flight values.

All parameterizations have tails to the left of the -x10 dotted line, which means that all parameterizations overpredicted these values compared to the flight values, though the tails are most apparent in the B+T and Davis parameterizations. These small flight values, most below 10^{-3}, occur during four different research flights (Figure A3), and at different altitude, temperature, relative humidity, particle surface area, and measured N_2O_5 and particle nitrate concentration with no strong correlations to any of these metrics (Table A4).

3.3.2 Evaluation of the model-implemented Gaston uptake parameterization

In this section, I will discuss the factors influencing $\gamma(N_2O_5)$ in the parameterization that may lead to the low bias seen in Figures 2 and 3. I correlated Gaston $\gamma(N_2O_5)$ with relative humidity, temperature, and O:C ratio. In the Gaston parameterization, both relative humidity and O:C impose empirically derived limits to the interactions with the organic coating, and I expected these limits to influence the resulting $\gamma(N_2O_5)$. Temperature has been shown to have an impact on $\gamma(N_2O_5)$ (Hallquist et al., 2003), and in the Gaston parameterization it is used in calculations of the mean molecular speed of gas-phase N_2O_5.

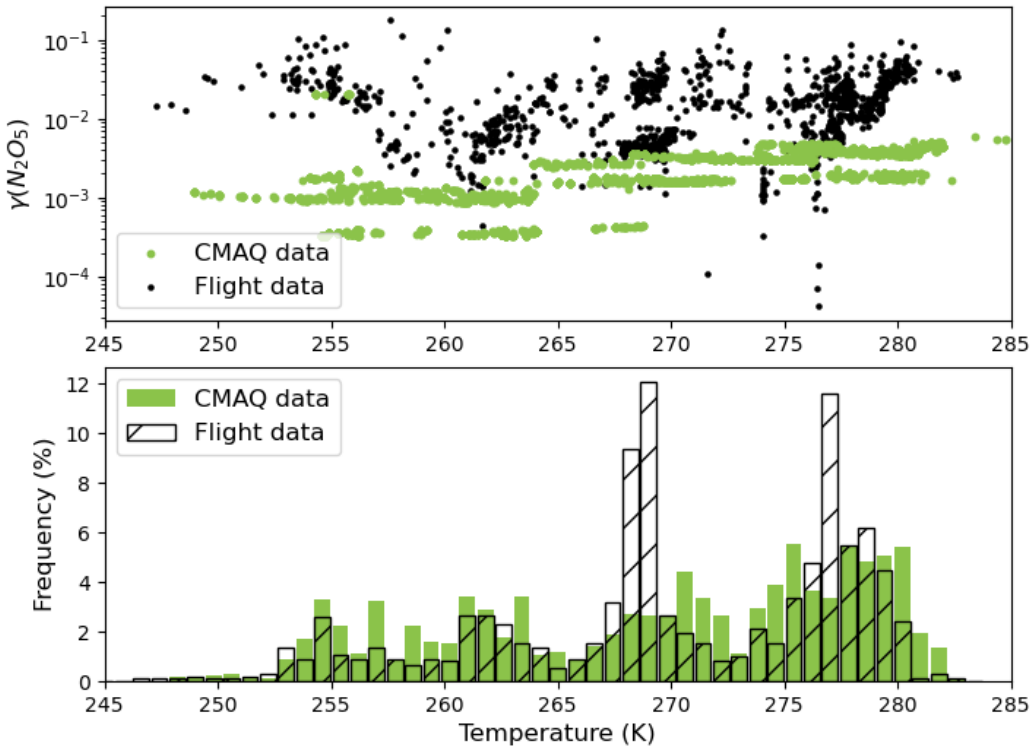

Figure 4. Relationship between modelled temperature and Gaston $\gamma(N_2O_5)$ (top) and frequency of temperature measurements (bottom) during the WINTER 2015 campaign. Results from the CMAQ model are shown in green, field measurements are shown in black. The model $\gamma(N_2O_5)$ does not align with the field data, and neither dataset shows a strong dependence on temperature. The model captures the general trend of temperature measurements.

Figure 4 shows there is a moderate positive dependence of modelled Gaston $\gamma(N_2O_5)$ on modeled temperature in the period studied here ($Slope = 4.6 \times 10^{-4}, R^2 = 0.46, p < 0.05$). Modelled $\gamma(N_2O_5)$ values appear to have 3 modes resulting in the streaky organization of green dots in figure 4 when plotted against temperature, and these modes exist across temperature ranges. This $\gamma(N_2O_5)$ versus temperature relationship shown in green does not match the measured $\gamma(N_2O_5)$ versus temperature relationship shown in black. McDuffie et al. did not find a statistically significant correlation between temperature and box model uptake values ($R^2 = 0.001, p > 0.05$) (McDuffie et al., 2018b). One complicating factor is that modelled temperature

seems to have a smoother distribution across all values compared to measured temperature which shows two distinct peaks in frequency.

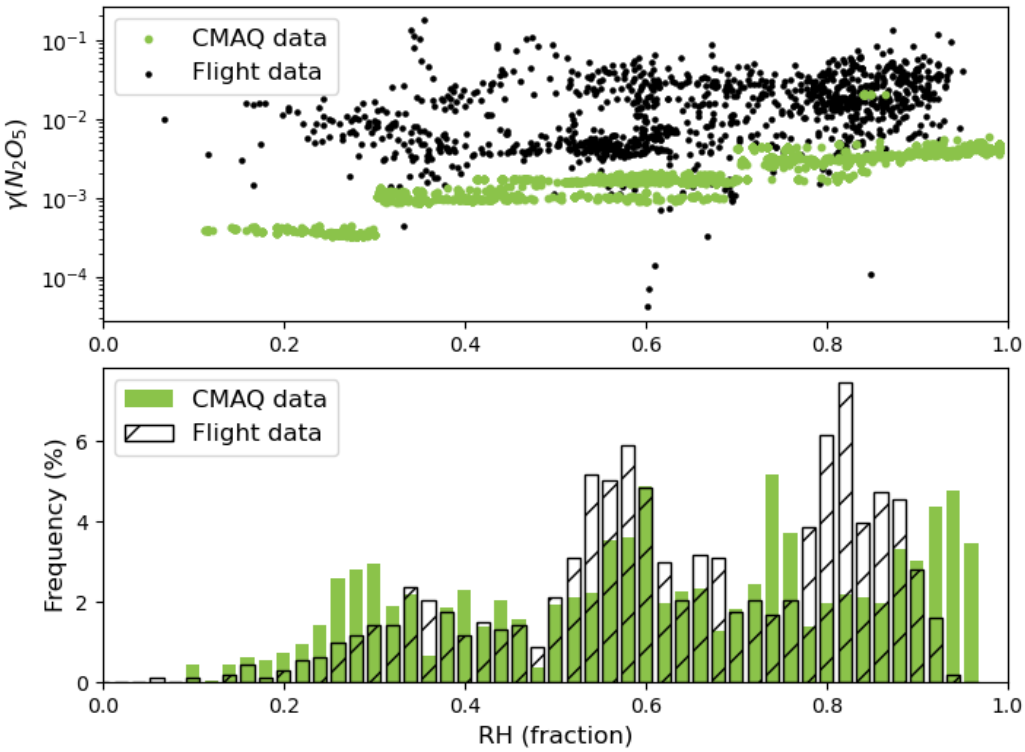

Figure 5. Relationship between relative humidity (RH) and $\gamma(N_2O_5)$ (top) and frequency of RH measurements (bottom) during the WINTER 2015 campaign. Results from the CMAQ model are shown in green, field measurements are shown in black. The model $\gamma(N_2O_5)$ does not align with the field data. Field data shows a general increasing trend with modeled relative humidity but modelled $\gamma(N_2O_5)$ demonstrates a strong, stepwise dependence on RH.

The Gaston parameterization assumes a positive relationship between $\gamma(N_2O_5)$ and RH such that the empirically-derived k_{org}, D_{org}, and H_{org} of the particle organic coating cause uptake to increase with increasing RH in a stepwise function (Gaston et al., 2014). There are three relative humidity ranges in the Gaston parameterization that delineate the possible ranges of $\gamma(N_2O_5)$. Modelled $\gamma(N_2O_5)$ clearly reflects these RH ranges, as seen in Figure 5. At RH less than 0.3, $\gamma(N_2O_5)$ is below 3×10^{-3} because it is limited by k_{org}, D_{org}, and H_{org}. There is then a step up to larger $\gamma(N_2O_5)$ of RH between 0.3 and 0.7, and a final step to the largest values of $\gamma(N_2O_5)$

at RH greater than 0.7. These trends are not seen in the flight data. The correlation strength between modelled uptake and RH is high ($Slope = 2.3 \times 10^{-2}, R^2 = 0.84, p < 0.05$), compared to the weak positive relationship seen in the flight data ($R^2 = 0.075, p < 0.05$) (McDuffie et al., 2018b). The modelled RH does replicate measured RH well, although the model tends to predict more low RH values than high RH values compared to the measurements.

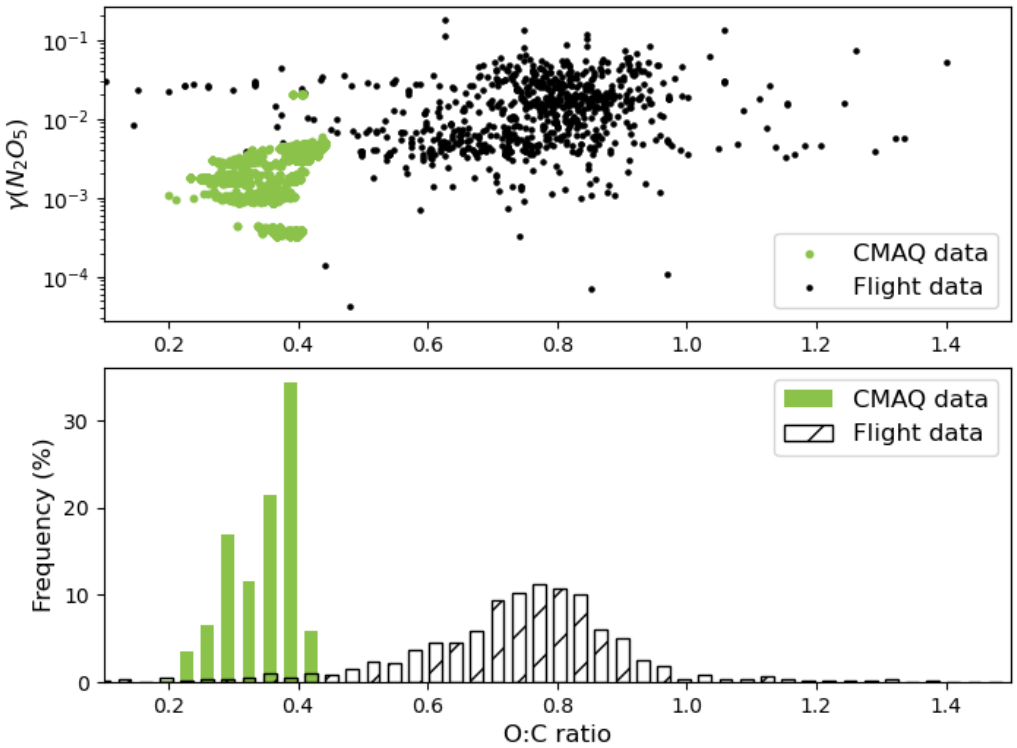

Figure 6. Relationship between O:C and $\gamma(N_2O_5)$ during WINTER 2015 campaign. Results from the CMAQ model are shown in green, field measurements made during the WINTER 2015 field campaign that align with the time and location for each model data point are shown in grey. The model $\gamma(N_2O_5)$ does not align with the field data. Neither dataset shows a clear trend with modelled O:C.

The Gaston parameterization empirically limits $\gamma(N_2O_5)$ based on O:C ratio of the organic fraction of the aerosol particle. This dependence on O:C is meant to represent organic layer composition, as laboratory studies have shown that $\gamma(N_2O_5)$ depends on particle organic composition and phase state (Griffiths et al., 2009; Gross et al., 2009; Thornton & Abbatt, 2005).

Gaston et al. (2014) found that organic mass fraction was a key variable for predicting uptake and that O:C could be used as a reasonably good representation of organic-phase composition. Therefore, the proposed parameterization of organic-phase coatings included two ranges of O:C based on laboratory measurements with a divide at 0.7 (Gaston et al., 2014). Lower values of O:C correspond to lower $\gamma(N_2O_5)$ because the coating is less oxidized, while higher values of O:C correspond to higher $\gamma(N_2O_5)$.

Model O:C is biased low as seen in Figure 6. The cut-off between large O:C and small O:C in the Gaston parameterization occurs at O:C = 0.7, but CMAQ modelled O:C does not go beyond this value. AMS data collected during the WINTER 2015 field campaign for the period of the box model data shows a peak at O:C = 0.8 (black hatched bars) and a range of 0.10 to 1.76. The mean of modelled O:C occurs at O:C = 0.36 with a range of 0.20 – 0.44. These results are consistent with previous attempts to model the O:C during WINTER using the GEOS-Chem model (Schroder et al., 2018). During WINTER, Schroder et al. found that POA was almost half of the total organic aerosol, and that model parameterizations of primary organic aerosol (POA) greatly influenced both total O:C and POA/SOA fractions (Schroder et al., 2018). In our O:C calculations, I included only five low-to-intermediate POA species, representative of vehicle emissions (Murphy et al., 2017). While this does not indicate how much of the total OA mass was POA compared to secondary organic aerosol (SOA), it does imply that there are likely missing POA from other sources such as residential wood burning. In our calculation of O:C, I also excluded the empirically derived pcSOA species, which represents potential combustion emissions in the CMAQ model and was introduced to account for missing SOA mass due to various processes and chamber study limitations (Murphy et al., 2017). This SOA species has an individual O:C of 0.667 in CMAQ v5.4,

so inclusion of pcSOA in our calculations would not increase total O:C beyond the Gaston cut-off of 0.7.

The limits of the CMAQ model to predict the organic phase composition of the aerosol particles is a source of error in our calculations of $\gamma(N_2O_5)$ using the Gaston parameterization. The Gaston uptake has a statistically significant weak positive correlation with O:C ($Slope = 6.5 \times 10^{-2}, R^2 = 0.29, p < 0.05$), similar to the weak positive relationship seen in the flight data ($R^2 = 0.017, p < 0.05$) (McDuffie et al., 2018b). I expect that for larger modelled values of O:C, the uptake coefficient will also be larger. Thus, changing the calculations of O:C to include more wood burning POA may improve the ability of the Gaston parameterization to capture the full range of $\gamma(N_2O_5)$ values.

Overall, the Gaston parameterization is limited by the dependence on RH and O:C that I use here. I use discrete values of the organic phase coefficients k_{org}, D_{org}, and H_{org} that are based on ranges in RH and O:C, rather than calculating these values as a function of the organic phase composition, temperature, and RH. There are limited laboratory studies from which to develop such a function, and the existing ranges that I use here are based on one study (Gaston et al., 2014). I also assumed there was no RH, temperature, or composition dependence to the formation of the organic coating; all organics regardless of particle composition, RH, or temperature were treated as forming an organic film over the aqueous core. Laboratory studies show that there is both an RH and O:C dependence on the liquid-liquid phase separation in particles, where phase separation is less likely at high RH and high O:C (Ohno et al., 2021; Wu et al., 2018; You et al., 2014). In addition, I assumed the organic phase would form a continuous film over the aqueous core and this process would occur at all particle sizes. Both of these

assumptions may not hold for real particles (Kucinski et al., 2019; Qiu & Molinero, 2015). Further research into the RH and compositional dependence of phase-separation and the resulting effects on organic-phase coefficients k_{org}, D_{org}, and H_{org} is needed to improve the ability of the Gaston parameterization to capture the full range of observed $\gamma(N_2O_5)$ values.

3.3.3 Yield of $ClNO_2$ from particles

I tested four combinations of $\Phi(ClNO_2)$ and $\gamma(N_2O_2)$ parameterizations in the CMAQ fine mode (Table 2). I assessed the similarity of the two model $\Phi(ClNO_2)$ results of one $\gamma(N_2O_5)$ parameterization using the Mann-Whitney U test for non-parametric data. I did not remove zero values from the model datasets for similarity comparisons. At a 95% confidence, all parameterization combinations were statistically significantly different ($P < 0.05$). This indicates that the $\gamma(N_2O_5)$ parameterization impacts particle N_2O_5 concentration to the extent that particle-phase reactions in the model are significantly different, and assessment of particle-phase reaction mechanisms should consider which heterogeneous reaction schemes are used.

Table 4 lists the descriptive statistics of $\Phi(ClNO_2)$ for the four parameterization combinations, as well as the performance metrics when compared against the box model $\Phi(ClNO_2)$ values during the WINTER 2015 campaign. I excluded zero values from the model results when calculating the minimum value to facilitate comparison with the flight data minimum. The yield of $ClNO_2$ is a range from 0-1 with a non-Gaussian distribution. Regardless of $\gamma(N_2O_2)$ parameterization used, the bias statistics show that the Sarwar parameterization overestimates $\Phi(ClNO_2)$ (positive NMB) and the Staudt parameterization underestimates $\Phi(ClNO_2)$ (negative NMB). The Staudt parameterization reduces error in $\Phi(ClNO_2)$ prediction compared to the Sarwar parameterization. The normalized mean error is between 77-79% for

both Staudt yield cases compared to close to or greater than 100% NME for the Sarwar yield cases. The Sarwar parameterization predicts larger values of yield while the Staudt parameterization predicts lower average and minimum yield values. The median for the Staudt parameterizations is about half of the flight median, while the median yield with the Sarwar parameterization is more than double the flight median. Thus, both yield parameterizations miss one end of the yield range, either by a tendency towards overprediction (Sarwar) or underprediction (Staudt).

Table 4: Descriptive statistics of $\Phi(ClNO_2)$ data and model performance metrics

	Maximum	Minimum	Median	NMB (%)	NME (%)
Box model flight data	1.00	2.52×10^{-3}	0.14		
Davis-Sarwar	9.71×10^{-1}	4.64×10^{-2}	0.32	39.5%	97.2%
Davis-Staudt	6.94×10^{-1}	1.18×10^{-3}	0.07	-61.7%	79.1%
Gaston-Sarwar	9.82×10^{-1}	4.63×10^{-2}	0.38	78.0%	125.9%
Gaston-Staudt	7.01×10^{-1}	5.90×10^{-4}	0.09	-50.5%	77.6%

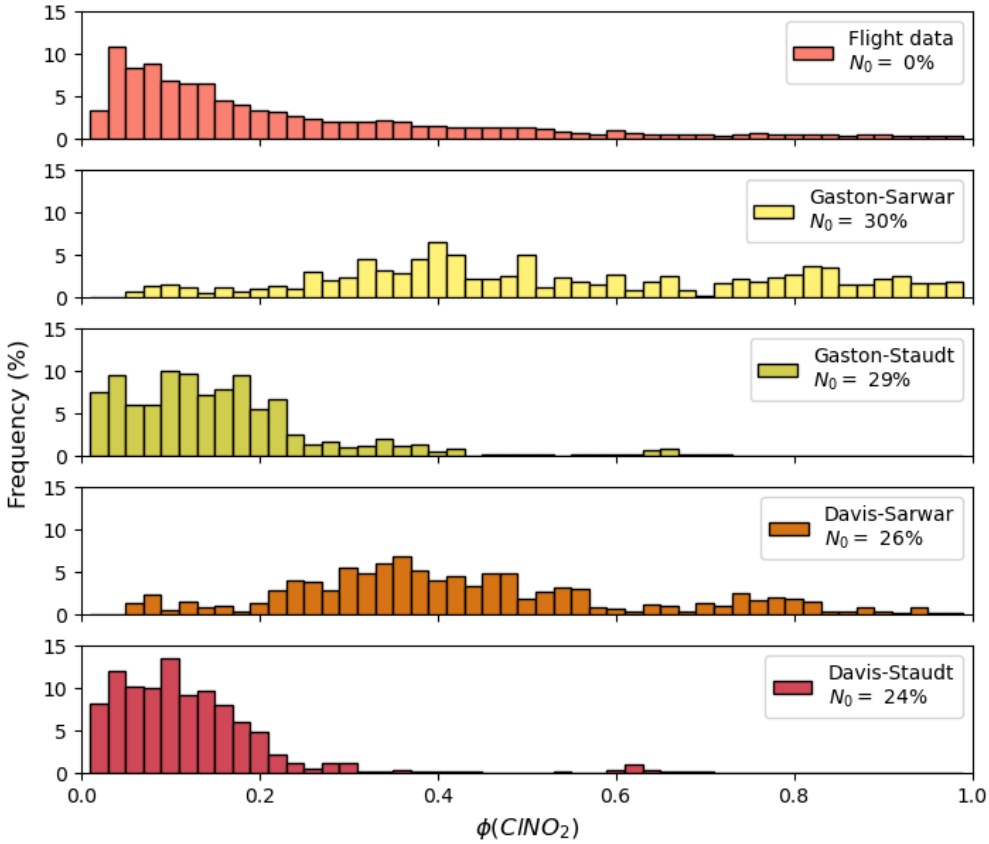

Figure 7. Frequency distribution of $\Phi(ClNO_2)$. The top panel, the box model results of the WINTER flight data, shows a smoothly decreasing frequency of $\Phi(ClNO_2)$ from 0 to 1. To improve the resolution of the frequency distributions, yield values equal to zero were removed from the figures. None of the box model values are equal to zero (N0 = 0%). For each of the model predictions, about 25% of the yield values are equal to zero.

This pattern of over/under prediction can be seen in Figure 7. The frequency of yield values in the flight data decreases from 0 to 1, showing there is a much higher frequency of small $\Phi(ClNO_2)$ compared to large. Both Sarwar yield parameterizations (Gaston-Sarwar in yellow, Davis-Sarwar in brown) have very few small yield values or large yield values. The frequency distribution of the Sarwar parameterization peaks near 0.5 yield. In comparison, the Staudt parameterization predicts small $\Phi(ClNO_2)$ with more frequency than the flight data. The Staudt

parameterization is unable to capture the larger yield values, with a maximum around 0.7 for Staudt yield combinations.

All parameterization combinations predicted $\Phi(ClNO_2) = 0$ in 25-30% of the cases where box model data was available. The number of instances of $\Phi(ClNO_2) = 0$ are listed in the top right corner of each panel in Figure 7. The CMAQ model assumes $\Phi(ClNO_2) = 0$ unless conditions on particle water and chloride content are met: water mixing ratio must be greater than 5×10^{-1} μg/m^3, and chloride mixing ratio must be greater than 1×10^{-4} μg/m^3 and $1 \times 10^{-4} \times [H_2O] \times MW_{Cl}/MW_{H_2O}$. There are several instances of low chloride (<10^{-11} μg/m^3), though most cases of $\Phi(ClNO_2) = 0$ occur when particle water is low (Figure A4). The $\Phi(ClNO_2) = 0$ instances occur throughout the WINTER campaign area.

All parameterization combinations were statistically significantly different from the flight data at 95% confidence when compared using the Mann-Whitney U test for non-parametric data. The inability of the model parameterizations to replicate box model yield values can be seen in Figure 8, where the modelled yield values are plotted against the flight data. The Staudt parameterizations (right column, Gaston in green, Davis in purple) show a clear tendency towards underestimation in the scatterplots. The Sarwar parameterizations (left column, Gaston in yellow, Davis in brown) are more evenly distributed along the yield range in the scatterplots. Box and whiskers show the distribution within bins of flight data. The first three bins in the Staudt parameterization have medians and means close to the 1:1 line, although the whiskers and outliers in the first two bins extend for almost half of the yield range. In comparison, the same bin means and medians in the Sarwar parameterization cases overestimate the flight data with ranges over most of the total yield range. Half of the flight data is within these first three bins,

meaning that the Staudt parameterization performs moderately well about 50% of the time. The Sarwar parameterization does a better job of predicting the larger flight yield values. Instances of zero yield are included at green bars along the x-axis in each panel. Most instances where the model predicts $\Phi(ClNO_2) = 0$ occur at low yield values, but several instances in each parameterization do occur when the box model calculated a large yield and, therefore, potentially higher production of $ClNO_2$.

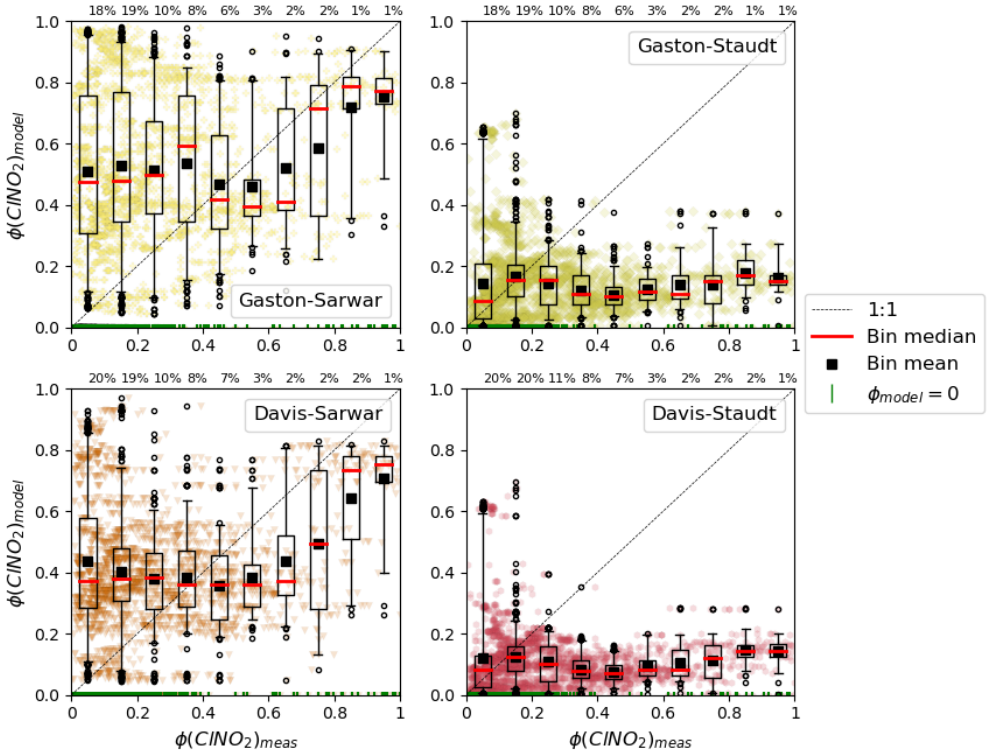

Figure 8. Binned scatterplots of CMAQ modelled yield versus box model yields from WINTER flight data. Boxes contain the interquartile range (25th to 75th percent of data contained within the boxes) for each bin, the whiskers extend to 5-95% of the data. Outliers are denoted by black circles. The solid red line in each box is the bin median, the black square is the bin mean. Top row is the Sarwar parameterization and bottom row is the Staudt parameterization. Modelled $\Phi(ClNO_2) = 0$ values are shown in the figure but are not included in the binned boxplots. The percentage of data points in each bin range is shown above the bin along the upper x-axis, excluding $\Phi(ClNO_2) = 0$ values. All $\Phi(ClNO_2) = 0$ instances are marked with a green line along the x-axis.

3.3.4 Impact of particle chloride concentration on yield

For all four parameterization cases shown in Figure 8, the model is unable to replicate the largest box model yield values. The Sarwar cases are closer to the 1:1 line but still underestimate yield when the box model calculates the largest yield values. Since both parameterizations can only reach larger yield values when particle chloride concentrations are high (E4 and 5), the low bias at the highest box model yield values indicates that the model is underestimating particle chloride. The prevalence of $\Phi(ClNO_2) = 0$ that occur when chloride concentration is too low also may indicate that the model tends to underpredict particle chloride in the fine mode.

I compared chloride concentrations in both the coarse mode and the fine mode to test whether the limitations of the yield parameterizations were affected by modal distributions of particle chloride in the model. Figure 9 shows that there is more chloride in the coarse mode compared to the fine mode for the Gaston-Staudt case, as well as for flight data collected by PILS-IC (Guo et al., 2016). The CMAQ fine and coarse mode distributions of particle chloride are statistically significantly different ($p < 0.05$). The maximum chloride concentration in the coarse mode is 4.7 μg/m^3, though the frequency of these large chloride values is very low. In comparison, the fine mode chloride during the WINTER period is always less than 0.2 μg/m^3, which inhibits formation of $ClNO_2$. The very low chloride content in the fine mode is also consistent with the high frequency of $\Phi(ClNO_2) = 0$ cases. The flight paths during WINTER were over several urban areas and coastal regions. It is possible that flight measurements of particle chloride are high compared to fine mode predictions because of model underestimates in either urban or coastal Cl emissions. During the winter, there is also extensive use of road salt to aid in ice melt. Road

salt may contribute to particle chloride, a chloride source that is currently not included in the CMAQ model (McNamara et al., 2020).

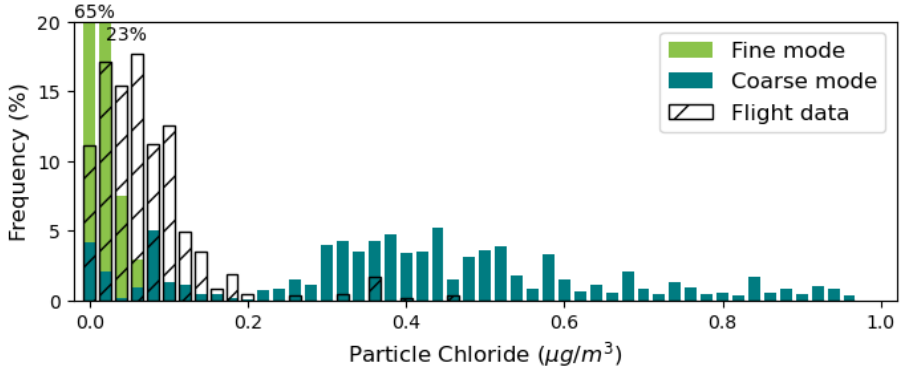

Figure 9. Frequency distribution of particle chloride in the fine mode (green bars) and coarse mode (blue bars) for the Gaston-Staudt parameterization case. Flight data is shown in black hatched bars. The first two fine mode bins extend beyond the y-axis scale and the frequencies are shown over the respective bars.

3.3.5 Comparison of fine and coarse particle modes

The previous analysis of model heterogeneous mechanism performance focused on the fine mode. I chose to assess the fine mode initially because of the preponderance of particle surface area in this mode, on average 93% of the surface area was in the combined Aitken and accumulation modes. Because the loss of N_2O_5 depends on particle surface area as in (E6), I hypothesized that the fine mode would drive heterogenous chemistry and be responsible for most of the loss of N_2O_5 and production of $ClNO_2$. However, coarse mode particle chloride concentration is significantly larger than fine mode, which indicates that fine and coarse mode yield may differ. Here, I test the hypothesis that fine mode drives N_2O_5 loss and $ClNO_2$ production by comparing the fine and coarse mode loss of N_2O_5 ($L(N_2O_5)$) and production of $ClNO_2$ ($P(ClNO_2)$) throughout the WINTER period for the Gaston-Staudt parameterization case.

$$L(N_2O_5)_i = -\frac{d[N_2O_5]}{dt} = k_{het,i}[N_2O_5] = \frac{\gamma(N_2O_5)_i * SA_i * c}{4}[N_2O_5] \quad (6)$$

$$P(ClNO_2)_i = \frac{d[ClNO_2]}{dt} = -L(N_2O_5)_i * \Phi(ClNO_2)_i \quad (7)$$

The loss of gas-phase N_2O_5 depends on k_{het}, which includes the effect of both the particle composition and total available surface area. Therefore, in areas with very low N_2O_5 concentrations I expect to see little loss to the particle phase, but in areas with very high N_2O_5 concentration the loss may still be small because of slow reaction rates limited by the uptake coefficient of small particle surface area. The relationship between $ClNO_2$ concentration and $\Phi(ClNO_2)$ is direct: as $\Phi(ClNO_2)$ increases, so can the production of $ClNO_2$. Within the particle, the production of $ClNO_2$ depends on the available NO_2^+, and therefore N_2O_5 that enters the particle. The production of $ClNO_2$ depends on the loss of N_2O_5 from the gas-phase and the yield of $ClNO_2$ in the particle. In areas with a large model-derived yield, the production of $ClNO_2$ may still be small if there is no particle-phase N_2O_5 available. I calculated $P(ClNO_2)$ according to (E7), where the uptake of N_2O_5 and yield of $ClNO_2$ are mode-specific but concentration of N_2O_5 is the same for both fine and coarse modes.

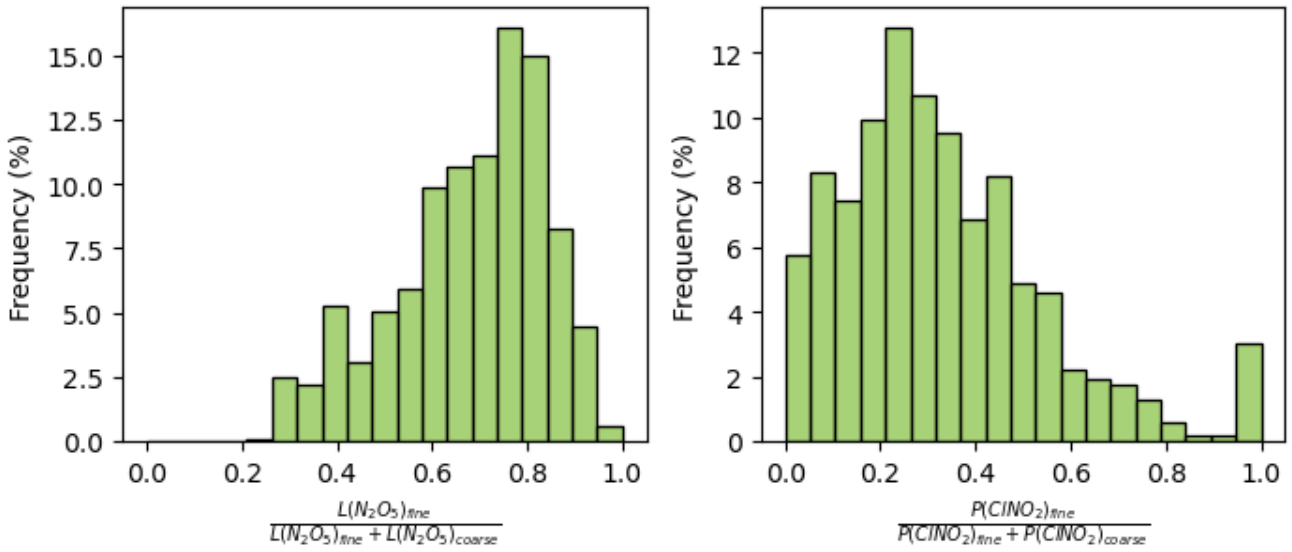

Figure 10. Frequency distributions of the ratio of N_2O_5 loss (left) and $ClNO_2$ production (right) in the fine mode over total loss or production (sum of fine and coarse modes) for the Gaston-Staudt case.

Figure 10 shows the ratio of fine mode $L(N_2O_5)$ and $P(ClNO_2)$ to the total loss and production for the Gaston-Staudt case. The left panel shows that the fine mode tends to contribute more to the loss of N_2O_5 than the coarse mode (higher frequency at larger ratios). Because the same N_2O_5 concentration is used to calculate loss of N_2O_5 for each mode, the difference between fine and coarse mode are a result of the differences in surface area and uptake. The coarse mode surface area is limited to 0-10 μg/m^3 throughout the WINTER period and represents 7% on average of the total surface area while the fine mode makes up most of the model surface area. However, in the Gaston-Staudt case, the average coarse mode uptake ($\bar{\gamma}(N_2O_5) = 0.011$) is almost an order of magnitude larger on average than the fine mode ($\bar{\gamma}(N_2O_5) = 0.0024$), which somewhat compensates for the smaller surface area in the coarse mode.

The larger coarse mode uptake means that the coarse mode has a different composition than the fine mode to the extent that uptake is impacted. Two ways in which particle composition

increase uptake are through the calculation of organic layer thickness and the calculation of O:C in the organic layer, both of which depend on the organic species in the particle. Because uptake is larger in the coarse mode compared to the fine mode, I expect that the coarse mode either has a higher O:C (more oxidized coating allowing for more N_2O_5 to diffuse through) or a thinner organic coating (overall lower concentration of organic-phase species). By increasing O:C in the fine mode, the CMAQ model may be better able to predict larger uptake values and increase the total loss of N_2O_5 to the particle. During the entire WINTER period, the fine mode accounts for 82.8% of the total N_2O_5 loss and the coarse mode accounts for 17.2% of the loss.

The right panel of Figure 10 shows the ratio of $ClNO_2$ production in the fine mode compared to total production of $ClNO_2$. In the case of $P(ClNO_2)$, the peak in frequency occurs around 0.2, meaning that the fine mode is contributing less on average to total production than the coarse mode. This means that for the Gaston-Staudt case, the larger yield in the coarse mode is compensating for the smaller N_2O_5 loss. Even though there is less N_2O_5 entering the coarse mode particles, the higher concentration of particle chloride means the reaction to form $ClNO_2$ is more likely to occur. If more chloride were included in the fine mode, either by increasing emission from existing sources or by considering potentially missing sources (e.g., road salt), fine mode production would likely increase. The coarse mode is responsible for 60.3% of the total $ClNO_2$ production during the WINTER period, while the fine mode accounts for 39.7%. Despite the very small total surface area of the coarse mode, this mode is a large contributor to both the loss of N_2O_5 and production of $ClNO_2$ in the Gaston-Staudt parameterization case and must be considered when comparing concentrations of N_2O_5 and $ClNO_2$ to flight data.

3.4 Impact of heterogeneous chemistry on ambient concentrations

I have shown that both the Gaston parameterization and the Staudt parameterizations reduce $\gamma(N_2O_5)$ and $\Phi(ClNO_2)$ in the fine mode compared to the existing model parameterizations. This implies that the concentration of N_2O_5 should increase and the concentration of $ClNO_2$ should decrease when using these parameterizations compared to the existing model methods. The small coarse mode contribution to the loss of N_2O_5 indicates that the effect on N_2O_5 concentration is less impacted by uptake to coarse mode particles than fine mode. In comparison, the coarse mode contribution to $ClNO_2$ production was large, which means the effect on $ClNO_2$ concentration with the Staudt parameterization may be regulated by the competing effects of small yield in the fine mode but large yield in the coarse mode. In the following sections, I evaluate model performance of N_2O_5 and $ClNO_2$ concentration, as well as particle nitrate.

3.4.1 *N_2O_5 concentration*

Concentration of N_2O_5 during the WINTER campaign was measured by cavity ring-down spectroscopy (CRDS), with an instrument limit of detection of 1 pptv (Dubé et al., 2006). Table 5 lists the descriptive statistics of model N_2O_5 concentration, regardless of whether the corresponding flight values are below LOD = 1 pptv. For calculation of performance statistics, I remove instances of model N_2O_5 concentration where the corresponding flight value is below the LOD. The flight data is compared against the three model uptake parameterization cases listed in Section 3.3.1: Gaston in fine and coarse mode, B+T in fine and coarse mode, and Davis in fine and coarse mode.

Table 5: Descriptive statistics of N_2O_5 concentration and model performance metrics

	Maximum (ppb)	Minimum (ppb)	Mean ($\pm 1\sigma$) (ppb)	RMSE (ppb)	NMB (%)	NME (%)
Flight data	3.35	1×10^{-3}	$2.35 \times 10^{-1}(4.11 \times 10^{-1})$			
Gaston	1.41	9.93×10^{-8}	$1.44 \times 10^{-1}(2.07 \times 10^{-1})$	3.74×10^{-1}	-23.3%	67.0%
B+T	8.41×10^{-1}	9.47×10^{-8}	$6.22 \times 10^{-2}(1.15 \times 10^{-1})$	3.94×10^{-1}	-69.2%	77.2%
Davis	5.36×10^{-1}	9.57×10^{-8}	$4.19 \times 10^{-2}(6.51 \times 10^{-2})$	4.27×10^{-1}	-79.3%	84.0%

The negative NMB for all parameterizations indicates that all three uptake methods underestimate N_2O_5 concentration compared to flight values. This is consistent with the inability of all three parameterizations to capture the smallest $\gamma(N_2O_5)$ values, meaning they tend to assume more loss of gas-phase N_2O_5 to the particle. N_2O_5 concentration calculated using the Gaston uptake parameterization has the least bias and error ($NMB = -23.3\%$ and $NME = 67.0\%$) because the Gaston parameterization tends to predict lower $\gamma(N_2O_5)$ than the other two parameterizations. The Davis parameterization has the largest magnitude of bias ($NMB = -79.3\%$), which is consistent with the tendency towards overprediction of $\gamma(N_2O_5)$. The Davis parameterization also has the largest error, both NME and RMSE, of the three parameterizations tested, indicating that the Davis parameterization is the least accurate at modelling gas-phase N_2O_5 concentration when the parameterization is used for both fine and coarse mode uptake calculations. The Gaston parameterization has the least bias and error and has the largest mean value, closest to the mean of the flight data.

Although all parameterizations tend to underpredict N_2O_5 concentration, Figure 11 shows that the Gaston parameterization is closest to replicating measured N_2O_5 concentration between 0.1 to 1 ppb, where the bulk of the flight data occurs. On average, the model predicts the magnitude of N_2O_5 concentration (black squares in each bin), but the numerous outliers (open

circles) indicate that the individual data points may not capture measured data well. In both the B+T and Davis parameterizations, the interquartile range, median, and mean of data for bins over $5 \times 10^{-2}\ ppb$ are entirely below the 1:1 line. These parameterizations predict higher uptake coefficients, resulting in more loss of N_2O_5 to the particle and less ambient N_2O_5. The Gaston parameterization in comparison has bin means and medians closer to the 1:1 line for higher concentrations of N_2O_5, likely due to the much smaller predicted uptake coefficients. While the B+T parameterization had the best performance for prediction of $\gamma(N_2O_5)$, the Gaston parameterization tends to perform better for predictions of N_2O_5 concentration.

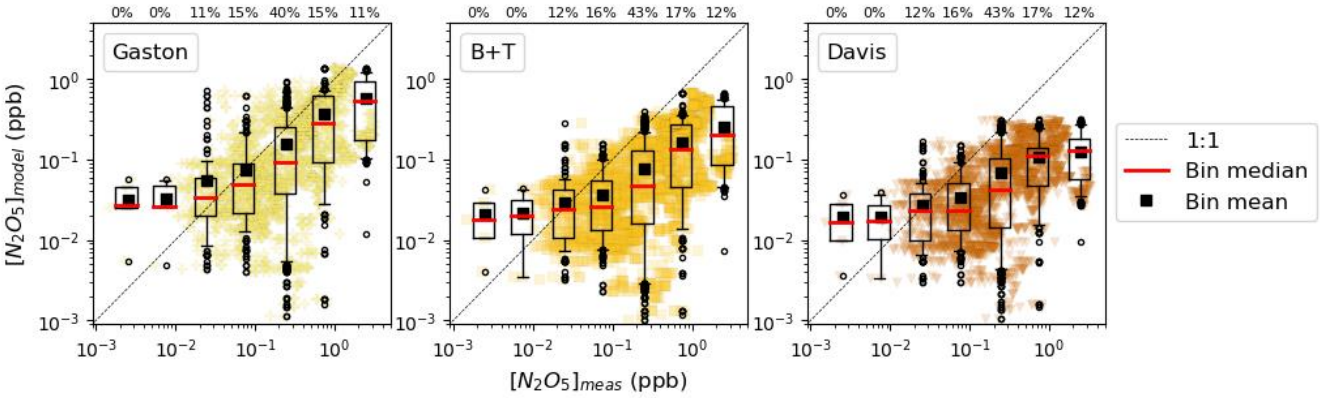

Figure 11. Binned scatterplot of model versus measured N_2O_5 concentration. All measured values below the LOD=1 ppt were removed. Boxes contain the interquartile range (25th to 75th percent of data contained within the boxes) for each bin, the whiskers extend to 5-95% of the data. Outliers are denoted by black circles. The solid red line in each box is the bin median, the black square is the bin mean. The percentage of data points in each bin is shown above the bin along the upper x-axis.

3.4.2 $ClNO_2$ concentration

Flight data of $ClNO_2$ was collected by high-resolution time-of-flight chemical-ionization mass spectrometer (HR-ToF-CIMS) with an instrument detection limit of 1 pptv $ClNO_2$ (Haskins et al., 2018; Lee et al., 2018). Table 6 lists the model descriptive statistcs of $ClNO_2$ concentration, regardless of whether the corresponding flight value is below LOD = 1 pptv. For calculation of

performance metrics, I remove instances of model $ClNO_2$ concentration with a corresponding flight value below the LOD.

Table 6: Descriptive statistics of $ClNO_2$ concentration and model performance metrics

	Maximum (ppb)	Minimum (ppb)	Mean ($\pm 1\sigma$) (ppb)	RMSE (ppb)	NMB (%)	NME (%)
Flight data	2.55	1.00×10^{-3}	1.47×10^{-1} ($\pm 2.70 \times 10^{-1}$)			
Davis-Sarwar	7.14×10^{-1}	2.30×10^{-9}	7.32×10^{-2} ($\pm 1.07 \times 10^{-1}$)	2.37×10^{-1}	-37.9%	76.9%
Davis-Staudt	4.91×10^{-1}	1.12×10^{-9}	3.62×10^{-2} ($\pm 6.05 \times 10^{-2}$)	2.64×10^{-1}	-69.2%	78.4%
Gaston-Sarwar	6.27×10^{-1}	1.29×10^{-9}	5.58×10^{-2} ($\pm 9.59 \times 10^{-2}$)	2.39×10^{-1}	-52.4%	73.8%
Gaston-Staudt	4.43×10^{-1}	5.40×10^{-10}	3.08×10^{-2} ($\pm 5.70 \times 10^{-2}$)	2.64×10^{-1}	-73.7%	79.2%

All combinations of uptake-yield parameterizations predicted $ClNO_2$ concentrations with NME between 73% - 80% when compared to flight data. The Sarwar yield parameterization predicted $ClNO_2$ concentration with smaller magnitude of bias and RMSE than the Staudt yield parameterization. All parameterization combinations underpredicted $ClNO_2$ concentration, indicated by the negative NMB and means smaller than the flight mean. The Gaston-Staudt case had the largest magnitude of underprediction (NMB = -73.7%). The Davis-Sarwar case had the smallest bias (NMB = -37.9%) because the Davis uptake allowed more N_2O_5 to enter the particle.

Binned scatterplots of model $ClNO_2$ concentration versus measured concentration are shown in Figure 12. Instances of $\Phi(ClNO_2) = 0$ are marked with a green star. This highlights that the lowest model predicted $ClNO_2$ concentrations for all cases occur when $\Phi(ClNO_2) = 0$ in the fine mode. This is expected since there is not additional $ClNO_2$ being produced from the particle in that time step. Predicted $ClNO_2$ concentrations when $\Phi(ClNO_2) = 0$ are not always small because ambient concentrations stay appreciable. In addition, coarse mode $\Phi(ClNO_2)$ may not be zero, which contributes to increased $ClNO_2$ production when fine mode production is zero.

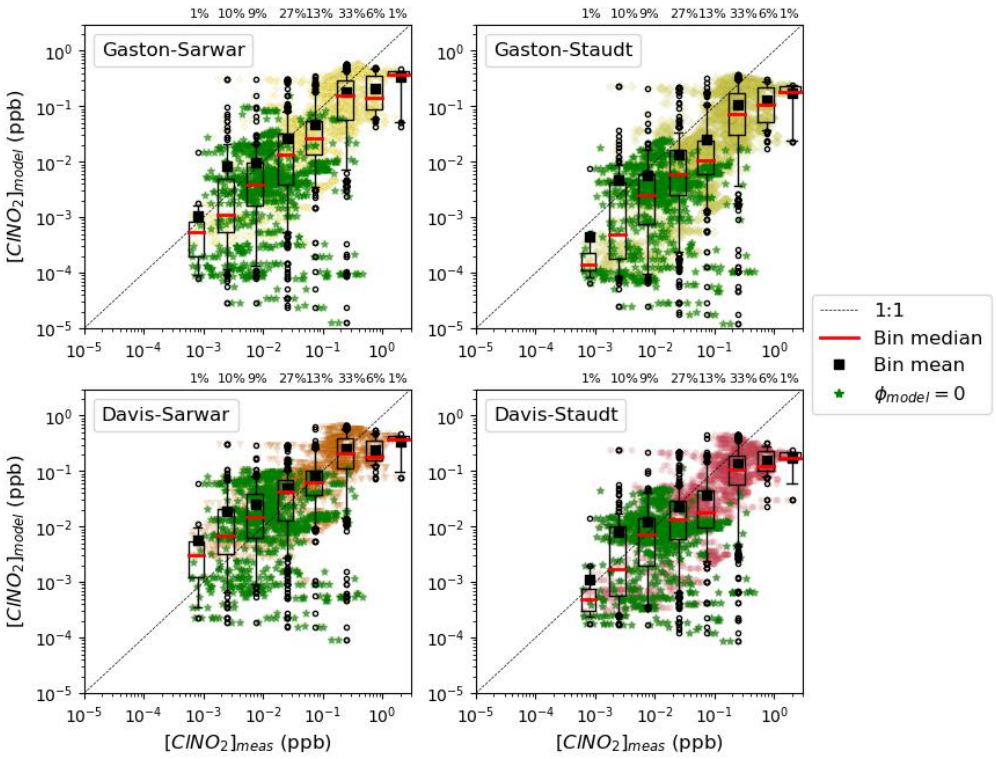

Figure 12. Binned scatterplots of modelled $ClNO_2$ concentration versus flight measurements. Boxes contain the interquartile range (25th to 75th percent of data contained within the boxes) for each bin, the whiskers extend to 5-95% of the data. Outliers are denoted by black circles. The solid red line in each box is the bin median, the black square is the bin mean. Top row is the Sarwar parameterization and bottom row is the Staudt parameterization. Measured $[ClNO_2] < 6 \times 10^{-4}\ ppb$ values (below instrument LOD) are removed. The percentage of data points in each bin range is shown above the bin along the upper x-axis. Green stars in each panel show where a model $ClNO_2$ concentration has a corresponding $\Phi(ClNO_2) = 0$ prediction.

The Gaston cases have smaller minimum $ClNO_2$ concentrations than the Davis cases by a factor of 10. When using the Gaston uptake, regardless of yield parameterization, model predicted $ClNO_2$ is lower. The bin medians for the Gaston cases are lower than the bin medians for the corresponding Davis cases. The Sarwar cases (left column) have bin medians close to the 1:1 line for most data points. The Davis-Sarwar slightly overpredicts at the smallest $ClNO_2$ concentrations. The Staudt cases (right column) consistently underpredict $ClNO_2$. While the

Staudt parameterization captures small yield values well, the significant underprediction in large fine-mode yields means that the Staudt parameterization tends to underpredict $ClNO_2$ concentrations. The Gaston-Staudt case had the most underprediction in $ClNO_2$ concentration and largest NME. Considering that the coarse mode was responsible for 60.3% of total $ClNO_2$ produced during the WINTER period in the Gaston-Staudt case, the underpredictions in $ClNO_2$ concentrations would likely be much greater without the modulating effect of the coarse mode contributions.

3.4.3 Influence on particle nitrate

Both the uptake of N_2O_5 to particles and the yield of $ClNO_2$ from particles affect particle nitrate composition. I can use particle nitrate to assess the overall impact of both heterogeneous mechanisms on model performance. Here, I compare the particle NO_3 concentrations using the four combinations of uptake and yield listed in Table 2. I do not assess the B+T uptake parameterization. I compare all model results against the PILS-IC measured NO_3 mixing ratios. The instrument detection limit is 0.05 $\mu g/m^3$, and measurements were made for particles with a <1 µm diameter during the WINTER campaign (Guo et al., 2016). This size distribution does not easily map on to on the CMAQ modes, so I compared PILS measurements with the combined Aitken + accumulation (fine mode) results. Because the accumulation mode extends beyond 1 µm and more particles are included in the CMAQ results, I expect that the model results will overestimate measurements.

Table 7 lists the performance metrics for each model parameterization case compared against flight data. As expected, the positive NMB shows that the model results are generally higher than the measured values. The distributions and means of both cases with the same

uptake (i.e., both Gaston cases and both Davis cases) are more similar than both cases with the same yield. For example, both Davis cases have maximum concentrations greater than 10 μg/m^3 and means of 8.11 μg/m^3 while both Gaston cases have maxima less than 10 μg/m^3 and means around 7.6 μg/m^3. The Gaston cases have higher normalized mean error ($NME = 92 - 93\%$) but comparable bias to the Davis cases ($NMB = 33 - 34\%$). This means that, on average, the Gaston cases overestimate particle nitrate a similar amount to the Davis cases, but the Gaston cases tend to be less accurate at predicting individual nitrate concentrations. The Davis-Staudt case had the lowest NMB, NME, and RMSE, though it still overpredicted both mean and maximum compared to flight data.

Table 7: Descriptive statistics of particle nitrate and model performance metrics

	Maximum (μg/m^3)	Minimum (μg/m^3)	Mean ($\pm 1\sigma$) (μg/m^3)	RMSE (μg/m^3)	NMB (%)	NME (%)
Flight data	4.86	5.10×10^{-2}	7.64×10^{-1} (7.90×10^{-1})			
Davis-Sarwar	14.6	6.20×10^{-13}	8.11×10^{-1} (1.03)	1.17	34.3%	77.7%
Davis-Staudt	12.8	6.20×10^{-13}	8.11×10^{-1} (1.00)	1.08	33.4%	76.0%
Gaston-Sarwar	9.77	6.20×10^{-13}	7.55×10^{-1} (9.55×10^{-1})	1.20	34.4%	93.4%
Gaston-Staudt	8.81	6.20×10^{-13}	7.60×10^{-1} (9.42×10^{-1})	1.16	34.6%	92.4%

The mixed influence of the four parameterization combinations on particle NO_3 shows how the competing effects of heterogeneous chemistry mechanisms – uptake adding nitrate to the particle and yield removing nitrate from the particle – may be impacting modelled particle nitrate in different ways and at different times or locations throughout the WINTER campaign period. Statistically the Davis cases have the least error, but the Gaston parameterizations predict lower particle NO_3 means and maxima, closer to the flight data. By increasing CMAQ modelled O:C, which would allow for larger uptake values predicted by the Gaston parameterization,

modelled particle nitrate in the fine mode would likely increase, which may result in greater overestimates.

3.5 Conclusions

Atmospheric aerosol particles are chemically complex. The presence of insoluble organic constituents can lead to phase separation of organic and inorganic components. Existing CMAQ parameterizations of $\gamma(N_2O_5)$ do not account for the organic component of particles, resulting in an overestimation of $\gamma(N_2O_5)$. The existing CMAQ parameterization of $\Phi(ClNO_2)$ does not account for reactions that compete with chlorination and hydrolysis of N_2O_5, leading to an overestimation of $\Phi(ClNO_2)$. In this study, I implemented two chemically representative model parameterizations of $\gamma(N_2O_5)$ and $\Phi(ClNO_2)$ in CMAQ and evaluated their performance relative to existing parameterizations.

The added Gaston parameterization for $\gamma(N_2O_5)$ includes the effects of an organic coating on particles which inhibits N_2O_5 uptake. The Gaston parameterization performed best at predicting measured N_2O_5 concentrations. None of the three parameterizations tested were able to capture the full range of box model flight $\gamma(N_2O_5)$ values. The Gaston parameterization tended to predict smaller $\gamma(N_2O_5)$ values and was limited by the parameterization dependence on relative humidity and organic-phase composition. The Gaston parameterization may be improved by removing the stepwise dependence of k_{org}, D_{org}, and H_{org} on RH. More laboratory studies should be conducted to better understand this relationship. The CMAQ model predictions of uptake using the Gaston parameterization may also be improved by including more POA in the calculation of O:C. The Gaston parameterization is also impacted by the treatment of F at large

radii, as discussed in Section 3.2 and A2 of the Appendix. I did not assess the sensitivity of the model parameterization to the radius cut-off values I assigned, so more work should be done to determine how these cut-offs impact model performance.

The Staudt parameterization for $\Phi(ClNO_2)$ includes the catalytic role for sulfate in the hydrolysis of N_2O_5 that effectively limits the chlorination reaction leading to $ClNO_2$ production. Because of the low concentration of chloride predicted in the CMAQ fine mode, I found that the Staudt parameterization tends to underpredict $\Phi(ClNO_2)$. In the fine mode, the existing Sarwar parameterization tends to overpredict $\Phi(ClNO_2)$ compared to flight data and the Staudt yield predicts low $\Phi(ClNO_2)$ values better. The coarse mode Staudt parameterization predicted large yield values because of the higher concentrations of particle chloride in the coarse mode compared to the fine mode. All yield parameterizations produced erroneous $ClNO_2$ concentrations: the Sarwar cases tended to overpredict $ClNO_2$ concentration relative to the flight data and Staudt cases tended to underpredict. Improving model performance of fine mode particle chloride is necessary to address the discrepancies between the model yield and flight-derived values. Because chloride content in the fine mode is so low, the Staudt yield is biased low. If the Staudt yield were to be adjusted up to account for this bias without first adjusting particle chloride, then the yield parameterization would likely overpredict yield in cases where particle chloride is accurate. Future studies should address potential missing sources of particle chloride in the model that may be affecting fine mode predictions.

I found that the coarse mode contributed to total N_2O_5 loss and $ClNO_2$ production, affecting ambient concentrations predicted during the WINTER period. In the Gaston-Staudt case, the small surface area in the coarse mode limited the impact on $L(N_2O_5)$, as the coarse

mode accounted for only 17.2% of total loss. However, the coarse mode was responsible for 60.3% of the total $P(ClNO_2)$ despite contributing very little to the total particle surface area available for reactions. When assessing model performance of heterogeneous NO_x chemistry, it is important to consider how the coarse mode particle composition differs from fine mode.

In all parameterization cases tested, the model overestimated fine mode particle nitrate. Heterogeneous NO_x chemistry has large impacts on particle nitrate, which has large impacts on the effects of human health. Changes to the heterogeneous mechanisms discussed here may improve model predictions of particle nitrate. None of the tested chemistry schemes were able to capture the full range of observed values in uptake, yield, or gas- or particle-phase concentrations. Therefore, when selecting mechanisms for nocturnal heterogeneous chemistry, I recommend that the mechanisms be as representative of the chemistry and physics of the reactions as possible. Both the Gaston and Staudt mechanisms improve the model parameterizations based on our understanding of the processes affecting heterogeneous NO_x. However, I did not evaluate the how these parameterizations affected daytime NO_2 or ozone concentrations, which is a potential next step in model evaluation, and is explored in Chapter 4.

Data Availability

Modified CMAQ code can be found at https://doi.org/10.21231/NVZC-MF25. Data for the WINTER 2015 field campaign can be found at https://data.eol.ucar.edu/project/WINTER. The EPA EQUATES data used in the CMAQ simulations is available at https://doi.org/10.15139/S3/F2KJSK.

References

Alexander, B., Hastings, M. G., Allman, D. J., Dachs, J., Thornton, J. A., & Kunasek, S. A. (2009). Quantifying atmospheric nitrate formation pathways based on a global model of the oxygen isotopic composition (δ17O) of atmospheric nitrate. *Atmospheric Chemistry and Physics*, *9*(14), 5043–5056. https://doi.org/10.5194/ACP-9-5043-2009

Anttila, T., Kiendler-Scharr, A., Tillmann, R., & Mentel, T. F. (2006). On the Reactive Uptake of Gaseous Compounds by Organic-Coated Aqueous Aerosols: Theoretical Analysis and Application to the Heterogeneous Hydrolysis of N2O5. *Journal of Physical Chemistry A*, *110*(35), 10435–10443. https://doi.org/10.1021/JP062403C

Appel, K. W., Bash, J. O., Fahey, K. M., Foley, K. M., Gilliam, R. C., Hogrefe, C., et al. (2021). The Community Multiscale Air Quality (CMAQ) model versions 5.3 and 5.3.1: system updates and evaluation. *Geoscientific Model Development*, *14*(5), 2867–2897. https://doi.org/10.5194/gmd-14-2867-2021

Badger, C. L., Griffiths, P. T., George, I., Abbatt, J. P. D., & Cox, R. A. (2006). Reactive Uptake of N2O5 by Aerosol Particles Containing Mixtures of Humic Acid and Ammonium Sulfate. *Journal of Physical Chemistry A*, *110*(21), 6986–6994. https://doi.org/10.1021/JP0562678

Bauer, S. E., Balkanski, Y., Schulz, M., Hauglustine, D. A., & Dentener, F. (2004). Global modeling of heterogenous chemistry on mineral aerosol surfaces: Influence on tropospheric ozone chemistry and comparison to observations. *Journal of Geophysical Research D: Atmospheres*, *109*(2). https://doi.org/10.1029/2003JD003868

Behnke, W., George, C., Scheer, V., & Zetzsch, C. (1997). Production and decay of ClNO2 from the reaction of gaseous N2O5 with NaCl solution: Bulk and aerosol experiments. *Journal of Geophysical Research Atmospheres*, *102*(3), 3795–3804. https://doi.org/10.1029/96JD03057

Bergin, R. A., Harkey, M., Hoffman, A., Moore, R. H., Anderson, B., Beyersdorf, A., et al. (2022). Observation-based constraints on modeled aerosol surface area: implications for heterogeneous chemistry. *Atmos. Chem. Phys*, *22*, 15449–15468. https://doi.org/10.5194/acp-22-15449-2022

Bertram, T. H., & Thornton, J. A. (2009). Toward a general parameterization of N2O5 reactivity on aqueous particles: the competing effects of particle liquid water, nitrate and chloride. *Atmospheric Chemistry and Physics*, *9*, 8351–8363.

Bertram, T. H., Thornton, J. A., Riedel, T. P., Middlebrook, A. M., Bahreini, R., Bates, T. S., et al. (2009). Direct observations of N2O5 reactivity on ambient aerosol particles. *Geophysical Research Letters*, *36*(L19803), 1–5. https://doi.org/10.1029/2009GL040248

Binkowski, F. S., & Roselle, S. J. (2003). Models-3 Community Multiscale Air Quality (CMAQ) model aerosol component 1. Model description. *Journal of Geophysical Research D: Atmospheres*, *108*(6). https://doi.org/10.1029/2001jd001409

Brown, S. S., Ryerson, T. B., Wollny, A. G., Brock, C. A., Peltier, R., Sullivan, A. P., et al. (2006). Variability in Nocturnal Nitrogen Oxide Processing and Its Role in Regional Air Quality. *Science*, *311*, 76–70.

Brown, S. S., Dubé, W. P., Fuchs, H., Ryerson, T. B., Wollny, A. G., Brock, C. A., et al. (2009). Reactive uptake coefficients for N_2O_5 determined from aircraft measurements during

the Second Texas Air Quality Study: Comparison to current model parameterizations. *Journal of Geophysical Research*, *114*, D00F10. https://doi.org/10.1029/2008JD011679

Byun, D., & Schere, K. L. (2006). Review of the Governing Equations, Computational Algorithms, and Other Components of the Models-3 Community Multiscale Air Quality (CMAQ) Modeling System. *Applied Mechanics Reviews*, *59*(2). https://doi.org/10.1115/1.2128636

Canagaratna, M. R., Jimenez, J. L., Kroll, J. H., Chen, Q., Kessler, S. H., Massoli, P., et al. (2015). Elemental ratio measurements of organic compounds using aerosol mass spectrometry: characterization, improved calibration, and implications. *Atmos. Chem. Phys*, *15*, 253–272. https://doi.org/10.5194/acp-15-253-2015

Chang, W. L., Bhave, P. V., Brown, S. S., Riemer, N., Stutz, J., & Dabdub, D. (2011). Heterogeneous Atmospheric Chemistry, Ambient Measurements, and Model Calculations of N2O5: A Review. *Aerosol Science and Technology*, *45*(6), 665–695. https://doi.org/10.1080/02786826.2010.551672

Chang, W. L., Brown, S. S., Stutz, J., Middlebrook, A. M., Bahreini, R., Wagner, N. L., et al. (2016). Evaluating N2O5 heterogeneous hydrolysis parameterizations for CalNex 2010. *Journal of Geophysical Research: Atmospheres*, *121*(9), 5051–5070. https://doi.org/10.1002/2015JD024737

Davis, J. M., Bhave, P. V., & Foley, K. M. (2008). Parameterization of N2O5 reaction probabilities on the surface of particles containing ammonium, sulfate, and nitrate. *Atmos. Chem. Phys*, *8*, 5295–5311.

Dubé, W. P., Brown, S. S., Osthoff, H. D., Nunley, M. R., Ciciora, S. J., Paris, M. W., et al. (2006). Aircraft instrument for simultaneous, in situ measurement of NO3 and N2O5 via pulsed cavity ring-down spectroscopy. *Rev. Sci. Instrum*, *77*, 34101. https://doi.org/10.1063/1.2176058

Emery, C., Jung, J., Koo, B., & Yarwood, G. (2015). *Improvements to CAMx Snow Cover Treatments and Carbon Bond Chemical Mechanism for Winter Ozone. Final Report*. Salt Lake City, UT: Ramboll Environ. Retrieved from http://www.deq.utah.gov/locations/U/uintahbasin/docs/2014/03Mar

Evans, M. J., & Jacob, D. J. (2005). Impact of new laboratory studies of N2O5 hydrolysis on global model budgets of tropospheric nitrogen oxides, ozone, and OH. *Geophysical Research Letters*, *32*(9), 1–4. https://doi.org/10.1029/2005GL022469

Finlayson-Pitts, B. J., Ezell, M. J., & Pitts Jr., J. N. (1989). Formation of chemically active chlorine compounds by reactions of atmospheric NaCl particles with gaseous N2O5 and ClONO2. *Nature*, *337*, 241–244.

Foley, K. M., Pouliot, G. A., Eyth, A., Aldridge, M. F., Allen, C., Appel, K. W., et al. (2023). 2002–2017 anthropogenic emissions data for air quality modeling over the United States. *Data in Brief*, *47*, 109022. https://doi.org/10.1016/j.dib.2023.109022

Folkers, M. (2001). *Bestimmung der Reaktionswahrscheinlichkeit von N2O5 an troposphärisch relevanten Aerosolen*. Universität su Köln.

Folkers, M., Mentel, Th. F., & Wahner, A. (2003). Influence of an organic coating on the reactivity of aqueous aerosols probed by the heterogeneous hydrolysis of N2O5. *Geophysical Research Letters*, *30*(12), 1644. https://doi.org/10.1029/2003GL017168

Gaston, C. J., Thornton, J. A., & Ng, N. L. (2014). Reactive uptake of N2O5 to internally mixed inorganic and organic particles: The role of organic carbon oxidation state and inferred organic phase separations. *Atmospheric Chemistry and Physics*, *14*(11), 5693–5707. https://doi.org/10.5194/ACP-14-5693-2014

Griffiths, P. T., Badger, C. L., Cox, R. A., Folkers, M., Henk, H. H., & Mentel, T. F. (2009). Reactive uptake of N2O5 by aerosols containing dicarboxylic acids. Effect of particle phase, composition, and nitrate content. *Journal of Physical Chemistry A*, *113*(17), 5082–5090. https://doi.org/10.1021/JP8096814/ASSET/IMAGES/JP-2008-096814_M023.GIF

Gross, S., Iannone, R., Xiao, S., & Bertram, A. K. (2009). Reactive uptake studies of NO3 and N2O5 on alkenoic acid, alkanoate, and polyalcohol substrates to probe nighttime aerosol chemistry. *Physical Chemistry Chemical Physics*, *11*(36), 7792–7803. https://doi.org/10.1039/B904741G

Guo, H., Sullivan, A. P., Campuzano-Jost, P., Schroder, J. C., Lopez-Hilfiker, F. D., Dibb, J. E., et al. (2016). Fine particle pH and the partitioning of nitric acid during winter in the northeastern United States. *Journal of Geophysical Research: Atmospheres*, *121*(17), 10,355-10,376. https://doi.org/10.1002/2016JD025311

Hallquist, M., Stewart, D. J., Stephenson, S. K., & Cox, R. A. (2003). Hydrolysis of N2O5 on sub-micron sulfate aerosols. *Physical Chemistry Chemical Physics*, *5*, 3453–3463. https://doi.org/10.1039/b301827j

Harkey, M., & Holloway, T. (2013). Constrained dynamical downscaling for assessment of climate impacts. *Journal of Geophysical Research Atmospheres*, *118*(5), 2136–2148. https://doi.org/10.1002/jgrd.50223

Harkey, M., Holloway, T., Kim, E. J., Baker, K. R., & Henderson, B. (2021). Satellite Formaldehyde to Support Model Evaluation. *Journal of Geophysical Research: Atmospheres*, *126*(4), e2020JD032881. https://doi.org/10.1029/2020JD032881

Haskins, J. D., Jaeglé, L., Shah, V., Lee, B. H., Lopez-Hilfiker, F. D., Campuzano-Jost, P., et al. (2018). Wintertime Gas-Particle Partitioning and Speciation of Inorganic Chlorine in the Lower Troposphere Over the Northeast United States and Coastal Ocean. *Journal of Geophysical Research: Atmospheres*, *123*(22), 12,897-12,916. https://doi.org/10.1029/2018JD028786

Holmes, C. D., Bertram, T. H., Confer, K. L., Graham, K. A., Ronan, A. C., Wirks, C. K., & Shah, V. (2019). The Role of Clouds in the Tropospheric NOx Cycle: A New Modeling Approach for Cloud Chemistry and Its Global Implications. *Geophysical Research Letters*, *46*(9), 4980–4990. https://doi.org/10.1029/2019GL081990

Hu, J. H., & Abbatt, J. P. D. (1997). Reaction Probabilities for N2O5 Hydrolysis on Sulfuric Acid and Ammonium Sulfate Aerosols at Room Temperature. *Journal of Physical Chemistry A*, *101*(5), 871–878. https://doi.org/10.1021/JP9627436

Jacob, D. J. (2000). Heterogeneous chemistry and tropospheric ozone. *Atmospheric Environment*, *34*, 2131–2159.

Jaeglé, L., Shah, V., Thornton, J. A., Lopez-Hilfiker, F. D., Lee, B. H., McDuffie, E. E., et al. (2018). Nitrogen Oxides Emissions, Chemistry, Deposition, and Export Over the Northeast United States During the WINTER Aircraft Campaign. *Journal of Geophysical Research: Atmospheres*, *123*(21), 12,368-12,393. https://doi.org/10.1029/2018JD029133

Kane, S. M., Caloz, F., & Leu, M.-T. (2001). Heterogeneous Uptake of Gaseous N2O5 by (NH4)2SO4, NH4HSO4, and H2SO4 Aerosols. *Journal of Physical Chemistry A*, *105*, 6465–6470. https://doi.org/10.1021/jp010490x

Kucinski, T. M., Dawson, J. N., & Freedman, M. A. (2019). Size-Dependent Liquid-Liquid Phase Separation in Atmospherically Relevant Complex Systems. *Journal of Physical Chemistry Letters*, *10*(21), 6915–6920. https://doi.org/10.1021/ACS.JPCLETT.9B02532/ASSET/IMAGES/LARGE/JZ9B02532_0004.JPEG

Lee, B. H., Lopez-Hilfiker, F. D., Veres, P. R., McDuffie, E. E., Fibiger, D. L., Sparks, T. L., et al. (2018). Flight Deployment of a High-Resolution Time-of-Flight Chemical Ionization Mass Spectrometer: Observations of Reactive Halogen and Nitrogen Oxide Species. *Journal of Geophysical Research: Atmospheres*, *123*(14), 7670–7686. https://doi.org/10.1029/2017JD028082

Lei, H., & Wang, J. X. L. (2014). Sensitivities of NOx transformation and the effects on surface ozone and nitrate. *Atmospheric Chemistry and Physics*, *14*, 1385–1396. https://doi.org/10.5194/acp-14-1385-2014

Li, Y., Carlton, A. G., & Shiraiwa, M. (2021). Diurnal and Seasonal Variations in the Phase State of Secondary Organic Aerosol Material over the Contiguous US Simulated in CMAQ. *ACS Earth and Space Chemistry*. https://doi.org/10.1021/ACSEARTHSPACECHEM.1C00094

Luecken, D. J., Yarwood, G., & Hutzell, W. T. (2019). Multipollutant modeling of ozone, reactive nitrogen and HAPs across the continental US with CMAQ-CB6. *Atmospheric Environment*, *201*, 62–72. https://doi.org/10.1016/J.ATMOSENV.2018.11.060

MacIntyre, H. L., & Evans, M. J. (2010). Sensitivity of a global model to the uptake of N2O5 by tropospheric aerosol. *Atmospheric Chemistry and Physics*, *10*(15), 7409–7414. https://doi.org/10.5194/ACP-10-7409-2010

McDuffie, E. E., Fibiger, D. L., Dubé, W. P., Lopez Hilfiker, F., Lee, B. H., Jaeglé, L., et al. (2018a). ClNO 2 Yields From Aircraft Measurements During the 2015 WINTER Campaign and Critical Evaluation of the Current Parameterization. *Journal of Geophysical Research: Atmospheres*, *123*(22), 12,994-13,015. https://doi.org/10.1029/2018JD029358

McDuffie, E. E., Fibiger, D. L., Dubé, W. P., Lopez-Hilfiker, F., Lee, B. H., Thornton, J. A., et al. (2018b). Heterogeneous N2O5 Uptake During Winter: Aircraft Measurements During the 2015 WINTER Campaign and Critical Evaluation of Current Parameterizations. *Journal of Geophysical Research: Atmospheres*, *123*(8), 4345–4372. https://doi.org/10.1002/2018JD028336

McNamara, S. M., Kolesar, K. R., Wang, S., Kirpes, R. M., May, N. W., Gunsch, M. J., et al. (2020). Observation of Road Salt Aerosol Driving Inland Wintertime Atmospheric Chlorine Chemistry. *ACS Central Science*, *6*, 684–694. https://doi.org/10.1021/acscentsci.9b00994

Mentel, T. F., Sohn, M., & Wahner, A. (1999). Nitrate effect in the heterogeneous hydrolysis of dinitrogen pentoxide on aqueous aerosols. *Physical Chemistry Chemical Physics*, *1*(24), 5451–5457. https://doi.org/10.1039/a905338g

Mesinger, F., DiMego, G., Kalnay, E., Mitchell, K., Shafran, P. C., Ebisuzaki, W., et al. (2006). North American regional reanalysis. *Bulletin of the American Meteorological Society*, *87*(3), 343–360. https://doi.org/10.1175/BAMS-87-3-343

Mozurkewich, M., & Calvert, J. G. (1988). Reaction probability of N2O5 on aqueous aerosols. *Journal of Geophysical Research: Atmospheres*, *93*(D12), 15889–15896. https://doi.org/10.1029/JD093ID12P15889

Murphy, B. N., Woody, M. C., Jimenez, J. L., Carlton, A. M. G., Hayes, P. L., Liu, S., et al. (2017). Semivolatile POA and parameterized total combustion SOA in CMAQv5.2: Impacts on source strength and partitioning. *Atmospheric Chemistry and Physics*, *17*(18), 11107–11133. https://doi.org/10.5194/ACP-17-11107-2017

National Emissions Inventory Collaborative. (2019). 2016v1 Emissions Modeling Platform. Retrieved from http://views.cira.colostate.edu/wiki/wiki/10202

Nolte, C. G., Appel, K. W., Kelly, J. T., Bhave, P. V., Fahey, K. M., Collett, J. L., et al. (2015). Evaluation of the Community Multiscale Air Quality (CMAQ) model v5.0 against size-resolved measurements of inorganic particle composition across sites in North America. *Geoscientific Model Development*, *8*(9), 2877–2892. https://doi.org/10.5194/gmd-8-2877-2015

Ohno, P. E., Qin, Y., Ye, J., Wang, J., Bertram, A. K., & Martin, S. T. (2021). Fluorescence Aerosol Flow Tube Spectroscopy to Detect Liquid-Liquid Phase Separation. *ACS Earth and Space Chemistry*, *5*(5), 1223–1232. https://doi.org/10.1021/ACSEARTHSPACECHEM.1C00061/ASSET/IMAGES/LARGE/SP1C00061_0005.JPEG

Osthoff, H. D., Roberts, J. M., Ravishankara, A. R., Williams, E. J., Lerner, B. M., Sommariva, R., et al. (2008). High levels of nitryl chloride in the polluted subtropical marine boundary layer. https://doi.org/10.1038/ngeo177

Pouliot, G. A., Foley, K. M., Beidler, J., Vukovich, J., & Baker, K. R. (2020). Multi-Year Reanalysis of EPA's Fire Emissions Inventory. In *19th Annual CMAS Conference*.

Prabhakar, G., Parworth, C. L., Zhang, X., Kim, H., Young, D. E., Beyersdorf, A. J., et al. (2017). Observational assessment of the role of nocturnal residual-layer chemistry in determining daytime surface particulate nitrate concentrations. *Atmospheric Chemistry and Physics*, *17*(23), 14747–14770. https://doi.org/10.5194/ACP-17-14747-2017

Pye, H. O. T., Murphy, B. N., Xu, L., Ng, N. L., Carlton, A. G., Guo, H., et al. (2017). On the implications of aerosol liquid water and phase separation for organic aerosol mass. *Atmos. Chem. Phys*, *17*, 343–369. https://doi.org/10.5194/acp-17-343-2017

Qiu, Y., & Molinero, V. (2015). Morphology of Liquid-Liquid Phase Separated Aerosols. *Journal of the American Chemical Society*, *137*(33), 10642–10651. https://doi.org/10.1021/JACS.5B05579/ASSET/IMAGES/LARGE/JA-2015-05579R_0006.JPEG

Richards, L. W. (1983). Comments on the oxidation of NO2 to nitrate—day and night. *Atmospheric Environment (1967)*, *17*(2), 397–402. https://doi.org/10.1016/0004-6981(83)90057-4

Riemer, N., Vogel, H., Vogel, B., Schell, B., Ackermann, I., Kessler, C., & Hass, H. (2003). Impact of the heterogeneous hydrolysis of N2O5 on chemistry and nitrate aerosol formation in the lower troposphere under photosmog conditions. *Journal of Geophysical Research: Atmospheres*, *108*(4), 1–21. https://doi.org/10.1029/2002jd002436

Riemer, N., Vogel, H., Vogel, B., Anttila, T., Kiendler-Scharr, A., & Mentel, T. F. (2009). Relative importance of organic coatings for the heterogeneous hydrolysis of N2O5 during

summer in Europe. *Journal of Geophysical Research: Atmospheres*, *114*(D17), 17307. https://doi.org/10.1029/2008JD011369

Roberts, J. M., Osthoff, H. D., Brown, S. S., Ravishankara, A. R., Coffman, D., Quinn, P., & Bates, T. (2009). Laboratory studies of products of N2O5 uptake on Cl− containing substrates. *Geophysical Research Letters*, *36*(20), 20808. https://doi.org/10.1029/2009GL040448

Ryder, O. S., Ault, A. P., Cahill, J. F., Guasco, T. L., Riedel, T. P., Cuadra-Rodriguez, L. A., et al. (2014). On the Role of Particle Inorganic Mixing State in the Reactive Uptake of N_2O_5 to Ambient Aerosol Particles. *Environmental Science & Technology*, *48*(3), 1618–1627. https://doi.org/10.1021/es4042622

Sarwar, G., Simon, H., Bhave, P., & Yarwood, G. (2012). Examining the impact of heterogeneous nitryl chloride production on air quality across the United States. *Atmos. Chem. Phys*, *12*, 6455–6473. https://doi.org/10.5194/acp-12-6455-2012

Schroder, J. C., Campuzano-Jost, P., Day, D. A., Shah, V., Larson, K., Sommers, J. M., et al. (2018). Sources and Secondary Production of Organic Aerosols in the Northeastern United States during WINTER. *Journal of Geophysical Research: Atmospheres*, *123*(14), 7771–7796. https://doi.org/10.1029/2018JD028475

Skamarock, W. C., Klemp, J. B., Dudhia, J., Gill, D. O., Barker, D. M., Duda, M. G., et al. (2008). *A Description of the Advanced Research WRF Version 3*.

Spicer, C. W. (1983). Smog Chamber Studies of NOx Transformation Rate and Nitrate/Precursor Relationships. *Environmental Science and Technology*, *17*(2), 112–120.

Staudt, S., Gord, J. R., Karimova, N. V., Mcduffie, E. E., Brown, S. S., Gerber, R. B., et al. (2019). Sulfate and Carboxylate Suppress the Formation of ClNO2 at Atmospheric Interfaces. *ACS Earth Space Chem*, *3*(9). https://doi.org/10.1021/acsearthspacechem.9b00177

Thornton, J. A., & Abbatt, J. P. D. D. (2005). N2O5 reaction on submicron sea salt aerosol: Kinetics, products, and the effect of surface active organics. *Journal of Physical Chemistry A*, *109*(44), 10004–10012.

Thornton, J. A., Braban, C. F., & Abbatt, J. P. D. (2003). N2O5 hydrolysis on sub-micron organic aerosols: the effect of relative humidity, particle phase, and particle size. *Physical Chemistry Chemical Physics*, *5*, 4593–4603. https://doi.org/10.1039/b307498f

Thornton, J. A., Kercher, J. P., Riedel, T. P., Wagner, N. L., Cozic, J., Holloway, J. S., et al. (2010). A large atomic chlorine source inferred from mid-continental reactive nitrogen chemistry. *Nature*, *464*, 271–274. https://doi.org/10.1038/nature08905

Wang, Z., Wang, W., Tham, Y. J., Li, Q., Wang, H., Wen, L., et al. (2017). Fast heterogeneous N2O5 uptake and ClNO2 production in power plant and industrial plumes observed in the nocturnal residual layer over the North China Plain. *Atmospheric Chemistry and Physics*, *17*, 12361–12378. https://doi.org/10.5194/acp-17-12361-2017

Wu, F. M., Wang, X. W., Jing, B., Zhang, Y. H., & Ge, M. F. (2018). Liquid-liquid phase separation in internally mixed magnesium sulfate/glutaric acid particles. *Atmospheric Environment*, *178*, 286–292. https://doi.org/10.1016/J.ATMOSENV.2018.02.012

Xu, L., Pye, H. O. T., He, J., Chen, Y., Murphy, B. N., & Ng, N. L. (2018). Experimental and model estimates of the contributions from biogenic monoterpenes and sesquiterpenes to secondary organic aerosol in the southeastern United States. *Atmospheric Chemistry and Physics*, *18*(17), 12613–12637. https://doi.org/10.5194/ACP-18-12613-2018

You, Y., Smith, M. L., Song, M., Martin, S. T., & Bertram, A. K. (2014). Liquid–liquid phase separation in atmospherically relevant particles consisting of organic species and inorganic salts. *International Reviews in Physical Chemistry*, *33*(1), 43–77. https://doi.org/10.1080/0144235X.2014.890786

Chapter 4 Investigating the role of nocturnal chemistry on daytime NO_x air quality

Highlights

- On average, NO_3 reactions dominate nocturnal NO_x loss in the summer, but dominant wintertime nocturnal NO_x loss pathway varies by location across the US.
- Daytime reactions account for 84% of total NO_x loss in July and 78% of total loss in January.
- Modeling N_2O_5 uptake on uncoated particles more than doubles nocturnal NO_x loss compared to modeling uptake on particles with organic coatings.
- The impact of different model representations of heterogeneous chemistry has a greater impact on daytime NO_2 concentration in the winter than the summer.

Abstract

Nocturnal loss pathways of NO_x reservoir species impact daytime concentrations of NO_2. It is important to understand the role of nocturnal loss pathways, such as N_2O_5 uptake and NO_3 reactions, in local air quality. However, there is spatial and seasonal variability in dominant nocturnal NO_x loss pathway across the United States. Here, I use the EPA Community Multiscale Air Quality (CMAQ) model to calculate the contribution of different loss pathways to the NO_x budget. Reactions of NO_3 with biogenic and anthropogenic volatile organic compounds (VOCs) are the dominant nocturnal loss mechanism in the summer, but the dominant nocturnal loss pathway varies by location in winter. Local meteorological conditions such as planetary boundary

layer height, wind speed, and temperature are moderate predictors of the variability in nocturnal loss. Daytime loss pathways account for 84% of total NO_x loss on average in July and 78% of total loss in January, which highlights how most NO_x loss occurs during the day rather than at night. By changing the model representation of heterogeneous chemistry to remove organic coatings from particles, N_2O_5 uptake became the dominant nocturnal loss pathway in January, and this resulted in a 7.3% decrease in early morning NO_2 concentration.

4.1 Introduction

Nitrogen oxides ($NO_x \equiv NO + NO_2$) play a central role in atmospheric chemistry and affect the production of secondary pollutants like ozone (O_3) and particulate matter (PM) (Jacob et al., 1996; Pandis et al., 1992). It is therefore important to understand NO_x chemistry and its various production and loss pathways. However, complex nocturnal chemistry makes quantifying the NO_x budget and its spatial distribution difficult (Brown et al., 2004; Schultz et al., 2000; Stroud et al., 2003).

At night, the absence of sunlight allows reservoir species of NO_2 to build up (Brown et al., 2006; Platt et al., 1984; Wu et al., 1973). These species include nitrate radical (NO_3), dinitrogen pentoxide (N_2O_5), and nitryl chloride ($ClNO_2$) (Wayne et al., 1991). The reaction of NO_3 with VOCs results in a variety of products that may act as a sink for NO_x (e.g., HNO_3) or regenerate NO_2 (Atkinson, 1991; Ng et al., 2017). Alternatively, NO_3 can react with NO_2 to form N_2O_5, which in turn may enter into the particle phase (Mozurkewich & Calvert, 1988; Wayne et al., 1991). Within the particle phase, N_2O_5 reacts with particle-phase species such as water or chloride to form HNO_3 and $ClNO_2$, among other products (Bertram & Thornton, 2009; Finlayson-Pitts et al., 1989).

At sunrise, NO_3, N_2O_5, and $ClNO_2$ photo-dissociate to form NO_2, thus the nocturnal reaction pathways influence the NO_x budget (Wayne et al., 1991). If the loss of NO_3 and N_2O_5 are low at night, and yield of $ClNO_2$ is large, then these species will rapidly decompose to NO_2 when the sun rises, contributing to an elevated concentration of NO_x during the morning. Alternatively, if loss of NO_3 through gas-phase reactions or the loss of N_2O_5 through heterogeneous uptake are high, then early morning NO_x concentrations may be lower (Brown et al., 2004; Edwards et al., 2017).

The impact of nocturnal loss on the NO_x budget shows variability spatially and seasonally. Numerous field studies have compared nocturnal NO_x loss pathways for summer and winter seasons (Table 1). More than half of studies listed in Table 1 (56%) found that N_2O_5 uptake dominates nocturnal NO_x loss, and that N_2O_5 uptake can dominate loss in both summer and winter. Of cases where NO_3 loss pathways dominate, 79% occurred during the summer. NO_3 + VOC reactions proceed more through biogenic than anthropogenic VOC (Warneke et al., 2004), contributing to the prevalence of NO_3 loss during the summer when biogenic emissions are high (Sindelarova et al., 2014). In some locations, N_2O_5 uptake and NO_3 + VOC loss are roughly equal on average, but variability occurs in specific air masses. For example, field campaigns in coastal New England during the summer found that total NO_x loss at night is due to NO_3 + VOC reactions and N_2O_5 uptake in about equal amounts (Aldener et al., 2006; Ambrose et al., 2007), but air masses with high NO_2 concentrations favor more N_2O_5 uptake while air masses with high biogenic VOC concentrations drive more NO_3 loss (Brown et al., 2007). When considering more polluted continental air masses in the northeastern US, N_2O_5 loss is influenced by particle composition, specifically by sulfate content (Brown et al., 2006). The season of measurement can impact the dominant loss pathway by affecting prevailing wind direction and therefore the transport of

pollutants. For example, in Weybourne, United Kingdom, influx of marine air during the summer led to the NO_x loss being dominated by NO_3 + marine VOC reactions, but wintertime continental air masses were more polluted so N_2O_5 loss pathways dominated (Allan et al., 1999).

Table 1. Seasonal distribution of dominant nocturnal NO_x loss pathways

Reference	Dominant loss pathway*	Location
Summer		
Geyer et al 2001	NO_3 + monoterpenes	Lindenberg, Germany
Allan et al 1999	NO_3 + marine VOC	Weyborne, UK
Aldener et al 2006	Equal N_2O_5 and NO_3	New England coast
Ambrose et al 2007	Equal N_2O_5 and NO_3	Appledore Island, Maine
Brown et al 2004	NO_3 + biogenic VOC	New England coast
Brown et al 2006 (both)	N_2O_5 uptake	Pennsylvania and Ohio
Brown et al 2006 (both)	NO_3 + biogenic VOC	New York
Brown et al 2007 (JGR)	NO_3 + biogenic VOC	New England coast
Tsai et al 2014	N_2O_5 uptake	Los Angeles Basin, California
Wang et al 2005	NO_3 loss	Phoenix, Arizona
McLaren et al 2004	N_2O_5 uptake	Lower Fraser Valley, British Columbia
Zaveri et al 2010	NO_3 loss	Boston, Massachusetts
Stutz et al 2004	N_2O_5 uptake	Houston, Texas
Stutz et al 2010	NO_3 + VOC	Houston, Texas
Wang et al 2017	N_2O_5 uptake	Mt. Tai, Shandong, China
Brown et al 2011	NO_3 + anthropogenic VOC	Houston, Texas
Edwards et al 2017	NO_3 + biogenic VOC	Southeast United States
Vicars et al 2013	N_2O_5 uptake	Coastal Los Angeles
Wang et al 2018	N_2O_5 uptake	Beijing, China
Masumoto et al 2006	NO_3 + marine VOC	Izu-Oshima Island, Japan
Fall		
Brown et al 2007 (ACP)	NO_3 loss and deposition	Boulder, Colorado
Brown et al 2009	NO_3 + VOC	Houston, Texas
Martinez et al 2000	N_2O_5 uptake	Helgoland, Germany
Winter		
Geyer et al 2001	N_2O_5 uptake	Lindenberg, Germany
Allan et al 1999	N_2O_5 loss	Weyborne, UK
Apodaca et al 2008	N_2O_5 uptake to ice	Fairbanks, Alaska
Jaeglé et al 2018	N_2O_5 uptake	United States northeast coast
Fibiger et al 2018	NO_3 loss	Putnam County, Georgia
Wagner et al 2013	N_2O_5 uptake	Boulder, Colorado
Kenagy et al 2018	N_2O_5 uptake	United States northeast coast
McDuffie et al 2019	N_2O_5 uptake	Salt Lake valley, Utah
Brown et al 2016	N_2O_5 uptake	Hong Kong

Spring		
Crowley et al 2010	NO_3 + biogenic VOC	Taunus Observatory, Germany
Year-round		
Stone et al 2014	N_2O_5 uptake	Southern United Kingdom
Vrekoussis et al 2007	N_2O_5 uptake	Crete, Greece
Heintz et al 1996	N_2O_5 loss	Rügen, German

* Dominant loss pathway as reported in each publication. Green indicates NO_3 loss dominates, blue indicates N_2O_5 loss dominates, yellow means the authors reported the two pathways were roughly equal on average.

The spatial and seasonal distribution of nocturnal NO_x loss depends on a variety of factors including temperature, ambient VOC concentrations and speciation, relative humidity, particle number and surface area concentrations, and nocturnal boundary layer physics (Allan et al., 1999; Ambrose et al., 2007; Brown et al., 2006; Brown et al., 2007; Fibiger et al., 2018; Vrekoussis et al., 2007; Wang et al., 2006). The large heterogeneity in these conditions can make it difficult to extrapolate dominant nocturnal NO_x loss pathways from existing site-specific field studies. Models can be used to evaluate the impact of nocturnal loss on the NO_x budget over larger areas. For example, Alexander et al (2009) used the GEOS-Chem global model at 1˚ spatial and 6 hr temporal resolution to assess nitrate formation pathways and found that NO_2 + OH was the dominant formation pathway, followed by N_2O_5 hydrolysis (N_2O_5 + H_2O), and NO_3 + VOC contributed 4% to HNO_3 formation. However, this analysis included both daytime and nighttime reactions, which contributed to the dominance of NO_2 + OH reactions over other HNO_3 formation pathways. In addition, not all NO_x loss pathways contribute to HNO_3 formation, thus N_2O_5 uptake to particles and NO_3 + VOC reactions that did not result in HNO_3 were not considered (Alexander et al., 2009). Liang et al (1998) used a chemical transport model with 4˚ x 5˚ resolution to evaluate seasonal changes of dominant loss processes over the US. On average, NO_3 + BVOC pathways dominated in the summer and N_2O_5 uptake dominated in the winter (Liang et al., 1998). However,

as field studies have shown, there is heterogeneity in the dominant loss pathways during each season, which is not captured when using coarse model resolution.

Here, I use the EPA Community Multiscale Air Quality (CMAQ) model to improve our understanding of nocturnal NO_x loss across the contiguous United States. I examine nocturnal NO_x loss pathways during January and July of 2019 to explore the spatial and seasonal variability of nocturnal chemistry. Rather than assume one model parameterization of N_2O_5 heterogeneous chemistry is correct, I compare two model schemes to evaluate the relative importance of chemistry, meteorology, or emissions on daytime NO_2 concentrations.

4.2 Methods

4.2.1 Model configuration

I used CMAQ version 5.3.2 with aero7 aerosol chemistry (Appel et al., 2021), the Carbon Bond 6 chemical mechanism (Emery et al., 2015; Luecken et al., 2019), and in-line photolysis. CMAQ was run with 35 vertical layers with a top of approximately 100 hPa and a 12 km by 12 km horizontal resolution over the contiguous U.S. on the 12US1 domain (299 by 459 grid points) from the EPA Air QUAlity Time Series (EQUATES) project (Foley et al., 2023). I ran the model during two separate time periods: January 2019 and July 2019, each with a 10 day spin up period. According to the NOAA Annual Climate report for 2019, this year was anomalously wet in the upper Midwest region, and that there were temperature extremes in both January and July, indicating that these months may not be representative of average climatology (https://www.ncei.noaa.gov/access/monitoring/monthly-report/national/201913).

Meteorology, anthropogenic emissions, and fire emissions were from the EPA EQUATES project

data warehouse (US EPA, 2021). Biogenic emissions were calculated inline using the Biogenic Emission Inventory System (BEIS) version 3.6.1 with the Biogenic Emissions Landuse Database version 5 and seasonal switching between winter (January) and summer (July) conditions (Appel et al., 2021).

I ran the model a total of four times, twice each season, for two heterogeneous chemistry parameterizations. The no-coating case used CMAQv5.3.2 default heterogeneous chemistry for N_2O_5 uptake (Davis et al., 2008) and $ClNO_2$ yield (Bertram & Thornton, 2009; Sarwar et al., 2012). The coating case used an updated N_2O_5 uptake mechanism that accounted for organic coatings on particles (Gaston et al., 2014) and a $ClNO_2$ yield mechanism that accounted for the competitive effects of particle sulfate (Staudt et al., 2019). I first assessed loss using the coating parameterization, then compared these results against the no-coating case.

4.2.2 Loss calculations

For our initial analysis, I focused on loss of NO_x at night through two pathways: N_2O_5 heterogeneous uptake to particles (Eq. 1) and NO_3 gas-phase reactions (Eq. 2). The loss of gas-phase N_2O_5 depends on khet, which is a function of total available surface area (SA), mean molecular speed of N_2O_5 gas (c), and the modal uptake (γ). In the CMAQ model, N_2O_5 uptake is calculated for fine mode and coarse mode particles separately, where the fine mode calculation is a surface area weighting of Aitken and accumulation modes. Therefore, I used fine mode uptake for calculation of both Aitken and accumulation mode N_2O_5 loss in Eq. 1. Total loss via the N_2O_5 pathway is then the sum of each modal loss.

$$L(N_2O_5) = \sum_i [N_2O_5] k_{het,i} = \sum_i \frac{\gamma(N_2O_5)_i \times SA_i \times c}{4} \times [N_2O_5] \quad \text{Eq. 1}$$

For loss via NO_3 reactions, I considered all NO_3 reactions in the CMAQ cb6r3_ae7_aq mechanism that resulted in formation of HNO_3 or organic nitrates (NTR1 or NTR2). Monofunctional organic nitrates (NTR1) either photodissociate to NO_2 (R92 in the mechanism), which is not relevant at night, or react with OH to form NTR2 (R91). Multifunctional organic nitrates (NTR2) heterogeneously form HNO_3, so I treated NO_3 reactions that form NTR2 and NTR1 as sink reactions. Table 2 lists the reactions I included, as well as their reaction rates and reaction number for reference to the CMAQ mechanism files.

$$L(NO_3) = \sum_j [NO_3][VOC]_j k_j \qquad \text{Eq. 2}$$

Table 2. Nocturnal NO_3 loss reactions

Reaction	Rate coefficient k (molecules/s/cm3)	Rxn number
$HCHO + NO_3 \rightarrow HNO_3 + HO_2 + CO$	5.5×10^{-16}	R100
$ALD2 + NO_3 \rightarrow C2O3 + HNO_3$	$1.4 \times 10^{-12} e^{-1.86\times10^3/T}$	R107
$ALDX + NO_3 \rightarrow CXO3 + HNO_3$	6.3×10^{-15}	R111
$GLYD + NO_3 \rightarrow C2O3 + HNO_3$	$1.4 \times 10^{-12} e^{-1.86\times10^3/T}$	R115
$GLY + NO_3 \rightarrow HNO_3 + 1.5CO + 0.5XO2 + 0.5RO2 + HO2$	$1.4 \times 10^{-12} e^{-1.86\times10^3/T}$	R118
$MGLY + NO_3 \rightarrow HNO_3 + C2O3 + XO2 + RO2$	$1.4 \times 10^{-12} e^{-1.86\times10^3/T}$	R120
$ISPD + NO_3 \rightarrow 0.717HNO_3 + 0.142NTR2 + 0.142NO_2 + 0.142XO2 + 0.142XO2 + 0.113GLYD + 0.113MGLY + 0.717PAR + 0.717CXO3 + 0.284RO2$	$4.1 \times 10^{-12} e^{-1.86\times10^3/T}$	R160
$HPLD + NO_3 \rightarrow HNO_3 + ISPD$	$6.0 \times 10^{-12} e^{-1.86\times10^3/T}$	R164
$CRES + NO_3 \rightarrow HNO_3 + 0.3CRO + 0.48XO2 + 0.12XO2H + 0.24GLY + 0.24MGLY + 0.48OPO3 + 0.1XO2N + 0.7RO2$	$2.7 \times 10^{-12} e^{3.6\times10^2/T}$	R191
$CRON + NO_3 \rightarrow HNO_3 + NTR2 + 0.5CRO$	$2.7 \times 10^{-12} e^{3.6\times10^2/T}$	R195
$OPEN + NO_3 \rightarrow HNO_3 + OPO3$	3.8×10^{-12}	R204
$CAT1 + NO_3 \rightarrow HNO_3 + CRO$	1.7×10^{-10}	R206
$ISOP + NO_3 \rightarrow 0.35NO_2 + 0.65NTR2 + 0.64XO2H + 0.33XO2 + 0.03XO2N + RO2 + 0.35FORM + 0.35ISPD + ISOPRXN$	$3.03 \times 10^{-12} e^{3-4.48\times10^2/T}$	R157
$TERP + NO_3 \rightarrow 0.47NO_2 + 0.28XO2H + 0.75XO2 + 0.25XO2N + 0.94RO2 + 0.47ALDX + 0.53NTR2 + TERPNRO2$	$3.7 \times 10^{-12} e^{1.75\times10^2/T}$	R174
$APIN + NO_3 \rightarrow 0.47NO_2 + 0.28XO2H + 0.75XO2 + 0.25XO2N + 1.28RO2 + 0.47ALDX + 0.53NTR2$	$3.7 \times 10^{-12} e^{1.75\times10^2/T}$	R174a
$XOPN + NO_3 \rightarrow 0.5NO_2 + 0.5NTR2 + 0.45XO2H + 0.45XO2 + 0.1XO2N + RO2 + 0.25OPEN + 0.25GLY$	3.0×10^{-12}	R200

$ETH + NO_3 \rightarrow 0.5NO_2 + 0.5NTR1 + 0.5XO2H + 0.5XO2 + RO2 + 1.125FORM$	$3.3 \times 10^{-12} e^{-2.88 \times 10^3/T}$	R140
$OLE + NO_3 \rightarrow 0.5NO_2 + 0.5NTR1 + 0.48XO2H + 0.48XO2 + 0.04XO2N + RO2 + 0.5FORM + 0.25ALD2 + 0.375ALDX - 1PAR$	$4.66 \times 10^{-13} e^{-1.155 \times 10^3/T}$	R144
$IOLE + NO_3 \rightarrow 0.5NO_2 + 0.5NTR1 + 0.48XO2H + 0.48XO2 + 0.04XO2N + RO2 + 0.5ALD2 + 0.625ALDX + PAR$	3.7×10^{-13}	R148

I evaluated nocturnal loss by defining night as one hour after the monthly average sunset hour to one hour before the monthly average sunrise hour. The hour after sunset and before sunrise were included to avoid dusk and dawn, which would have some solar insolation and thus could result in photodissociation. I calculated the average loss during each nighttime hour and summed across an entire evening to find the total loss during a night. There are more nighttime hours during January than July, but the relative importance of NO_3 versus N_2O_5 loss pathways for one night are not affected by the length of the night.

I compared the relative impact of nocturnal loss reactions to daytime loss reactions on the total NO_x budget. Day was defined as the one hour after sunrise to one hour before sunset. This means the daytime period excluded dawn and dusk to avoid overlap with nocturnal reactions. Table 3 lists the species considered in daytime loss reactions. Again, I included any reactions in the cb6r3_ae7_aq mechanism that resulted in formation of HNO_3 or NTR2. I did not include reactions that formed NTR1 because NTR1 will photolyze and reform NO_2 during the day. I evaluated the reaction of NO_2 + OH separately from other OH + oxidized nitrogen species reactions because I hypothesized that the NO_2 + OH reaction would be a significant loss pathway.

Table 3. Daytime NO_x loss reactions.

Reaction	Rate coefficient k (molecules/s/cm3)	Rxn number

$NO_2 + OH \rightarrow HNO_3$	$\frac{k_0}{1+{}^{k_0}/_{k_1}} 0.6^{k_{end}}$ $k_0 = 1.8 \times 10^{-30} C_{air} \left(\frac{T}{300}\right)^{-3}$ $k_1 = 2.8 \times 10^{-11}$ $k_{end} = \frac{1}{1+\log\left(\frac{k_0}{k_1}\right)^2}$ $C_{air} = 7.33981 \times 10^{21} \frac{P}{T}$	R45
NO reactions		
$XO2N + NO \rightarrow 0.5NTR1 + 0.5NTR2$	$2.7 \times 10^{-12} e^{3.6\times10^2/T}$	R83
$BZO2 + NO \rightarrow 0.918NO_2 + 0.082NTR2 + 0.918GLY + 0.918OPEN + 0.918HO_2$	$2.7 \times 10^{-12} e^{3.6\times10^2/T}$	R176
$TO2 + NO \rightarrow 0.86NO_2 + 0.14NTR2 + 0.417GLY + 0.443MGLY + 0.66OPEN + 0.2XOPN + 0.86HO_2$	$2.7 \times 10^{-12} e^{3.6\times10^2/T}$	R181
$XLO2 + NO \rightarrow 0.86NO_2 + 0.14NTR2 + 0.221GLY + 0.675MGLY + 0.3OPEN + 0.56XOPN + 0.86HO_2$	$2.7 \times 10^{-12} e^{3.6\times10^2/T}$	R186
OH reactions		
$CRON + OH \rightarrow NTR2 + 0.5CRO$	1.53×10^{-12}	R194
$OPAN + OH \rightarrow 0.5NO_2 + 0.5GLY + CO + 0.5NTR2$	3.6×10^{-12}	R213
$INTR + OH \rightarrow 0.63XO2 + 0.37XO2H + RO2 + 0.444NO_2 + 0.183NO_3 + 0.104INTR + 0.592FORM + 0.331GLYD + 0.185FACD + 2.7PAR + 0.098OLE + 0.078ALDX + 0.266NTR2$	3.1×10^{-11}	R170

4.2.3 Model verification

Surface-level average hourly model output of NO_2 concentration was validated using hourly air quality system (AQS) NO_2 surface monitor measurements (available at https://aqs.epa.gov/aqsweb/airdata/download_files.html#Raw). Table 4 lists the average performance metrics for the coated and uncoated model results in January and July, and Figure 1 shows the correlation coefficient at each monitor location for the coated particle case. The model outputs when using heterogeneous N_2O_5 chemistry on particles with organic coatings have slightly better performance, indicated by the lower root mean square error (RMSE) and mean bias in January and lower mean bias in July. Overall, the two parameterizations result in similar predictions of hourly NO_2 concentration. Performance for both parameterizations is better in

July, with a lower RMSE and mean bias. The negative mean bias in all cases means that the model underpredicts NO_2 concentration compared to observations, though this may also be influenced by measurement error (Fehsenfeld et al., 1990). The correlation between model and observations shown in Figure 1 indicates that the model can capture the temporal trends in NO_2 hourly concentration.

Table 4. Model performance metrics compared against hourly NO_2 AQS measurements

Month	RMSE (ppb)	Mean Bias (ppb)
	Coated particles	
January	7.48	-3.56
July	4.99	-1.23
	Uncoated particles	
January	7.53	-3.70
July	4.99	-1.25

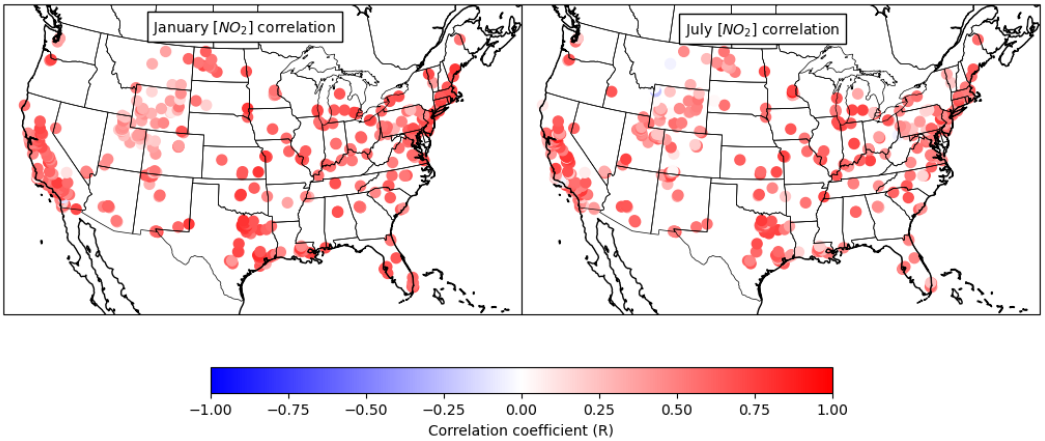

Figure 1. Spatial distribution of correlation between modeled and observed hourly NO_2 concentrations at AQS monitoring locations for model results using the particle organic coatings.

4.3 Results

4.3.1 Spatial and seasonal analysis of nocturnal loss over CONUS

Figure 2 shows the spatial distribution of loss via NO_3 reactions (left side) and N_2O_5 uptake (right side) for January (top row) and July (bottom row). Total N_2O_5 loss via uptake is an order of

magnitude smaller than loss of NO_3 through VOC reactions. The spatial and seasonal distribution of highest loss is different for the two pathways, highlighting the differences in chemistry and emissions driving loss.

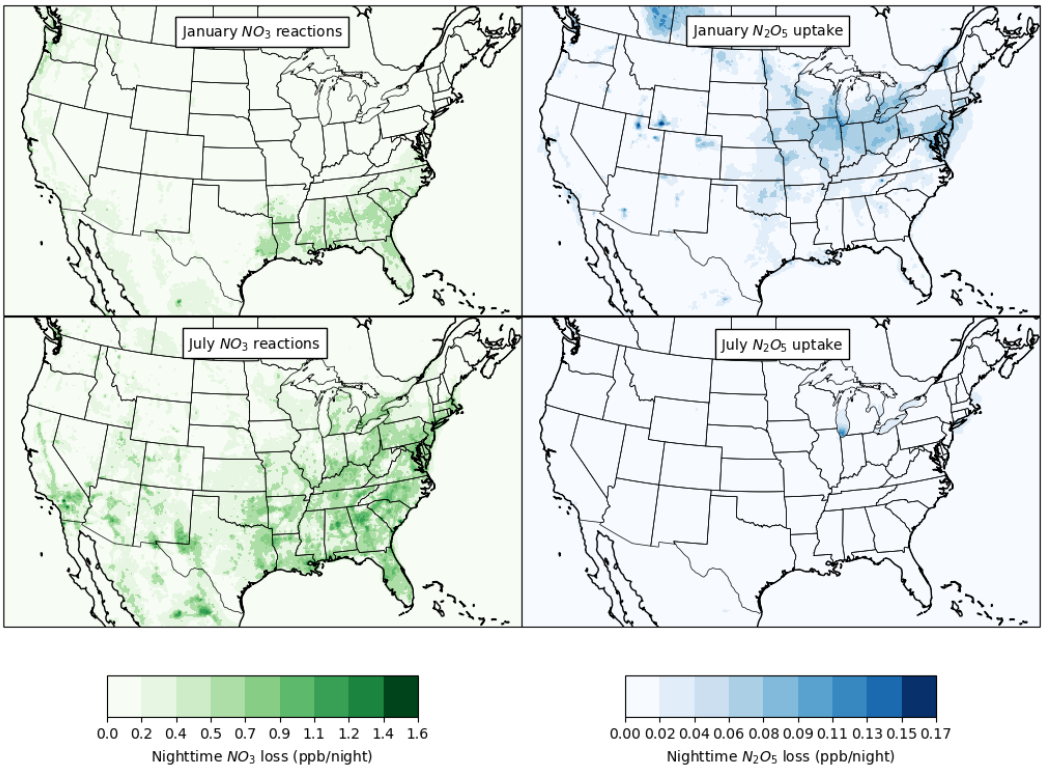

Figure 2. Average nighttime loss of NO_3 through VOC reactions (left side, in green) and N_2O_5 through heterogeneous uptake (right side, in blue) for January (top row) and July (bottom row) over CONUS. The scale of NO_3 loss is 10x of N_2O_5 loss.

Across both months, NO_3 reactions are greatest in the southeast US, an area with high biogenic VOC emissions (Millet et al., 2008). These results are consistent with previous studies that have found that NO_3 oxidation of biogenic VOCs is important for secondary organic aerosol formation, especially in the southeast US (Pye et al., 2010). While I do consider reactions with anthropogenic VOCs in the NO_3 loss pathway, urban centers with high anthropogenic VOC emissions do not stand out in Figure 2. However, the Permian Basin oil fields in west Texas, an area that has previously been shown to have high levels of alkanes and aromatics (Koss et al.,

2017), does show high NO_3 loss. The NO_3 loss in the Permian Basin region is only seen in July, not in January. Across CONUS, NO_3 reactions are more prevalent in July than January.

In comparison, N_2O_5 uptake is higher in January than July. Uptake in January is highest in the Rust Belt, northeast US, and several western cities. This is consistent with previous studies that have found N_2O_5 uptake tends to dominate in more polluted air masses (Allan et al., 1999; Brown et al., 2006). For example, the prevalence of sulfate aerosol over Ohio and Pennsylvania contributed to high uptake in this region (Brown et al., 2006). High NO_2 concentrations tended to push the equilibrium between NO_3 and N_2O_5 towards formation of more N_2O_5, thus enabling higher heterogeneous loss (Aldener et al., 2006). During July, N_2O_5 uptake is close to zero everywhere except over the Great Lakes and along the New England coast. The N_2O_5 uptake during July occurs over Lake Michigan close to Chicago. This area is known for the unique summertime meteorology resulting in high ozone levels along the coast, away from pollution centers (Acdan et al., 2023; Stanier et al., 2021; Vermeuel et al., 2019). The impact of Lake Michigan meteorology on N_2O_5 loss will be explored further in the next section.

4.3.2 Site-specific assessment of dominant loss pathways

To understand the contribution of each loss pathway on total nocturnal NO_x loss, I chose three regions that demonstrated different seasonal patterns of dominant nocturnal NO_x loss for further analysis, shown in Figure 3. Atlanta (ATL) is in the middle of the southeastern US and is dominated by NO_3 loss in both summer and winter. Salt Lake City (SLC) is characterized by high N_2O_5 uptake in January but little to no uptake in July. Lake Michigan (LM) shows high N_2O_5 uptake during the summer and winter.

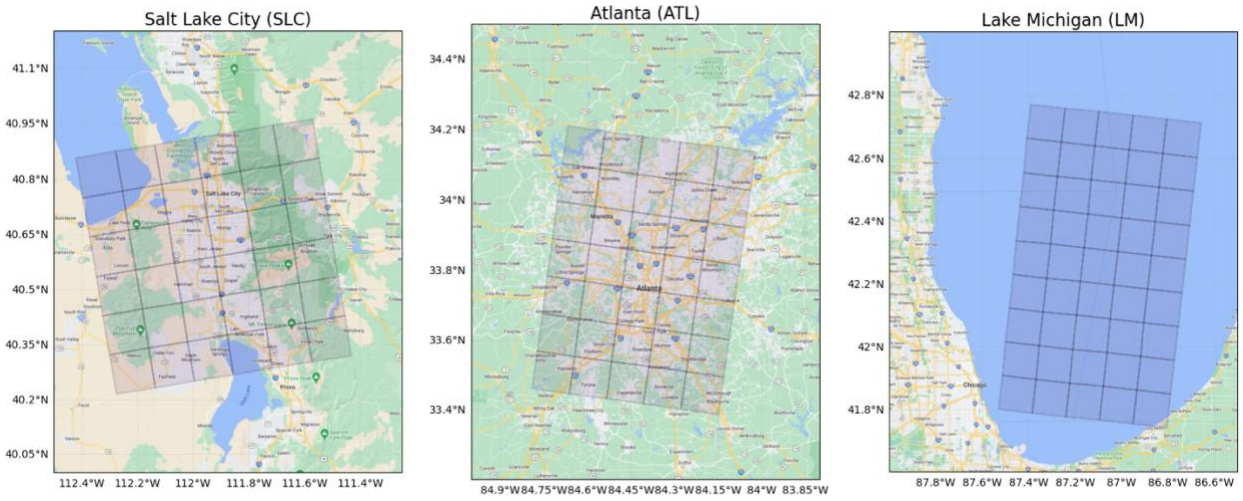

Figure 3. Maps of the study areas over Salt Lake City (SLC), Atlanta (ATL), and Lake Michigan (LM). The shaded area marks the CMAQ domain over each study area from which peak loss was calculated.

For each of the regions in Figure 3, I calculated the average nighttime NO_x loss in each season via NO_3 reactions and N_2O_5 uptake. While the loss of one NO_3 is equivalent to one oxidized nitrogen, each N_2O_5 lost at night corresponds to two oxidized nitrogen species. To account for total NO_x loss, the loss by N_2O_5 uptake was multiplied by two (Eq. 3). Figure 4 shows the contribution of each pathway to NO_x loss for January (triangles) and July (circles) in the three study regions. For all three regions in Figure 4, the location of the markers moves down when moving from summer to winter. This corresponds to a decrease in loss by NO_3 reactions. I then assessed the impact of average nightly and average daily meteorology on total nighttime N_2O_5 and NO_3 loss in each study region using linear regression. The heat map in Figure 5 shows the strength and direction of correlation (Pearson r) between the nocturnal loss pathway and each nighttime and daytime meteorological variable.

$$L(NO_2) = L(NO_3) + 2 \times L(N_2O_5) \quad \text{Eq. 3}$$

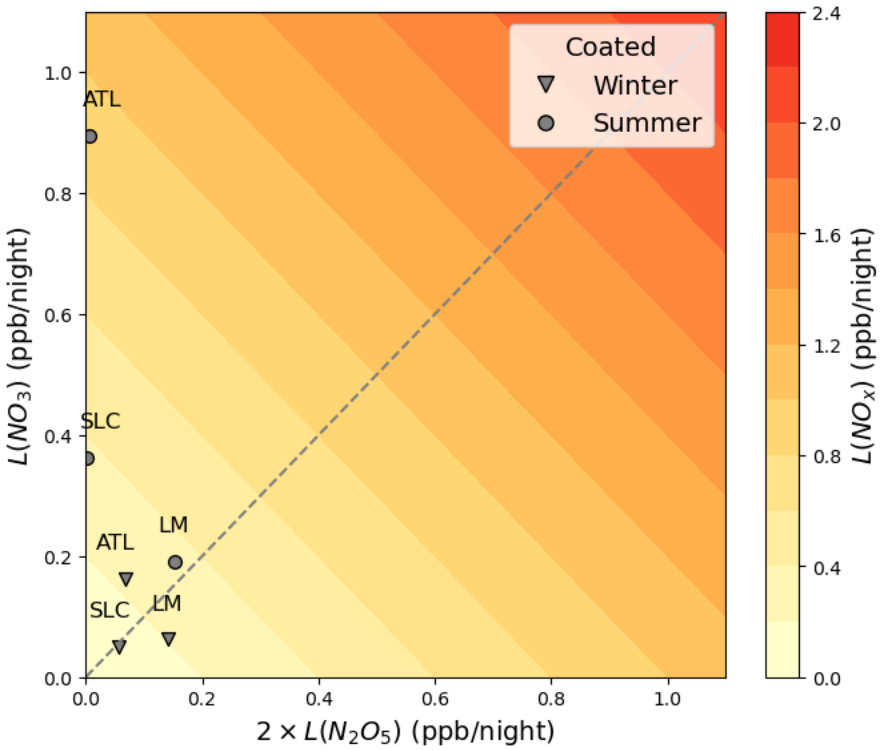

Figure 4. Contribution of NO_3-VOC reactions and N_2O_5 uptake on total NO_x loss for three representative locations: Atlanta (ATL), Salt Lake City (SLC), and over Lake Michigan (LM). Loss by NO_3-VOC reactions is plotted on the y-axis, and loss by N_2O_5 uptake is plotted along the x-axis. Each N_2O_5 molecule lost corresponds to two oxidized nitrogen molecules, so the x-axis is 2x N_2O_5 uptake. Shading is the total NO_x loss from both pathways. The three study regions are plotted as circles for July and triangles for January.

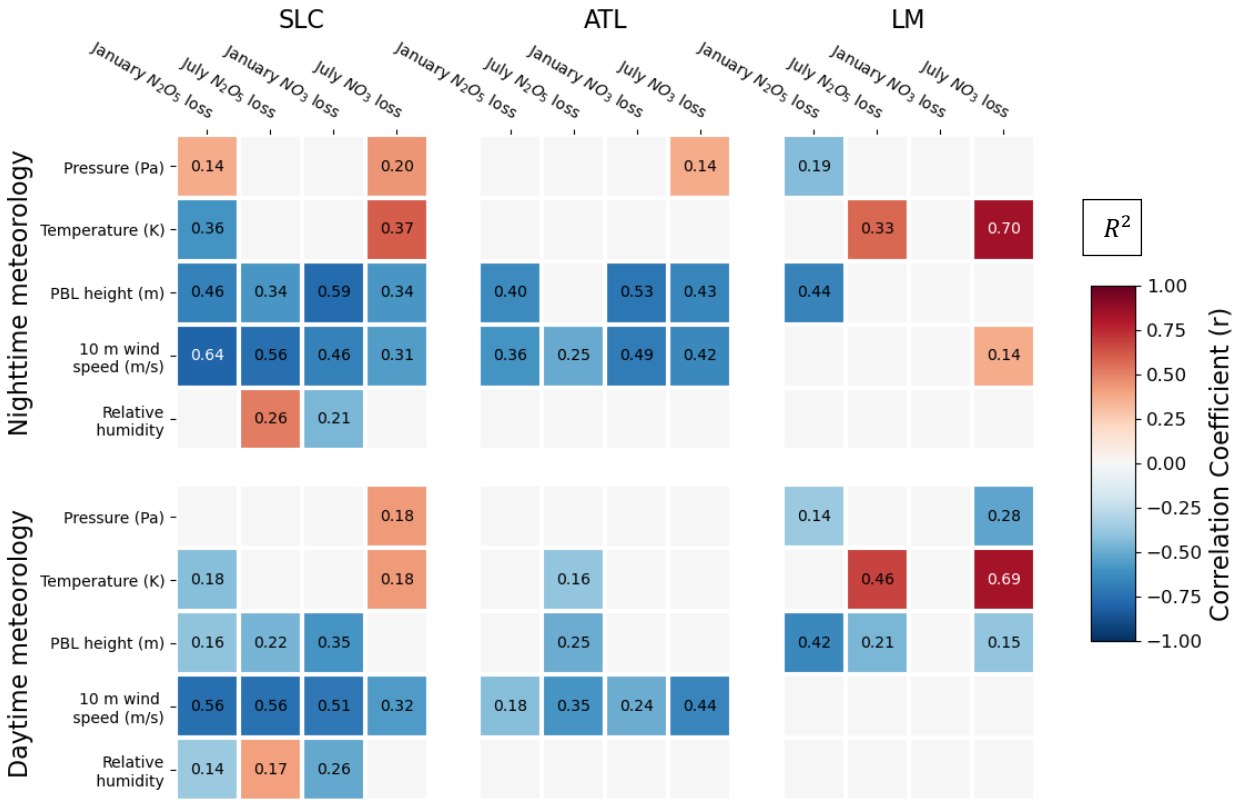

Figure 5. Heat maps of relationship between meteorology and nocturnal loss pathways. The color corresponds to the correlation coefficient (r), which describes the strength and direction of the relationship between the meteorological variable and the loss pathway. The number in each grid is the coefficient of determination (R^2), which represents the amount of variability in the loss pathway that is explained by the meteorological variable. When no statistically significant relationship exists at a 95% confidence level, the grid cell is left blank.

Loss of NO_x in Atlanta is dominated by NO_3 reactions in both summer and winter, which is different from the SLC and LM regions. This highlights the importance of biogenic emissions driving NO_3 reactions in the Atlanta area (Ng et al., 2017). The large decrease in NO_3 reactions and minimal increase in N_2O_5 uptake results in a 75% decrease ($-0.67\ ppb/night$) in total NO_x loss from summer to winter. Average nightly wind speed and planetary boundary layer (PBL) height are moderate predictors ($0.40 < R^2 < 0.55$) of nocturnal NO_3 loss in Atlanta. In general, daytime meteorology explains little of the variability in either NO_3 or N_2O_5 loss in Atlanta, indicating that these pathways depend on meteorology I did not assess (such as wind direction)

or other chemical variables such as VOC concentration or particle surface area. Loss through N_2O_5 uptake did not correlate with relative humidity in Atlanta in either January or July. This is interesting, given that increasing relative humidity often contributes to more particle water, which promotes uptake (Bertram et al., 2009; Phillips et al., 2016; Thornton et al., 2003).

Salt Lake City also has a large decrease (71%, $-0.25\ ppb/night$) in NO_x loss from summer to winter. This difference is mostly driven by the decrease in NO_3 reactions, to the point that wintertime NO_x loss in SLC is equally driven by N_2O_5 uptake and NO_3 reactions. Although small, this region shows the greatest increase in loss by N_2O_5 uptake when moving from summer to winter. This is likely due to inversions in winter, trapping polluted air close to the surface (Whiteman et al., 2001; Whiteman & McKee, 1977). These cold pools trap polluted air in the Salt Lake Valley and create high particle concentrations (Green et al., 2015; Holmes et al., 2015; Whiteman et al., 2014), thus increasing the available particle surface area for N_2O_5 uptake. Figure 6 shows that temperature inversions occur in both January and July during the night, but the inversion is stronger in January. Furthermore, during the day in January, the average planetary boundary layer height is 273 m above the surface, well below the height of the Wasatch and Oquirrh mountains that lie to the east and west of Salt Lake City. Nocturnal N_2O_5 loss has moderate inverse relationship with 10 wind speed and PBL height, where a shallower PBL and lower wind speeds will lead to higher nocturnal uptake. With a shallow PBL and low winds, pollution remains trapped in the valley, contributing to building particle surface area concentrations that lead to high N_2O_5 loss.

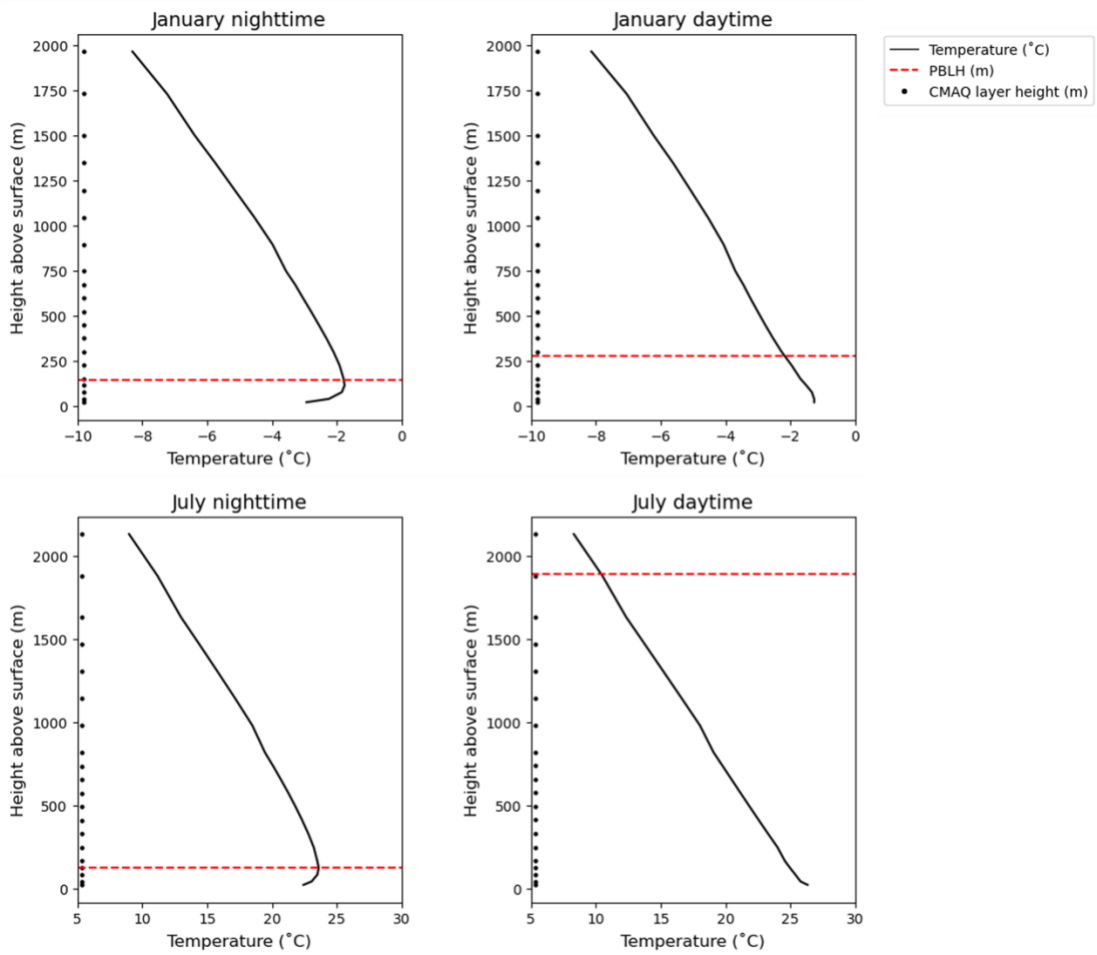

Figure 6. Vertical profile of temperature over the Salt Lake City area in January (top row) and July (bottom row) during the night (left) and day (right). The black line is the temperature profile, the dashed red line is the average planetary boundary layer height (PBLH) above the surface, and the black dots are the CMAQ layer height in meter above the surface. Note the change in temperature scale on the x-axis between January and July.

The Lake Michigan region has the smallest decrease in total NO_x loss (41%, $-0.14\ ppb/night$) in Figure 4. It is also the only region to show a decrease in N_2O_5 uptake when moving from summer to winter. The different spatial distribution of N_2O_5 uptake in Figure 2 indicates that the mechanisms driving N_2O_5 uptake in this area may differ between summer and winter. As shown in Figure 7, 10 m wind speed and direction, as well as divergence of the 10 m wind fields, vary between the summer and winter. In January, during both the day and night, there is divergence along the western shore of Lake Michigan and wind tends to travel towards

the east over the lake, bringing pollution over the lake but not contributing to a build-up along the southern end. In comparison, during the day in July, divergence is highest over the lake and convergence is highest over the western shore. This pattern is consistent with previous studies of the ozone season over Lake Michigan, where differential heating of the land/lake surfaces results in transport of pollution over the lake early in the day where it then reacts and is transported back over land in the afternoon (Acdan et al., 2023; Dye et al., 1995; Foley et al., 2011). The correlations in Figure 5 also indicate that differences in meteorology play a role in the spatial patterns of N_2O_5 loss. Decreasing pressure and decreasing PBL height tend to increase N_2O_5 loss in January, but increasing temperature is a better predictor of N_2O_5 loss in July. Temperature in July is also the best predictor of NO_3 loss over Lake Michigan with an $R^2 \approx 0.7$.

One important note for the correlations seen in Figure 5 is that these are based on only one month of data at a time. For some locations, certain meteorology has a seasonal dependence, but conditions do not have much variability on a day-to-day basis. For example, in Atlanta relative humidity is uniformly high during the summer, so the impact on N_2O_5 loss may be minimized by the lack of variability within the month. To better understand seasonal impacts, a multiyear analysis in each location could be conducted, or correlations could be assessed over the entire United States for a full year.

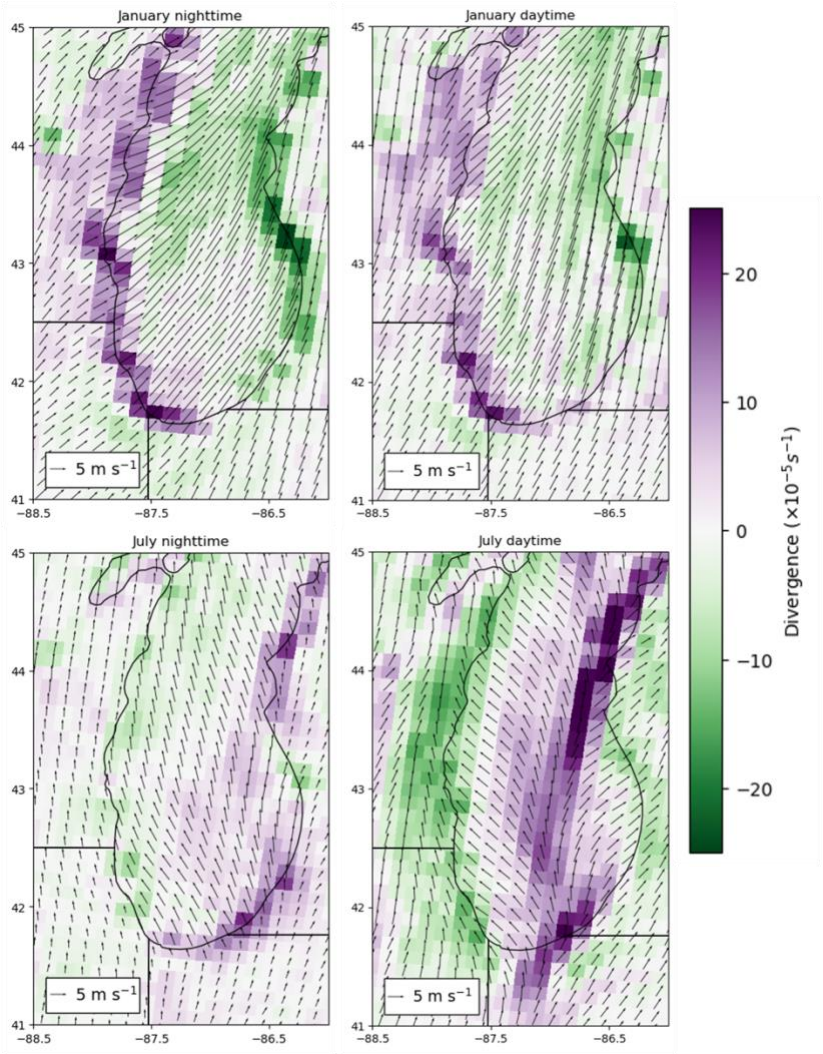

Figure 7. 10 m wind patterns over Lake Michigan during January (top row) and July (bottom row) during the night (left) and day (right). Arrow points toward where the wind is moving, and arrow length indicates the wind speed. Areas of convergence are marked in green, and areas of divergence are marked in purple.

4.3.3 Comparison with daytime NO_x loss pathways

Following analysis of nocturnal loss pathways, I evaluated the contribution of daytime loss to total NO_x removal. On average across the US, daytime reactions account for 84% of total NO_x loss in July and 78% of total loss in January. The relative contribution of each loss mechanism to total NO_x loss in the three study regions are shown in Figure 8.

Even for three disparate regions studied here, daytime pathways account for most NO_x loss. This highlights how most NO_x loss occurs during the day by the NO_2 + OH reaction. The second greatest loss pathway varied by location. In Lake Michigan, nocturnal N_2O_5 uptake was the second largest loss pathway in winter, but daytime OH and NO reactions were more important in the summer. In Atlanta, nocturnal NO_3 reactions were the second largest contributor to loss in winter, and similar in magnitude to summer loss by all OH and NO reactions. In Salt Lake City, daytime OH and NO reactions were the second largest contributor to total NO_x loss in winter and NO_3 reactions were more important in summer. Except over Lake Michigan in the winter, N_2O_5 is not a large contributor to total NO_x loss.

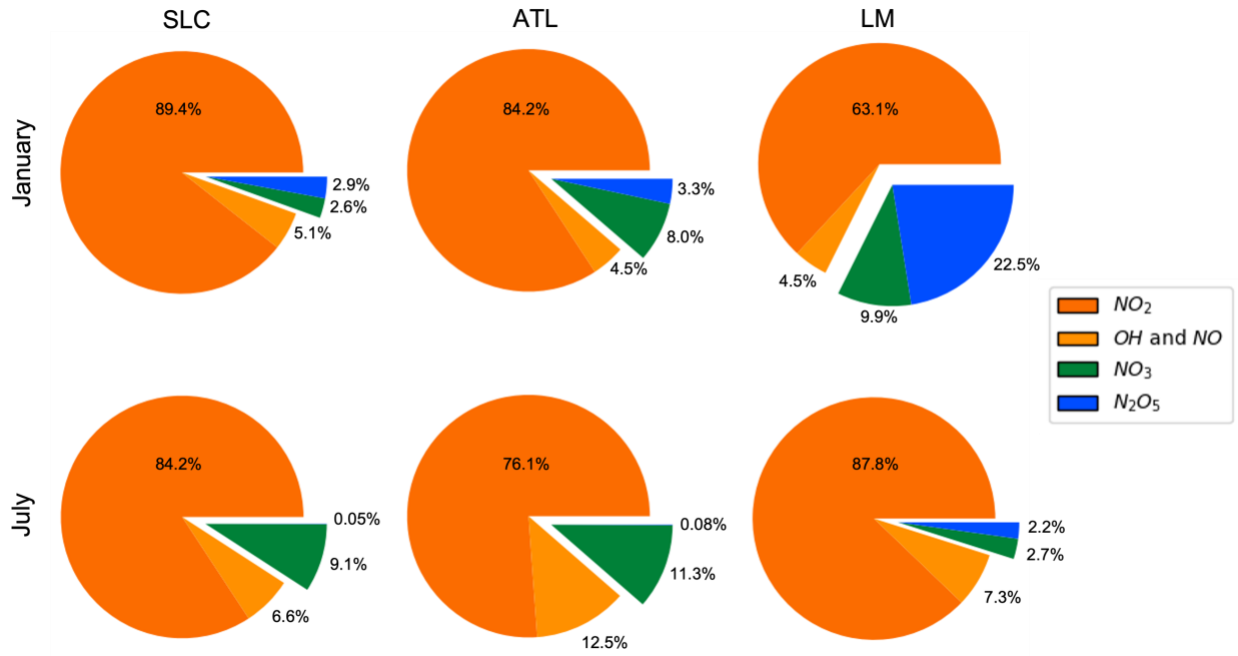

Figure 8. Pie charts of the contribution of each loss pathway on total NO_2 loss in January (top row) and July (bottom row). The three study regions are Salt Lake City (left column), Atlanta (middle), and Lake Michigan (right). Daytime loss pathways are labeled with warm colors. Nighttime loss pathways are labeled with cool colors. Each slice is labeled with the percent of total NO_x loss for that location and month attributable to the pathway.

4.3.4 Comparison of N_2O_5 uptake chemistry

There are several heterogeneous N_2O_5 uptake parameterization options in the CMAQ model, which will have an impact on the resulting loss of N_2O_5 (Davis et al., 2008; McDuffie et al., 2018). I compared N_2O_5 uptake using two different parameterizations to assess the impact on total nocturnal NO_x loss. The first parameterization, which I used in the previous sections of NO_x loss, represented phase-separated particles with an organic coating around an aqueous core (Gaston et al., 2014). The presence of organic coatings tends to reduce uptake of N_2O_5 to particles, which means loss by this pathway is lower than for particles with no coatings (Folkers et al., 2003; Riemer et al., 2009). The second parameterization does not include the effects of organics on uptake. This parameterization treats particles as aqueous and considers only the effects of particle sulfate, nitrate, and ammonium on uptake (Davis et al., 2008).

Figure 9 shows the spatial distribution of monthly average difference between the coating and no-coating parameterization cases for N_2O_5 and NO_3 loss. Although the absolute value of the difference between the two cases is similar for N_2O_5 and NO_3 loss, the relative change is much greater for N_2O_5 loss than NO_3 loss. The average decrease in NO_3 loss was -38% in July and -250% in January, while the average increase in N_2O_5 loss was 6000% in July and 11000% in January compared to the coating baseline. As expected, removing the organic coating from the particles increased N_2O_5 uptake everywhere with a maximum increase ($+0.45$ ppb lost) occurring in January. Loss by NO_3 mechanisms decreased everywhere when the organic particle coating was removed. As N_2O_5 is lost to the particle phase, NO_3 will react with NO_2 to form more N_2O_5 and maintain equilibrium in R1. This means there is less NO_3 to react with VOCs.

$$NO_3 + NO_2 \leftrightarrow N_2O_5 \qquad \text{R1}$$

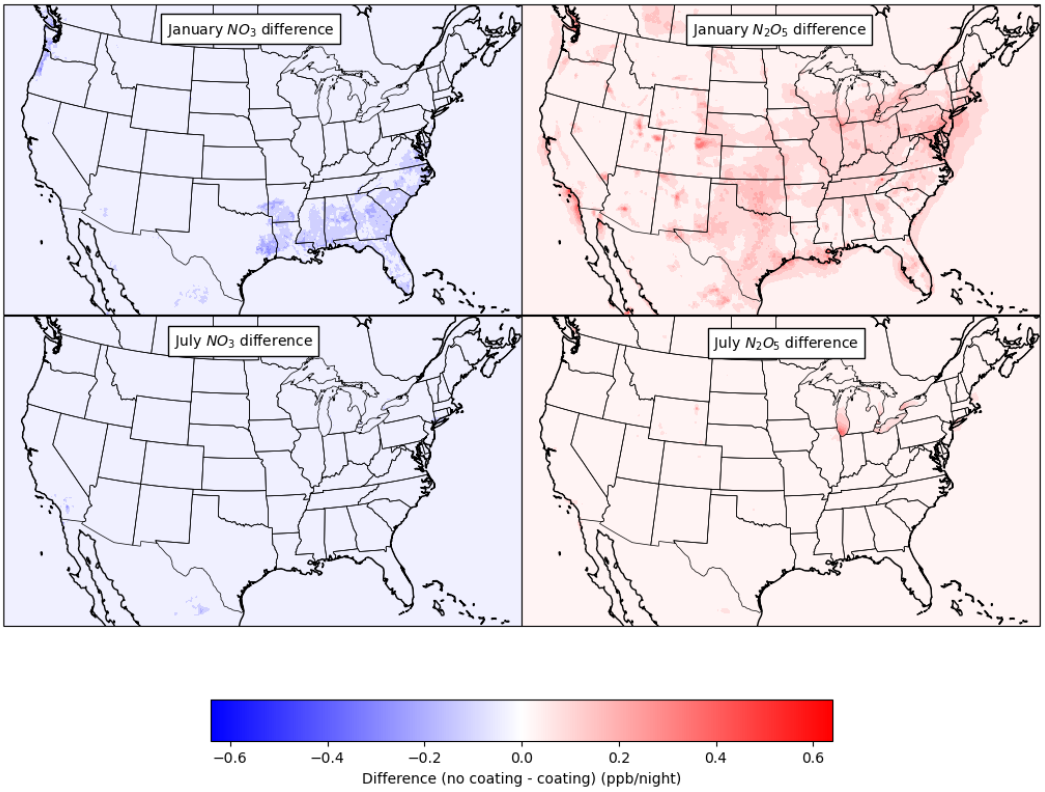

Figure 9. Magnitude of difference in N_2O_5 and NO_3 loss for two model parameterizations of heterogeneous uptake. Red indicates that there is more loss when the particles are modeled with no organic coating, and blue indicates that there is less loss when no organic coating is included. The top row is January, and the bottom row is July. Left column is the difference in NO_3 loss and the right column is the difference in N_2O_5 loss.

The decrease in NO_3 loss in January is highest in the southeast (-0.51 ppb), an area dominated by biogenic VOC emissions. A large fraction of organic particle composition in the CMAQ model is secondary organics from biogenic emissions (Pye et al., 2017), and the calculation of organic coatings used in the coating parameterization case has limited anthropogenic primary organic components (Murphy et al., 2017). Removing the organic coating has a greater influence on particles in biogenic-rich environments, and this will result in increased N_2O_5 uptake and decreased NO_3-VOC reactions in these areas. Although N_2O_5 loss does show an increase in these biogenic-rich areas in January, the greatest increases in N_2O_5 loss are seen over more polluted areas such as New Jersey, Pennsylvania, and major cities like Salt Lake City and Phoenix. In July,

the differences between the two cases are much smaller, with increases in N_2O_5 uptake greatest over Lake Michigan ($+0.37$ ppb).

I compared the impact of removing organic coatings on NO_x loss in the three study regions in Figure 10. For all seasons and locations, changing the heterogeneous uptake calculation decreased the contribution of NO_3 loss and increased the contribution of N_2O_5 loss. In winter, these changes resulted in dramatically higher nocturnal NO_x loss than seen in the baseline coating case. The difference between the two cases is smallest in Atlanta and Salt Lake City during the summer, where the decreased NO_3 contribution is approximately equal to the increased N_2O_5 contribution. In January, however, nocturnal NO_x loss increased compared to the baseline coating case because the contribution of N_2O_5 uptake more than doubled for both Atlanta and Salt Lake City.

The most significant difference between the coated and uncoated particle cases occurred over Lake Michigan in the summer. The contribution of N_2O_5 uptake to NO_x loss increased by a factor of three. Summertime Lake Michigan had the second highest nocturnal NO_x loss with the removal of organic particle coatings, after summertime Atlanta. The total NO_x chemistry region is sensitive to model representations of heterogeneous chemistry.

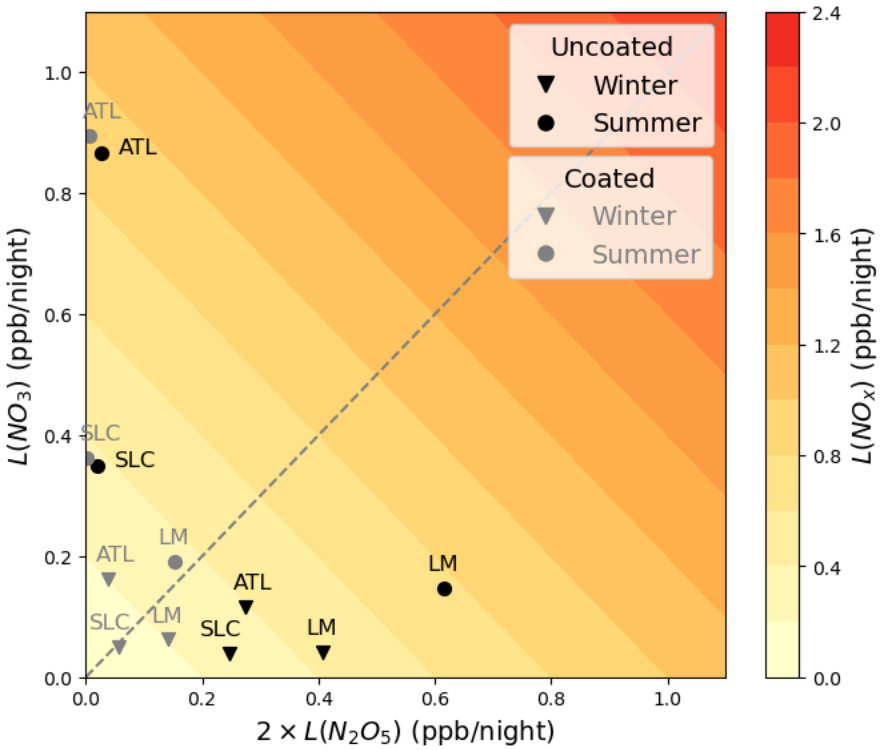

Figure 10. Contribution of NO_3-VOC reactions and N_2O_5 uptake on total NO_x loss for both the coating (grey) and no-coating (black) parameterizations. Loss by NO_3-VOC reactions is plotted on the y-axis, and loss by N_2O_5 uptake is plotted along the x-axis. Each N_2O_5 molecule lost corresponds to two oxidized nitrogen molecules, so the x-axis is 2x N_2O_5 uptake. Shading is the total NO_x loss from both pathways. The contributions to NO_x loss in each study region using the no-coating heterogeneous uptake parameterization are plotted as solid black circles (July) and triangles (January). The same three study regions from Figure 4 are plotted as grey circles for July and triangles for January.

4.3.5 Impact of NO_x production pathways

Thus far, I have focused on loss pathways of NO_x. However, the NO_x budget is also affected by production pathways, such as the formation of $ClNO_2$ from particles. $ClNO_2$ forms from particles containing both chloride and the nitronium ion (NO_2^+). Since the uptake of N_2O_5 contributes to particle NO_2^+ concentrations, $ClNO_2$ production can be calculated as a function of N_2O_5 uptake (Eq. 4).

$$P(ClNO_2) = -L(N_2O_5)_i \times \Phi(ClNO_2)_i = \frac{\gamma(N_2O_5)_i * SA_i * c}{4}[N_2O_5] \times \Phi(ClNO_2)_i \quad \text{Eq. 4}$$

The production of $ClNO_2$ contributes to the total NO_x budget, as $ClNO_2$ is also a reservoir species of NO_x. Larger concentrations of $ClNO_2$ at night will contribute to early morning NO_2 concentrations. I compared two parameterizations of $ClNO_2$ yield to assess the impact on the nocturnal NO_x budget. For the coated particles case, I included the competitive effects of sulfate on $ClNO_2$ yield (Staudt et al., 2019). For the uncoated particles, I did not include this effect on yield. I expected that $ClNO_2$ production would be lower in the coated particles both because of the reduction in available particle-phase N_2O_5 and because of the competition of sulfate for NO_2^+ compared to the uncoated particle case.

Across the US, $ClNO_2$ production is highest in January for both parameterization cases, and the uncoated particles with no sulfate competition had greater production than the coated particles with sulfate competition. Average production for the uncoated particles with no sulfate competition in January was $0.016\,ppb/night$ compared to $0.0022\,ppb/night$ for the coated particles. In July, average production is very low for both cases: $0.0011\,ppb/night$ in the uncoated case and $8.5 \times 10^{-5}\,ppb/night$ in the coated particle case. Figure 11 shows how the nightly $ClNO_2$ production varied across the three study regions and had different impacts on total nightly NO_x concentration.

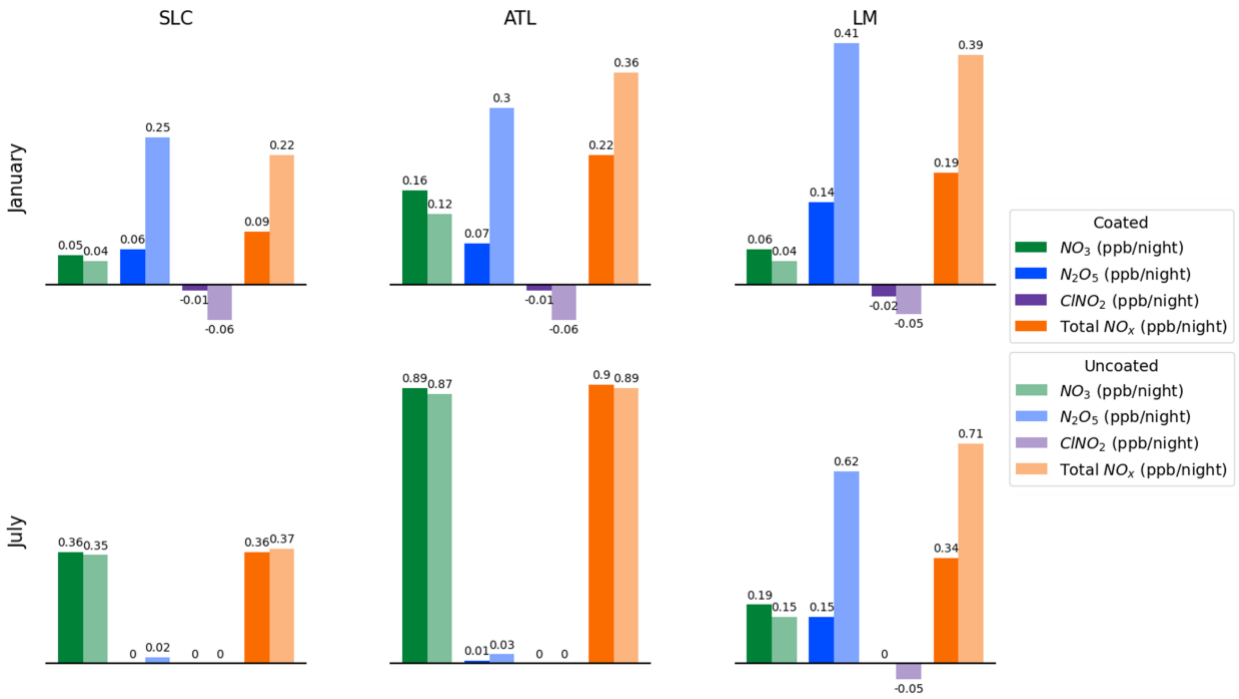

Figure 11. Contribution of nighttime loss and production pathways on total NO_x loss at night. The average contribution of each pathway in ppb/night is labeled above each bar. The orange bars are total NO_x loss at night, so that loss pathways (NO_3 in green and $2\times N_2O_5$ in blue) contribute positively to this and the production pathway ($ClNO_2$ in purple) contributes negatively.

The production of $ClNO_2$ is a function of N_2O_5 loss, so locations where N_2O_5 loss is very small also have negligible contributions from $ClNO_2$ production to total NO_x loss at night. $ClNO_2$ production is lowest in July for all three locations, although the uncoated particle case in Lake Michigan shows similar $ClNO_2$ production in January and July. Production is largest in Salt Lake City and Atlanta in January for the uncoated particle case, but largest over Lake Michigan for the coated particle case. This is consistent with the large uptake of N_2O_5 over Lake Michigan compared to the other two locations when using the coated particle uptake mechanism. In January, $ClNO_2$ production is responsible for a 11-20% decrease of total NO_x loss for the uncoated particles and between 3-10% decrease for the coated particles. In July, except over Lake Michigan in the uncoated particle case, $ClNO_2$ production does not contribute more than 0.005 ppb to the NO_x budget.

4.4 Discussion

4.4.1 Daytime air quality

The differences in the nighttime NO_x budget between the two cases indicates that the nocturnal loss and production pathways assessed here will have an impact on particle nitrate and NO_2 concentrations, which are important for daytime air quality. The uptake parameterization that includes organic coatings on particles results in a smaller nocturnal loss term than the uncoated particle case, which results in the coated particle case having a higher daytime NO_2 concentration and smaller average particle nitrate concentration than the uncoated particle case. The production of $ClNO_2$ has a small offset for the uncoated particles, but Figure 11 shows how this effect is not equal across the US.

The percent difference in daytime NO_2 concentration is shown in Figure 12 for the local hour of peak difference (9am in January and 6am in July). The hour of peak of difference in NO_2 concentration changes seasonally, corresponding to the time of local sunrise. Concentration differences in July begin during the evening when nocturnal loss is directly affecting ambient NO_2 concentration through R1. Because the coated case results in less loss of N_2O_5 during the night, the equilibrium in R1 keeps NO_2 concentrations high. These differences peak in the early morning at sunrise when N_2O_5 is then photolyzed. However, even at the peak of difference, July shows small percent differences in NO_2 concentration between the two parametrization cases, on average -1.83%.

In January, the decrease in NO_x loss through N_2O_5 uptake results in an average -7.30% difference in daytime NO_2 concentration between the two parameterization schemes across the

United States at 9am. The differences in NO_2 concentration in January are greater than zero at every hour. Like July, the minimum difference occurs in the afternoon and then begins to increase through the evening. However, the early morning peak shows a sharper increase than the steady increase seen in July. This indicates that in January there is a rapid photolysis of N_2O_5.

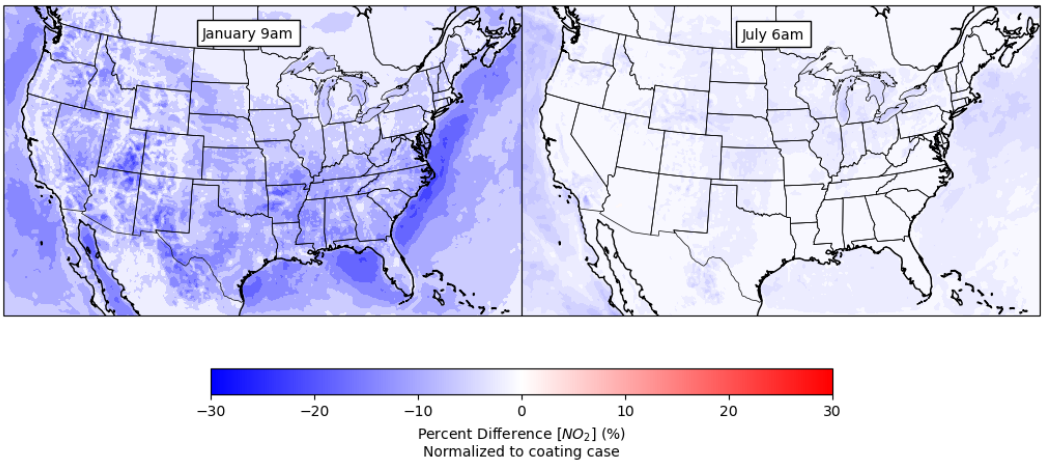

Figure 12. Average percent difference in NO_2 concentration ($\frac{[NO_2]_{uncoated}-[NO_2]_{coated}}{[NO_2]_{coated}}$) over CONUS for January at 9am local time (left) and July at 6am local time (right). Blue means that the uncoated parameterization case has a lower NO_2 concentration.

4.4.2 Consideration of other loss pathways

There are additional loss pathways besides gas-phase and heterogeneous reactions. Deposition, both wet and dry, is a significant loss of HNO_3, though less so for other oxidized nitrogen species (Butler et al., 2005; Munger et al., 1998). The CMAQ model outputs both wet and dry deposition information for numerous oxidized nitrogen species. I did not include deposition in the previous analysis of total NO_x loss because deposition in CMAQ is treated throughout the column, while I constrained our analysis to the surface layer. However, I did compare the relative contribution of wet versus dry deposition of nitrogen containing species during the day and night to the total loss by deposition.

Wet deposition was equal to or greater than dry deposition in all three locations in January, and in July dry deposition is only greater than wet deposition in Salt Lake City. This is consistent with previous findings for the southeast and upper Midwest US (Beachley et al., 2019; Li et al., 2016). Lake Michigan had the highest fractional loss via wet deposition compared to the other two locations (72% in January and 74% in July), while Salt Lake City had the smallest loss by wet deposition (62% in January and 48% in July), consistent with previous studies of nitrogen deposition patterns over the US (Zhang et al., 2012). Assessments of wet and dry nitrogen deposition across the US have found dry deposition more important in arid environments (Walker et al., 2019).

In Atlanta during January, nighttime wet deposition was three times greater than nighttime dry deposition (47% compared to 15%), and double dry (20%) and wet (18%) deposition during the day. In July, daytime wet deposition accounted for 63% of total loss by deposition, and daytime dry deposition accounted for 26%. However, it is misleading to extrapolate from average monthly wet deposition to individual days. Precipitation events are variable in frequency, duration, and intensity and the interannual variability of frequency, duration, and intensity is expected to change in a changing climate (Harp & Horton, 2023; Kim et al., 2022; Wright et al., 2019). On individual days, wet deposition by precipitation events can be a large contributor to total loss (Schichtel et al., 2019), so the large fraction loss by wet deposition compared to dry deposition in Atlanta and Lake Michigan may either be to slightly higher daily deposition or a few large precipitation events.

In addition to deposition, I did not consider other loss pathways such as direct uptake by the forest canopy (Kang et al., 2023), reactions on ice particles or snow surfaces (Apodaca et al.,

2008), or homogeneous loss with water (Stutz, 2004). During winter in Alaska, reactions of N_2O_5 on ice particles can contribute significantly to total NO_x loss (Apodaca et al., 2008), or loss to snowpack (Ayers & Simpson, 2006), but these pathways are likely more important at high latitudes rather than across the continental US. I also did not assess direct reactions between N_2O_5 or NO_3 with water vapor. The reaction of N_2O_5 with water vapor may be a dominant contributor to NO_x loss in some locations (Stutz, 2004). However, there is variability in the reaction rate of this mechanism, and heterogeneous N_2O_5 uptake is a larger contributor to NO_x loss in most locations (Brown et al., 2009).

4.5 Conclusions

I assessed predicted nocturnal NO_x loss pathways in January and July across the United States to understand the impact of nocturnal chemistry on the NO_x budget. Loss through NO_3 reactions is on average greater than loss by N_2O_5 and is greatest in areas with high biogenic VOC emissions such as the southeast US. Loss by N_2O_5 uptake is highest in more polluted regions such as over major cities. Although nocturnal pathways are important, daytime loss, specifically NO_2 + OH, dominates total NO_x loss across CONUS. In Atlanta and Lake Michigan in January, the second largest contributor to total NO_x loss is nocturnal pathways, but in Salt Lake City the second largest contributor is other daytime reactions.

Local meteorology plays a role in determining dominant loss pathway, but in some locations dominant loss is more driven by local chemistry. In Atlanta, local meteorology did not explain much of the variability in NO_3 or N_2O_5 loss, implying that other factors, such as BVOC concentration, NO_2 concentrations, or particle surface area and composition, that are more

important for determining loss. In Salt Lake City and over Lake Michigan, local meteorological conditions play a greater role in determining loss each night.

I also assessed the impact of different representations of N_2O_5 heterogeneous chemistry on nocturnal loss. Uptake is increased when particles are modeled without an organic coating. This increase in N_2O_5 uptake has a corresponding decrease in loss by NO_3 reactions, as NO_3 will react with NO_2 to maintain equilibrium with the lost N_2O_5. Not all regions are equally impacted by the differences in heterogenous chemistry. The effect is greatest over Lake Michigan and smallest in Salt Lake City. In addition to different representations of N_2O_5 uptake, representations of $ClNO_2$ production in the model affect the nocturnal NO_x budget. These differences are greatest in January, when uptake is also highest. The differences in nocturnal loss between the two parameterization cases results in higher daytime NO_2 concentrations for coated particles. Because the NO_x loss is small with organic coatings on particles, ambient NO_2 concentrations are higher than the model case without the organic particle coating. The difference in NO_2 concentration is greatest in January and small in July, emphasizing how nocturnal heterogeneous chemistry is an important loss term in the NO_x budget during the winter.

One limitation of this study is the short time range. I only assessed loss for two months, representing winter and summer, in one year. There may be interannual variability in dominant loss pathways, and there may be trends across years as emissions have changed. NO_x emissions have decreased across the US (U.S. EPA, 2021), and this will impact nighttime NO_3 and N_2O_5 concentrations. In addition, changes in particulate matter concentrations, especially during wildfire seasons, may also impact N_2O_5 loss by changing the available particle surface area and

composition. Future work should consider how changes in emissions over time have impacted dominant nocturnal loss pathways.

References

Acdan, J. J. M., Pierce, R. B., Dickens, A. F., Adelman, Z., & Nergui, T. (2023). Examining TROPOMI formaldehyde to nitrogen dioxide ratios in the Lake Michigan region: implications for ozone exceedances. *Atmospheric Chemistry and Physics*, *23*(14), 7867–7885. https://doi.org/10.5194/acp-23-7867-2023

Aldener, M., Brown, S. S., Stark, H., Williams, E. J., Lerner, B. M., Kuster, W. C., et al. (2006). Reactivity and loss mechanisms of NO3 and N2O5 in a polluted marine environment: Results from in situ measurements during New England Air Quality Study 2002. *Journal of Geophysical Research: Atmospheres*, *111*(D23). https://doi.org/10.1029/2006JD007252

Alexander, B., Hastings, M. G., Allman, D. J., Dachs, J., Thornton, J. A., & Kunasek, S. A. (2009). Quantifying atmospheric nitrate formation pathways based on a global model of the oxygen isotopic composition (δ17O) of atmospheric nitrate. *Atmospheric Chemistry and Physics*, *9*(14), 5043–5056. https://doi.org/10.5194/ACP-9-5043-2009

Allan, B. J., Carslaw, N., Coe, H., Burgess, R. A., & Plane, J. M. C. (1999). Observations of the Nitrate Radical in the Marine Boundary Layer. *Journal of Atmospheric Chemistry*, *33*(2), 129–154. https://doi.org/10.1023/A:1005917203307

Ambrose, J. L., Mao, H., Mayne, H. R., Stutz, J., Talbot, R., & Sive, B. C. (2007). Nighttime nitrate radical chemistry at Appledore Island, Maine during the 2004 International Consortium for Atmospheric Research on Transport and Transformation. *Journal of Geophysical Research*, *112*(D21), D21302. https://doi.org/10.1029/2007JD008756

Apodaca, R. L., Huff, D. M., & Simpson, W. R. (2008). The role of ice in N2O5 heterogeneous hydrolysis at high latitudes. *Atmospheric Chemistry and Physics*, *8*(24), 7451–7463. https://doi.org/10.5194/acp-8-7451-2008

Appel, K. W., Bash, J. O., Fahey, K. M., Foley, K. M., Gilliam, R. C., Hogrefe, C., et al. (2021). The Community Multiscale Air Quality (CMAQ) model versions 5.3 and 5.3.1: system updates and evaluation. *Geoscientific Model Development*, *14*(5), 2867–2897. https://doi.org/10.5194/gmd-14-2867-2021

Atkinson, R. (1991). Kinetics and Mechanisms of the Gas-Phase Reactions of the NO3 Radical with Organic Compounds. *Journal of Physical and Chemical Reference Data*, *20*(3), 459–507. https://doi.org/10.1063/1.555887

Ayers, J. D., & Simpson, W. R. (2006). Measurements of N_2O_5 near Fairbanks, Alaska. *Journal of Geophysical Research*, *111*(D14), D14309. https://doi.org/10.1029/2006JD007070

Beachley, G. M., Rogers, C. M., Lavery, T. F., Walker, J. T., & Puchalski, M. A. (2019). Long-Term Trends in Reactive Nitrogen Deposition in the United States. *EM (Pittsburgh, Pa.)*, *1*, http://nadp.slh.wisc.edu/committees/tdep/reports/EMissue2019/Long-term%20Trends%20in%20N%20Dep.pdf.

Bertram, T. H., & Thornton, J. A. (2009). Toward a general parameterization of N2O5 reactivity on aqueous particles: the competing effects of particle liquid water, nitrate and chloride. *Atmospheric Chemistry and Physics*, *9*, 8351–8363.

Bertram, T. H., Thornton, J. A., Riedel, T. P., Middlebrook, A. M., Bahreini, R., Bates, T. S., et al. (2009). Direct observations of N2O5 reactivity on ambient aerosol particles. *Geophysical Research Letters*, *36*(L19803), 1–5. https://doi.org/10.1029/2009GL040248

Brown, S. S., Dibb, J. E., Stark, H., Aldener, M., Vozella, M., Whitlow, S., et al. (2004). Nighttime removal of NOx in the summer marine boundary layer. *Geophysical Research Letters*, *31*(7). https://doi.org/10.1029/2004GL019412

Brown, S. S., Ryerson, T. B., Wollny, A. G., Brock, C. A., Peltier, R., Sullivan, A. P., et al. (2006). Variability in Nocturnal Nitrogen Oxide Processing and Its Role in Regional Air Quality. *Science*, *311*, 76–70.

Brown, S. S., Dubé, W. P., Osthoff, H. D., Stutz, J., Ryerson, T. B., Wollny, A. G., et al. (2007). Vertical profiles in NO_3 and N_2O_5 measured from an aircraft: Results from the NOAA P-3 and surface platforms during the New England Air Quality Study 2004. *Journal of Geophysical Research*, *112*(D22), D22304. https://doi.org/10.1029/2007JD008883

Brown, S. S., Dubé, W. P., Fuchs, H., Ryerson, T. B., Wollny, A. G., Brock, C. A., et al. (2009). Reactive uptake coefficients for N_2O_5 determined from aircraft measurements during the Second Texas Air Quality Study: Comparison to current model parameterizations. *Journal of Geophysical Research*, *114*, D00F10. https://doi.org/10.1029/2008JD011679

Butler, T. J., Likens, G. E., Vermeylen, F. M., & Stunder, B. J. B. (2005). The impact of changing nitrogen oxide emissions on wet and dry nitrogen deposition in the northeastern USA. *Atmospheric Environment*, *39*(27), 4851–4862. https://doi.org/10.1016/j.atmosenv.2005.04.031

Davis, J. M., Bhave, P. V., & Foley, K. M. (2008). Parameterization of N2O5 reaction probabilities on the surface of particles containing ammonium, sulfate, and nitrate. *Atmos. Chem. Phys*, *8*, 5295–5311.

Dye, T. S., Roberts, P. T., & Korc, M. E. (1995). Observations of transport processes for ozone and ozone precursors during the 1991 Lake Michigan Ozone Study. *Journal of Applied Meteorology*, *34*(8), 1877–1889. https://doi.org/10.1175/1520-0450(1995)034<1877:OOTPFO>2.0.CO;2

Edwards, P. M., Aikin, K. C., Dube, W. P., Fry, J. L., Gilman, J. B., de Gouw, J. A., et al. (2017). Transition from high- to low-NOx control of night-time oxidation in the southeastern US. *Nature Geoscience*, *10*(7), 490–495. https://doi.org/10.1038/ngeo2976

Emery, C., Jung, J., Koo, B., & Yarwood, G. (2015). *Improvements to CAMx Snow Cover Treatments and Carbon Bond Chemical Mechanism for Winter Ozone. Final Report*. Salt Lake City, UT: Ramboll Environ. Retrieved from http://www.deq.utah.gov/locations/U/uintahbasin/docs/2014/03Mar

Fehsenfeld, F. C., Drummond, J. W., Roychowdhury, U. K., Galvin, P. J., Williams, E. J., Buhr, M. P., et al. (1990). Intercomparison of NO2 measurement techniques. *Journal of Geophysical Research: Atmospheres*, *95*(D4), 3579–3597. https://doi.org/10.1029/JD095iD04p03579

Fibiger, D. L., McDuffie, E. E., Dubé, W. P., Aikin, K. C., Lopez-Hilfiker, F. D., Lee, B. H., et al. (2018). Wintertime Overnight NO_x Removal in a Southeastern United States Coal-fired

Power Plant Plume: A Model for Understanding Winter NO_x Processing and its Implications. *Journal of Geophysical Research: Atmospheres*, *123*(2), 1412–1425. https://doi.org/10.1002/2017JD027768

Finlayson-Pitts, B. J., Ezell, M. J., & Pitts Jr., J. N. (1989). Formation of chemically active chlorine compounds by reactions of atmospheric NaCl particles with gaseous N2O5 and ClONO2. *Nature*, *337*, 241–244.

Foley, K. M., Pouliot, G. A., Eyth, A., Aldridge, M. F., Allen, C., Appel, K. W., et al. (2023). 2002–2017 anthropogenic emissions data for air quality modeling over the United States. *Data in Brief*, *47*, 109022. https://doi.org/10.1016/j.dib.2023.109022

Foley, T., Betterton, E. A., Robert Jacko, P. E., & Hillery, J. (2011). Lake Michigan air quality: The 1994-2003 LADCO Aircraft Project (LAP). *Atmospheric Environment*, *45*(18), 3192–3202. https://doi.org/10.1016/j.atmosenv.2011.02.033

Folkers, M., Mentel, Th. F., & Wahner, A. (2003). Influence of an organic coating on the reactivity of aqueous aerosols probed by the heterogeneous hydrolysis of N2O5. *Geophysical Research Letters*, *30*(12), 1644. https://doi.org/10.1029/2003GL017168

Gaston, C. J., Thornton, J. A., & Ng, N. L. (2014). Reactive uptake of N2O5 to internally mixed inorganic and organic particles: The role of organic carbon oxidation state and inferred organic phase separations. *Atmospheric Chemistry and Physics*, *14*(11), 5693–5707. https://doi.org/10.5194/ACP-14-5693-2014

Green, M. C., Chow, J. C., Watson, J. G., Dick, K., & Inouye, D. (2015). Effects of Snow Cover and Atmospheric Stability on Winter PM2.5 Concentrations in Western U.S. Valleys. *Journal of Applied Meteorology and Climatology*, *54*(6), 1191–1201. https://doi.org/10.1175/JAMC-D-14-0191.1

Harp, R. D., & Horton, D. E. (2023). Observed Changes in Interannual Precipitation Variability in the United States. *Geophysical Research Letters*, *50*(13), e2023GL104533. https://doi.org/10.1029/2023GL104533

Holmes, H. A., Sriramasamudram, J. K., Pardyjak, E. R., & Whiteman, C. D. (2015). Turbulent Fluxes and Pollutant Mixing during Wintertime Air Pollution Episodes in Complex Terrain. *Environmental Science & Technology*, *49*(22), 13206–13214. https://doi.org/10.1021/acs.est.5b02616

Jacob, D. J., Heikes, E. G., Fan, S.-M., Logan, J. A., Mauzerall, D. L., Bradshaw, J. D., et al. (1996). Origin of ozone and NO_x in the tropical troposphere: A photochemical analysis of aircraft observations over the South Atlantic basin. *Journal of Geophysical Research: Atmospheres*, *101*(D19), 24235–24250. https://doi.org/10.1029/96JD00336

Kang, R., Huang, K., Gao, T., Mulder, J., Duan, L., Wang, C., et al. (2023). Forest Canopy Acts as an Atmospheric NOx Sink: Results From Micrometeorological Flux Measurements. *Journal of Geophysical Research: Atmospheres*, *128*(19), e2022JD037729. https://doi.org/10.1029/2022JD037729

Kim, J., Shu, E., Lai, K., Amodeo, M., Porter, J., & Kearns, E. (2022). Assessment of the standard precipitation frequency estimates in the United States. *Journal of Hydrology: Regional Studies*, *44*, 101276. https://doi.org/10.1016/j.ejrh.2022.101276

Koss, A., Yuan, B., Warneke, C., Gilman, J. B., Lerner, B. M., Veres, P. R., et al. (2017). Observations of VOC emissions and photochemical products over US oil- and gas-producing regions using high-resolution

H₃O⁺ CIMS (PTR-ToF-MS). *Atmospheric Measurement Techniques*, *10*(8), 2941–2968. https://doi.org/10.5194/amt-10-2941-2017

Li, Y., Schichtel, B. A., Walker, J. T., Schwede, D. B., Chen, X., Lehmann, C. M. B., et al. (2016). Increasing importance of deposition of reduced nitrogen in the United States. *Proceedings of the National Academy of Sciences*, *113*(21), 5874–5879. https://doi.org/10.1073/pnas.1525736113

Liang, J., Horowitz, L. W., Jacob, D. J., Wang, Y., Fiore, A. M., Logan, J. A., et al. (1998). Seasonal budgets of reactive nitrogen species and ozone over the United States, and export fluxes to the global atmosphere. *Journal of Geophysical Research: Atmospheres*, *103*(D11), 13435–13450. https://doi.org/10.1029/97JD03126

Luecken, D. J., Yarwood, G., & Hutzell, W. T. (2019). Multipollutant modeling of ozone, reactive nitrogen and HAPs across the continental US with CMAQ-CB6. *Atmospheric Environment*, *201*, 62–72. https://doi.org/10.1016/J.ATMOSENV.2018.11.060

McDuffie, E. E., Fibiger, D. L., Dubé, W. P., Lopez-Hilfiker, F., Lee, B. H., Thornton, J. A., et al. (2018). Heterogeneous N2O5 Uptake During Winter: Aircraft Measurements During the 2015 WINTER Campaign and Critical Evaluation of Current Parameterizations. *Journal of Geophysical Research: Atmospheres*, *123*(8), 4345–4372. https://doi.org/10.1002/2018JD028336

Millet, D. B., Jacob, D. J., Boersma, K. F., Fu, T., Kurosu, T. P., Chance, K., et al. (2008). Spatial distribution of isoprene emissions from North America derived from formaldehyde column measurements by the OMI satellite sensor. *Journal of Geophysical Research: Atmospheres*, *113*(D2), 2007JD008950. https://doi.org/10.1029/2007JD008950

Mozurkewich, M., & Calvert, J. G. (1988). Reaction probability of N2O5 on aqueous aerosols. *Journal of Geophysical Research: Atmospheres*, *93*(D12), 15889–15896. https://doi.org/10.1029/JD093ID12P15889

Munger, J. W., Fan, S.-M., Bakwin, P. S., Goulden, M. L., Goldstein, Allen. H., Colman, A. S., & Wofsy, S. C. (1998). Regional budgets for nitrogen oxides from continental sources: Variations of rates for oxidation and deposition with season and distance from source regions. *Journal of Geophysical Research: Atmospheres*, *103*(D7), 8355–8368. https://doi.org/10.1029/98JD00168

Murphy, B. N., Woody, M. C., Jimenez, J. L., Carlton, A. M. G., Hayes, P. L., Liu, S., et al. (2017). Semivolatile POA and parameterized total combustion SOA in CMAQv5.2: Impacts on source strength and partitioning. *Atmospheric Chemistry and Physics*, *17*(18), 11107–11133. https://doi.org/10.5194/ACP-17-11107-2017

Ng, N. L., Brown, S. S., Archibald, A. T., Atlas, E., Cohen, R. C., Crowley, J. N., et al. (2017). Nitrate radicals and biogenic volatile organic compounds: oxidation, mechanisms, and organic aerosol EPA Public Access non-photochemical mechanisms for use in state-of-the-art chemical transport and chemistry-climate models. *Atmos Chem Phys*, *17*(3), 2103–2162. https://doi.org/10.5194/acp-17-2103-2017-supplement

Pandis, S. N., Harley, R. A., Cass, G. R., & Seinfeld, J. H. (1992). Secondary organic aerosol formation and transport. *Atmospheric Environment. Part A. General Topics*, *26*(13), 2269–2282. https://doi.org/10.1016/0960-1686(92)90358-R

Phillips, G. J., Thieser, J., Tang, M., Sobanski, N., Schuster, G., Fachinger, J., et al. (2016). Estimating N₂O₅ uptake coefficients using ambient measurements ofNO₃, N₂O₅, ClNO₂ and particle-phase nitrate. *Atmospheric Chemistry and Physics*, *16*(20), 13231–13249. https://doi.org/10.5194/acp-16-13231-2016

Platt, U. F., Winer, A. M., Biermann, H. W., Atkinson, R., & Pitts, J. N. (1984). Measurement of Nitrate Radical Concentrations in Continental Air. *Environ. Sci. Technol*, *18*(5), 365–369. https://doi.org/10.1021/ES00123A015

Pye, H. O. T., Chan, A. W. H., Barkley, M. P., & Seinfeld, J. H. (2010). Global modeling of organic aerosol: the importance of reactive nitrogen (NO_x and NO₃). *Atmospheric Chemistry and Physics*, *10*(22), 11261–11276. https://doi.org/10.5194/acp-10-11261-2010

Pye, H. O. T., Murphy, B. N., Xu, L., Ng, N. L., Carlton, A. G., Guo, H., et al. (2017). On the implications of aerosol liquid water and phase separation for organic aerosol mass. *Atmos. Chem. Phys*, *17*, 343–369. https://doi.org/10.5194/acp-17-343-2017

Riemer, N., Vogel, H., Vogel, B., Anttila, T., Kiendler-Scharr, A., & Mentel, T. F. (2009). Relative importance of organic coatings for the heterogeneous hydrolysis of N2O5 during summer in Europe. *Journal of Geophysical Research: Atmospheres*, *114*(D17), 17307. https://doi.org/10.1029/2008JD011369

Sarwar, G., Simon, H., Bhave, P., & Yarwood, G. (2012). Examining the impact of heterogeneous nitryl chloride production on air quality across the United States. *Atmos. Chem. Phys*, *12*, 6455–6473. https://doi.org/10.5194/acp-12-6455-2012

Schichtel, B. A., Gebhart, K. A., Morris, K. H., Cheatham, J. R., Vimont, J., Larson, R. S., & Beachley, G. (2019). Long-term trends of wet inorganic nitrogen deposition in Rocky Mountain National Park: Influence of missing data imputation methods and associated uncertainty. *Science of The Total Environment*, *687*, 817–826. https://doi.org/10.1016/j.scitotenv.2019.06.104

Schultz, M. G., Jacob, D. J., Bradshaw, J. D., Sandholm, S. T., Dibb, J. E., Talbot, R. W., & Singh, H. B. (2000). Chemical NO x budget in the upper troposphere over the tropical South Pacific. *Journal of Geophysical Research: Atmospheres*, *105*(D5), 6669–6679. https://doi.org/10.1029/1999JD900994

Sindelarova, K., Granier, C., Bouarar, I., Guenther, A., Tilmes, S., Stavrakou, T., et al. (2014). Global data set of biogenic VOC emissions calculated by the MEGAN model over the last 30 years. *Atmos. Chem. Phys*, *14*, 9317–9341. https://doi.org/10.5194/acp-14-9317-2014

Stanier, C. O., Pierce, R. B., Abdi-Oskouei, M., Adelman, Z. E., Al-Saadi, J., Alwe, H. D., et al. (2021). Overview of the Lake Michigan Ozone Study 2017. *Bulletin of the American Meteorological Society*, *102*(12), E2207–E2225. https://doi.org/10.1175/BAMS-D-20-0061.1

Staudt, S., Gord, J. R., Karimova, N. V., Mcduffie, E. E., Brown, S. S., Gerber, R. B., et al. (2019). Sulfate and Carboxylate Suppress the Formation of ClNO2 at Atmospheric Interfaces. *ACS Earth Space Chem*, *3*(9). https://doi.org/10.1021/acsearthspacechem.9b00177

Stroud, C., Madronich, S., Atlas, E., Ridley, B., Flocke, F., Weinheimer, A., et al. (2003). Photochemistry in the arctic free troposphere: NOx budget and the role of odd nitrogen reservoir recycling. *Atmospheric Environment*, *37*(24), 3351–3364. https://doi.org/10.1016/S1352-2310(03)00353-4

Stutz, J. (2004). Vertical profiles of NO3, N2O5, O3, and NOx in the nocturnal boundary layer: 1. Observations during the Texas Air Quality Study 2000. *Journal of Geophysical Research*, *109*(D12), D12306. https://doi.org/10.1029/2003JD004209

Thornton, J. A., Braban, C. F., & Abbatt, J. P. D. (2003). N2O5 hydrolysis on sub-micron organic aerosols: the effect of relative humidity, particle phase, and particle size. *Physical Chemistry Chemical Physics*, *5*, 4593–4603. https://doi.org/10.1039/b307498f

US EPA. (2021). EQUATESv1.0: Emissions, WRF/MCIP, CMAQv5.3.2 Data -- 2002-2019 US_12km and NHEMI_108km (Version V5) [Data set]. UNC Dataverse. https://doi.org/10.15139/S3/F2KJSK

U.S. EPA. (2021). Our Nation's Air: Trends through 2021. Retrieved from https://gispub.epa.gov/air/trendsreport/2022/

Vermeuel, M. P., Novak, G. A., Alwe, H. D., Hughes, D. D., Kaleel, R., Dickens, A. F., et al. (2019). Sensitivity of Ozone Production to NOx and VOC Along the Lake Michigan Coastline. *Journal of Geophysical Research: Atmospheres*, *124*(20), 10989–11006. https://doi.org/10.1029/2019JD030842

Vrekoussis, M., Mihalopoulos, N., Gerasopoulos, E., Kanakidou, M., Crutzen, P. J., & Lelieveld, J. (2007). Two-years of NO3 radical observations in the boundary layer over the Eastern Mediterranean. *Atmospheric Chemistry and Physics*, *7*(2), 315–327. https://doi.org/10.5194/acp-7-315-2007

Walker, J. T., Beachley, G., Amos, H. M., Baron, J. S., Bash, J., Baumgardner, R., et al. (2019). Toward the improvement of total nitrogen deposition budgets in the United States. *Science of The Total Environment*, *691*, 1328–1352. https://doi.org/10.1016/j.scitotenv.2019.07.058

Wang, S., Ackermann, R., & Stutz, J. (2006). Vertical profiles of O3 and NOx chemistry in the polluted nocturnal boundary layer in Phoenix, AZ: I. Field observations by long-path DOAS. *Atmos. Chem. Phys*, *6*, 2671–2693.

Warneke, C., de Gouw, J. A., Goldan, P. D., Kuster, W. C., Williams, E. J., Lerner, B. M., et al. (2004). Comparison of daytime and nighttime oxidation of biogenic and anthropogenic VOCs along the New England coast in summer during New England Air Quality Study 2002. *Journal of Geophysical Research: Atmospheres*, *109*(D10). https://doi.org/10.1029/2003JD004424

Wayne, R. P., Barnes, I., Biggs, P., Burrows, J. P., Canosa-Mas, C. E., Hjorth, J., et al. (1991). The nitrate radical: Physics, chemistry, and the atmosphere. *Atmospheric Environment. Part A. General Topics*, *25*(1), 1–203. https://doi.org/10.1016/0960-1686(91)90192-A

Whiteman, C. D., & McKee, T. B. (1977). Observations of vertical atmospheric structure in a deep mountain valley. *Archiv Für Meteorologie, Geophysik Und Bioklimatologie Serie A*, *26*(1), 39–50. https://doi.org/10.1007/BF02246534

Whiteman, C. D., Zhong, S., Shaw, W. J., Hubbe, J. M., Bian, X., & Mittelstadt, J. (2001). Cold Pools in the Columbia Basin. *Weather and Forecasting*, *16*(4), 432–447. https://doi.org/10.1175/1520-0434(2001)016<0432:CPITCB>2.0.CO;2

Whiteman, C. D., Hoch, S. W., Horel, J. D., & Charland, A. (2014). Relationship between particulate air pollution and meteorological variables in Utah's Salt Lake Valley. *Atmospheric Environment*, *94*, 742–753. https://doi.org/10.1016/j.atmosenv.2014.06.012

Wright, D. B., Bosma, C. D., & Lopez-Cantu, T. (2019). U.S. Hydrologic Design Standards Insufficient Due to Large Increases in Frequency of Rainfall Extremes. *Geophysical Research Letters*, *46*(14), 8144–8153. https://doi.org/10.1029/2019GL083235

Wu, C. H., Morris, E. D., & Niki, H. (1973). Reaction of nitrogen dioxide with ozone. *The Journal of Physical Chemistry*, *77*(21), 2507–2511. https://doi.org/10.1021/j100907a003

Zhang, L., Jacob, D. J., Knipping, E. M., Kumar, N., Munger, J. W., Carouge, C. C., et al. (2012). Nitrogen deposition to the United States: distribution, sources, and processes. *Atmospheric Chemistry and Physics*, *12*(10), 4539–4554. https://doi.org/10.5194/acp-12-4539-2012

Chapter 5 Sensitivity of the CMAQ model to sea spray aerosol emission source functions

Highlights

- Changing sea spray source function in the CMAQ model results in a 18% decrease in accumulation mode particle number concentration and a 27% decrease in coarse mode particle number concentration
- Adding Aitken mode particles to CMAQ sea spray emissions more than doubles Aitken mode number concentration across the US
- The changes in sea spray source function affected heterogeneous loss of N_2O_5 in all modes by increasing surface area in the Aitken mode but decreasing surface area in the accumulation and coarse modes

Abstract

Sea spray aerosol (SSA) contribute to total aerosol mass in both continental and marine environments. Although these particles affect heterogeneous chemistry and climate, their emission in chemical transport models excludes the smallest particle sizes. I assessed the sensitivity of the EPA Community Multiscale Air Quality (CMAQ) model to representations of sea spray emission with the goal of highlighting the impact these particles have on heterogeneous chemistry. By changing the SSA source function in CMAQ, I decreased accumulation and coarse mode emissions, but increased Aitken mode emissions. The increase in Aitken mode emissions resulted in an over 200% increase in particle number and surface area concentrations in this

mode. The large increase in Aitken mode particles may be in part because CMAQ tends to underestimate emissions in this mode from other sources. The changes to modal surface area resulted in a similar impact to heterogeneous loss of N_2O_5 to the particle phase and an over 200% increase in Aitken mode heterogeneous N_2O_5 reaction rate. Future work should assess how modal SSA particle composition affects heterogeneous N_2O_5 loss in the CMAQ model.

5.1 Introduction

Sea spray aerosol (SSA) particles are formed through the physical interactions between wind and the ocean surface (Lewis & Schwartz, 2004; Prather et al., 2013). Sea spray particles affect the chemistry impacting air quality (Finlayson-Pitts, 2003; Simpson et al., 2015) by catalyzing reactions at the particle surface or altering the particle composition through bulk processes (Abbatt et al., 2012; Bertram et al., 2018). They also impact climate through direct and indirect radiative effects (DeMott et al., 2016; Murphy et al., 1998; Partanen et al., 2014). Despite their importance in these atmospheric processes, there is disagreement on how to best model SSA emissions in models, in part because of the complexities surrounding formation (Grythe et al., 2014; Meskhidze et al., 2013)

Several mechanisms influence SSA size, composition, and emission rates. Particles formed when high wind speeds pull spume off of wave crests are the largest in size (D >10 μm) (Monahan et al., 1983; Smith & Adamski, 1998). Although some SSA emission functions include spume droplet formation (Spada et al., 2013), these larger particles are often excluded from atmospheric chemistry models due to shorter atmospheric lifetimes associated with gravitational settling (Andreas, 1992; Quinn et al., 2015). Particles formed through jet drops are intermediate SSA of

sizes between 1-10 µm (Grythe et al., 2014; Lewis & Schwartz, 2004). Recent research indicates that jet drops can also produce submicron particles (Wang et al., 2017). Jet drop particles have variable composition that may be similar to bulk seawater, the sea surface microlayer, or neither (Blanchard, 1963; Jayarathne et al., 2016; Wang et al., 2017). Particles formed through film drops are typically smallest in size and have a composition representative of the sea surface microlayer but with enrichment in cations and organic carbon (Jayarathne et al., 2016; Keene et al., 2007; Spiel, 1998; Wang et al., 2015). Overall, the mechanism of SSA particle formation will affect the size distribution and the composition of the emitted particles.

There are several proposed representations of SSA formation in chemical transport models, called source functions. In their review of existing source functions, Grythe et al. (2014) found over 50 potential formulations that used some combination of wind, temperature, white cap coverage, surf zone area, and salinity to represent the flux of SSA particles. Each source function is only considered valid over a specific range of particle sizes because of the different formation mechanisms that are represented, and the data used in the development of the source function. For example, the Gong-Monahan function was derived using field measurements and laboratory data of open-ocean particle formation to model formation of particles of diameter 0.07-20 µm (Gong, 2003; Monahan & Spillane, 1986). In comparison, a source function using surf zone measurements rather than the open ocean data has a valid particle size of 0.8-10 µm (De Leeuw et al., 2000; De Leeuw et al., 2011). Other source functions have been derived from modifying existing functions with additional dependencies such as temperature (Jaeglé et al., 2011) or salinity (Neumann et al., 2016). Depending on the source function used, chemical transport models predict different size distributions and number fluxes of emitted SSA particles.

Here, I assess the current assumptions of modal SSA emissions in the EPA Community Multiscale Air Quality (CMAQ) model by adding in the formation of Aitken mode particles and changing the source function calculation. The CMAQ model is a chemical transport model by regulators to model air quality, so it is important to have accurate representations of particle formation mechanisms. Despite the growing body of literature showing that jet drops greatly impact the size distributions of emitted particles, there have been no updates to SSA emission in CMAQ since version 5.2.

The first representation of SSA in CMAQ was added to the model version 4.5 and used open-ocean formation by the Gong-Monahan method to create particles in the accumulation and coarse modes (Sarwar & Bhave, 2007). The density and composition of these particles is assumed to be constant in both modes regardless of formation location and time (Gantt et al., 2015; Nolte et al., 2008). The method was later adjusted to account for sea surface temperature (Gantt et al., 2015; Jaeglé et al., 2011; Ovadnevaite et al., 2014). In CMAQ version 4.7, formation of SSA by wave breaking along the coast was included by assuming 100% whitecap coverage in the Gong-Monahan method for a 50 m coastal surf zone, which improved the model underpredictions of several particle species, including Na^+ and Cl^- (Kelly et al., 2010). The surf-zone inclusion was removed for CMAQ versions 5.1 and later. To replace the surf zone approach, Gantt et al. (2015) forced the Gong-Monahan method to emit more particles of smaller diameter by decreasing a tunable parameter θ, which controls the size distribution of the emitted particles. The authors found that $\theta = 8$ increased fine mode SSA emissions relative to coarse mode emissions and improved predictions of particle composition compared to the original setting of $\theta = 30$. The representation of sea spray aerosol in CMAQ affect particle chloride concentrations and

chemistry, resulting in up to a 12 ppb increase in daily maximum 1 hr ozone (Kelly et al., 2010; Nolte et al., 2015; Sarwar & Bhave, 2007). Heterogeneous mechanisms such as N_2O_5 uptake are also affected by sea spray aerosol composition, which further affects daytime NO_x and ozone concentrations (Bertram et al., 2018; Bondy et al., 2017).

Our study presents an analysis of the sensitivity of particle size distributions and heterogeneous chemistry in CMAQ to representations of sea spray aerosol emissions. I evaluate the sensitivity of modal particle number and surface area concentration to the source function changes in Sect. 3. Further factors impacting SSA formation are discussed in Sect. 4.

5.2 Methods

This study employs CMAQ version 5.3.2 with aero7 aerosol chemistry (Appel et al., 2021), the Carbon Bond 6 chemical mechanism (Emery et al., 2015; Luecken et al., 2019), and in-line photolysis. CMAQ was run with 35 vertical layers with a top of approximately 100 hPa and a 12 km by 12 km horizontal resolution over the contiguous U.S. on the 12US1 domain (299 by 459 grid points) from the EPA Air QUAlity Time Series (EQUATES) project (Foley et al., 2023). I ran the model for July 2019 with a 10 day spin up period. Meteorology, anthropogenic emissions, and fire emissions were from the EPA EQUATES project data warehouse (US EPA, 2021). Biogenic emissions were calculated inline using the Biogenic Emission Inventory System (BEIS) version 3.6.1 with the Biogenic Emissions Landuse Database version 5 (Appel et al., 2021).

The default CMAQ configuration in the sea spray emission module includes a look-up table for geometric mean diameter (D_g) and standard deviation ($\boldsymbol{\sigma}_{\mathrm{g}}$) at each RH between 45-99%

(136 total values) for the accumulation mode and the coarse mode. The reference D_g are the modal geometric mean diameters described by Binkowski and Roselle (2003), and the D_g at each RH is calculated using the size correction factors in Eq. 1-2. (Gantt et al., 2015; Lewis & Schwartz, 2006; Zhang et al., 2005; Zhang et al., 2006). These size correction factors assume sea salt particles have a composition similar to that of bulk seawater and therefore their hygroscopicity is a function of the relative fraction of bulk seawater ions and respective water activity (Zhang et al., 2005). The validity of this assumption is assessed in Sect. 4.

$$C^{80}(RH) = \frac{C^0(RH)}{1.97} \qquad \text{Eq. 1}$$

$$C^0(RH) = 28.376 - 205.44RH + 653.37RH^2 - 1031.7RH^3 + 803.18RH^4 - 247.08RH^5 \qquad \text{Eq. 2}$$

Our work updates this sea spray emission module based on the Grythe et al. (2014) source function (with and without Aitken mode particles). In updating the CMAQ sea spray emission, I maintained the RH-dependent look-up tables of D_g and $\boldsymbol{\sigma}_{\mathrm{g}}$ using the same correction factors but included an additional set of tables for the Aitken mode. I first populated D_g look-up tables for the CMAQ sea spray emission module using the method discussed above, using only the RH size correction factors, which is currently employed in CMAQ (Gantt et al., 2015). For this method, I used geometric mean diameter and standard deviation of sea spray aerosol particles generated in the Scripps Ocean-Atmosphere Research Simulator (SOARS) combined wind tunnel and wave channel facility. Within the SOARS facility, SSA was generated from heavily filtered seawater originating off the Scripps pier with wave amplitude around 43 cm and whitecap equivalent 10

m wind speed of around 11 m/s. The particle sizes were measured at or below 45% RH, considered "dry", and this was our reference point for each subsequent RH diameter calculation. The D_g and $\boldsymbol{\sigma}_g$ tables were then populated with values assuming particle growth of the dry wave channel D_g and $\boldsymbol{\sigma}_g$ based on the Zhang et al. (2005) size correction factors.

In addition to D_g and $\boldsymbol{\sigma}_g$ tables, the default CMAQ sea spray emission module contains modal RH-dependent tables of number fluxes and an RH-dependent table of total volume flux, integrated over the entire accumulation and coarse modes. Rather than replicate these look-up tables, I had CMAQ calculate number flux in-line using the Grythe et al. (2014) source function (Eq. 3). This method is an adaptation of the Smith and Harrison (1998) method that has been extended to smaller particle sizes and includes the effects of sea surface temperature (Grythe et al., 2014; Jaeglé et al., 2011). I converted number flux to modal mass flux using Eq. 4 (Binkowski & Roselle, 2003). I then followed the existing module code to calculate the third and second wet and dry moments for each mode.

$$\frac{dF(D_p, U_{10}, T)}{dD_p} = T_w[235U_{10}^{3.5}A + 0.2U_{10}^{3.5}B + 6.8U_{10}^{3}C] \quad \text{Eq. 3}$$

$$A = exp\left(-0.55\left[\ln\frac{D_p}{0.1}\right]^2\right),\ B = exp\left(-1.5\left[\ln\frac{D_p}{3}\right]^2\right),\ C = exp\left(-\left[\ln\frac{D_p}{30}\right]^2\right)$$

$$T_w = 0.3 + 0.1T - 0.0076T^2 + 0.00021T^3$$

$$\frac{dMass}{dt} = \frac{\pi}{6}\rho d_{3.5}^3\frac{dF}{dD_p} \quad \text{Eq. 4}$$

I conducted three CMAQ simulations to compare the two sea spray source functions (Gong03 and Grythe14) and the impact of adding Aitken mode particles (noATKN and w/ATKN). Each simulation was conducted over the continental US on a 12 km by 12 km horizontal

resolution for the entire month of July 2019. The first simulation used the default conditions for the D_g and $\boldsymbol{\sigma}_{\mathrm{g}}$ tables and flux calculations, hereafter referred to as Gong03. For the second simulation, I updated the accumulation and coarse mode particle D_g and $\boldsymbol{\sigma}_{\mathrm{g}}$ tables with wave channel data and modified the flux source function to the Grythe et al. (2014) method but did not include Aitken mode particles. This case is hereafter referred to as Grythe14 noATKN. For the third model run, I added the Aitken mode tables and flux calculations to the Grythe et al. (2014) source function. This case is hereafter referred to as Grythe14 w/ATKN.

5.3 Results

By changing the SSA source function and adding Aitken mode particles, I changed the sea spray emission in all modes, resulting in different number concentrations of emitted sea spray aerosol. Figure 1 shows the modal number distributions for the three tested SSA source functions (Gong03, Grythe14 noATKN, Grythe14 w/ATKN). I added Aitken mode emissions to the Grythe14 w/ATKN case, represented by the solid blue line in Figure 1.

When using the Grythe14 source function, with or without Aitken mode, emission in the accumulation and coarse modes decreases relative to Gong03. The decrease in accumulation mode is expected, given that the source function is no longer forced towards smaller particles. Previously, Gantt et al. (2015) demonstrated that a smaller θ value in the Gong-Monahan source function would bias model SSA emission towards accumulation mode particles (Fig. S1 of Gantt et al. (2015)). To push the sea spray emission towards smaller sizes, the θ value was set at 8 rather than the original recommendation of 30 in Gong (2003). Without the theta correction

factor, the emission distribution between accumulation and coarse modes is no longer forced towards smaller particle sizes, and accumulation mode emission decreases.

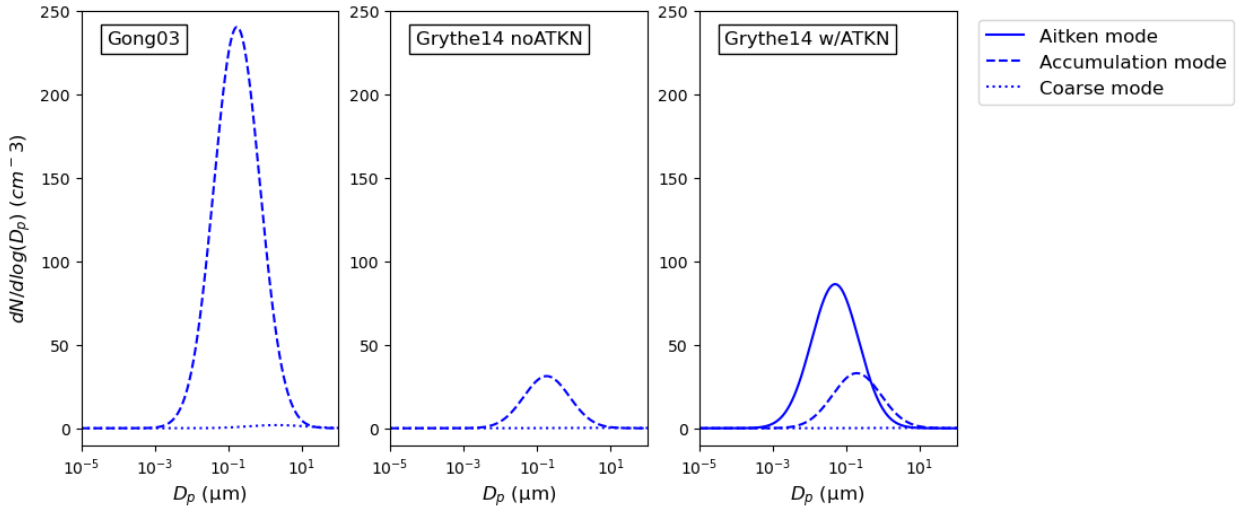

Figure 1. Average number distribution of emitted sea spray aerosol particles using the three different SSA source functions during July 2019.

Although the sea spray number flux distributions show a difference between the two source functions, the impact on total particle number concentrations over the entire CONUS area is small for the coarse and accumulation modes. Figure 2 shows the number distribution for the two source functions averaged over the entire CMAQ domain. Table 1 lists the percent differences in particle number concentration, geometric mean diameter, standard deviation, and surface area for each mode.

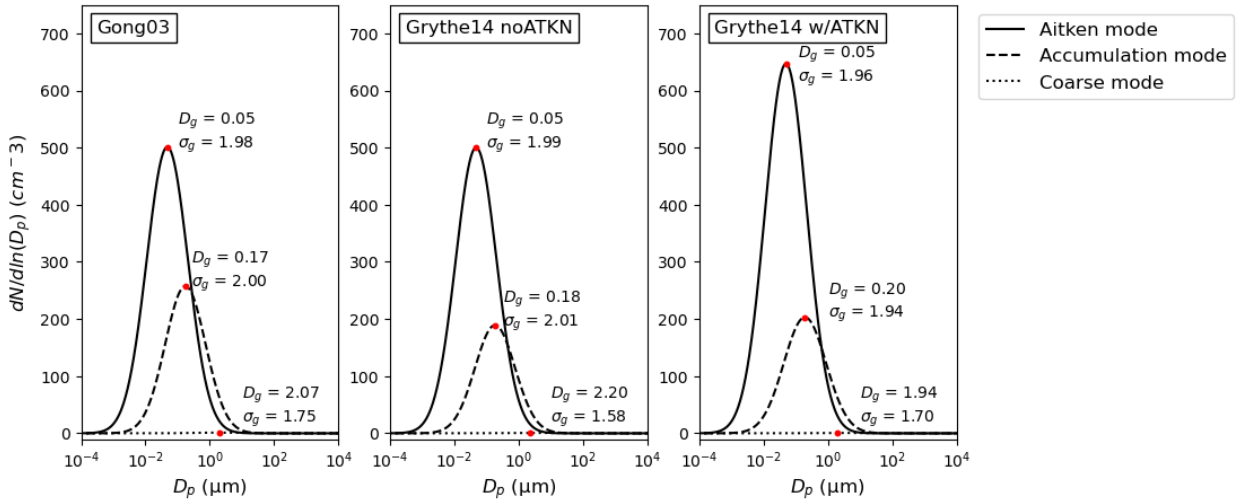

Figure 2. Modal number distributions, averaged over the entire study domain and time, for the three SSA source functions.

Both Grythe14 cases result in statistically significantly different number and surface area concentrations for all modes compared to the Gong03 case with a Mann-Whitney U test at 95% confidence. This is interesting given that no Aitken mode emissions were added to the Grythe14 noATKN case. Aitken mode particles in CMAQ are affected by production processes such as nucleation and primary emission as well as loss processes such as deposition, coagulation with accumulation mode particles, and growth by condensation to accumulation mode (Byun & Schere, 2006). Transport can affect particle number by both increasing and decreasing the concentration. The increase in Aitken mode particles cannot be due to additional primary emissions or nucleation in the Grythe14 noATKN case, therefore a decrease in one of the three loss pathways is responsible for the change. It is unlikely that the increase in Aitken mode particles is due to decreases in wet or dry deposition or transport because the same meteorological inputs were used in all cases. Similarly, no change was made to the gas-phase condensation growth pathways. Thus, this increase in the Aitken mode number concentration in

Grythe14 noATKN relative to Gong03 may be due to the decrease in coagulation with larger particles.

CMAQ counts intermodal coagulation as a decrease in Aitken mode number concentration and an increase in accumulation mode volume and surface area but not number concentration (Binkowski & Roselle, 2003). The rate of coagulation depends on the number of larger particles available to collide with, so a decrease in accumulation mode particles results in a decrease in intermodal coagulation. Previous work has shown that intermodal coagulation in CMAQ can have a significant impact on particle sizes and concentrations (Byun & Schere, 2006; Tsai et al., 2015).

The Grythe14 w/ATKN case increased Aitken mode number concentration as expected. The additional emission source more than doubled the average number concentration over CONUS. This implies that sea spray aerosols are responsible for approximately half of all Aitken mode particles. Some previous studies have found that SSA make up a large fraction of total aerosol mass and number, even at inland sites (Bondy et al., 2017; Textor et al., 2006; Xu et al., 2022), while other studies find that SSA is a small contributor to Aitken and accumulation modes (Quinn et al., 2017). The CMAQ model tends to underestimate particle number concentration while overestimating particle diameter (Nolte et al., 2015; Park et al., 2006), meaning that the model predicts few small particles. The addition of Aitken mode sea spray emissions may have resulted in such a large increase in total number of particles because the model currently tends to underestimate particles in this mode.

In the Grythe14 w/ATKN case, geometric mean diameter D_g increased by about 7% while standard deviation decreased slightly. This indicates that the particles in the Aitken mode were

more tightly clustered around a larger particle diameter than in the Gong03 case. The sea spray aerosol size distributions from the wave channel were fit to the CMAQ modes, but this was done assuming dry particles. The emitted sea spray particles would all have larger diameters depending on relative humidity, thus increasing average particle diameter in each mode. All Grythe14 D_g percent differences in Table 1 are positive except the Grythe14 noATKN Aitken mode and the Grythe14 w/ATKN coarse mode. The geometric mean diameter of Aitken mode particles in the Grythe14 noATKN case decreased while standard deviation increased. While particles on average got smaller, the spread increased so there were more small and large particles within the Aitken mode. In the Grythe14 w/ATKN coarse mode, D_g and $\boldsymbol{\sigma}_{\mathrm{g}}$ both decreased relative to Gong03, meaning that the particles were more tightly clustered around a smaller mean diameter. Since there were no changes to coarse mode chemistry or processing between the two Grythe14 cases, the difference in coarse mode D_g and $\boldsymbol{\sigma}_{\mathrm{g}}$ between the two cases may be due to coagulation with Aitken mode particles resulting in increased settling out of the largest particles (Tsai et al., 2015).

Table 1. Percent differences between Grythe14 and Gong03 source functions

	Grythe14 noATKN				**Grythe14 w/ATKN**			
	D_g (%)	**$\boldsymbol{\sigma}_g$ (%)**	**N_t (%)**	**SA (%)**	**D_g (%)**	**$\boldsymbol{\sigma}_g$ (%)**	**N_t (%)**	**SA (%)**
Aitken	-0.67	0.60	1.58	2.32	7.13	-0.25	241.12	285.89
Accumulation	5.70	0.63	-17.86	-10.50	15.58	-2.76	-16.60	-5.42
Coarse	4.24	-9.75	-27.22	-26.82	-5.52	-3.12	-27.01	-29.92

In addition to number concentration, particle surface area is impacted by the changed source functions (Figure 3). As expected, larger particle modes contribute more to surface area.

Accumulation mode accounts for most of the particle surface area on average for all three source functions. Aitken mode surface area is greatest in the Grythe14 w/ATKN case, again more than doubling relative to Gong03. Coarse mode surface area in both Grythe14 cases is lower than for Gong03, which is also consistent with the decrease in number concentration.

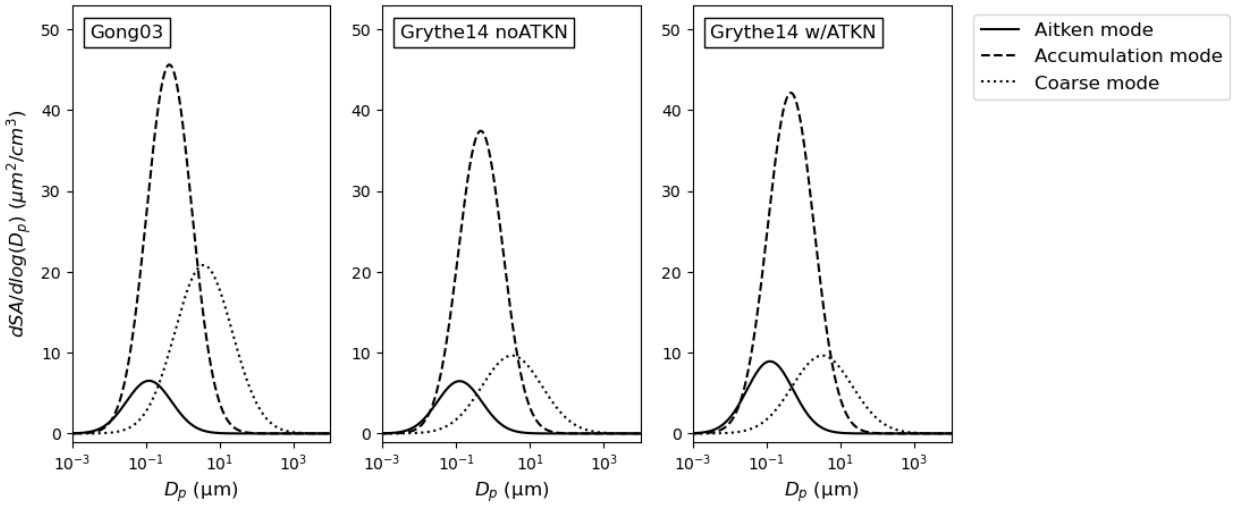

Figure 3. Surface area distributions, averaged over the entire study domain and time, for the three SSA source functions.

Particle surface area plays a role in modulating the impact of particles on air quality through heterogeneous reactions. For example, the loss of N_2O_5 to particles depends on modal surface area, as shown in Eq. 5. Because the particle surface area changed with each Grythe14 case, I expect that heterogeneous loss of N_2O_5 will be affected as well. Table 2 lists the mean reaction rate (k_{het}) for each case and the percent difference between the Grythe14 cases and Gong03. Heterogeneous reaction rate increased in the Aitken mode for both Grythe14 cases, while accumulation and coarse modes saw decreases in all cases, consistent with the changes in surface area.

$$L(N_2O_5) = \sum_i [N_2O_5] k_{het,i} = \sum_i [N_2O_5] \frac{\gamma(N_2O_5)_i \times SA_i \times c}{4} \qquad \text{Eq. 5}$$

Although the percent differences follow similar trends as surface area, they are not identical. This is because the uptake coefficient, gamma, depends on particle composition. The increase in sea spray aerosol emission changes the overall particle composition relative to the Gong03 case, resulting in changes to gamma. In all three cases, I used the default CMAQ uptake parameterizations for fine and coarse modes. The CMAQ model calculates N_2O_5 uptake for fine (Aitken + accumulation) and coarse modes rather than separately for each mode. In the fine mode, the default uptake parameterization assumes that uptake will increase with increasing sulfate and ammonium concentration and decrease with increasing nitrate (Davis et al., 2008). The assumed SSA composition in CMAQ is about 8% sulfate, with no contribution from nitrate or ammonium. The additional sulfate to total particle composition is likely responsible for the larger positive percent differences in Aitken mode k_{het} compared to surface area and the smaller negative percent differences in accumulation mode k_{het} compared to surface area.

In contrast to the fine modes, coarse mode gamma depends on particle water and chloride (Bertram & Thornton, 2009; Sarwar et al., 2012). The decrease in coarse mode SSA emissions in the Grythe14 cases means there is a smaller particle chloride contribution to this mode, and a resulting decrease in gamma relative to the Gong03 case. Thus, the percent differences for coarse mode k_{het} are more negative than coarse mode surface area.

Table 2. Average heterogeneous reaction rates and percent difference for each mode.

	Gong03	Grythe14 noATKN	Grythe14 w/ATKN
Aitken k_{het} (/s)	3.7e-06	3.8e-06	5.5e-06
(percent difference from Gong03)		(6.23%)	(294.18%)
Accumulation k_{het} (/s)	2.7e-05	2.4e-05	2.5e-05
(percent difference from Gong03)		(-7.85%)	(-4.64%)
Coarse k_{het} (/s)	1.6e-05	7.8e-06	7.0e-06
(percent difference from Gong03)		(-30.33%)	(-33.42%)

The increase in k_{het} in the Aitken mode and decrease in the coarse mode means that loss of N_2O_5 by heterogeneous uptake will occur more in fine mode particles in the Grythe14 cases relative to the Gong03 case. The decrease in accumulation mode will offset the increase in Aitken mode k_{het} to some degree, although this is a small change in the Grythe14 w/ATKN case relative to the Aitken mode increase. The ratio of loss of N_2O_5 in the fine mode relative to total loss can be seen in the frequency distribution in Figure 4. As expected, there is a slight increase in fine mode loss of N_2O_5 relative to total loss in the Grythe14 noATKN case, and a larger increase in the Grythe14 w/ATKN case. Adding this new Aitken mode SSA emission source, which contains inorganic composition only, results in more loss of N_2O_5 to fine mode particles, thus affecting both air quality and particle composition. However, I did not modify sea spray aerosol modal composition, which may have resulted in an overestimate of the impact of SSA on increasing N_2O_5 uptake. A large body of laboratory and field studies indicate that smaller sea spray particles have a different composition than larger particles with a larger organic fraction (Ault et al., 2013; Kaluarachchi et al., 2022; Lee et al., 2020). I discuss the impact of sea spray aerosol composition in the next section.

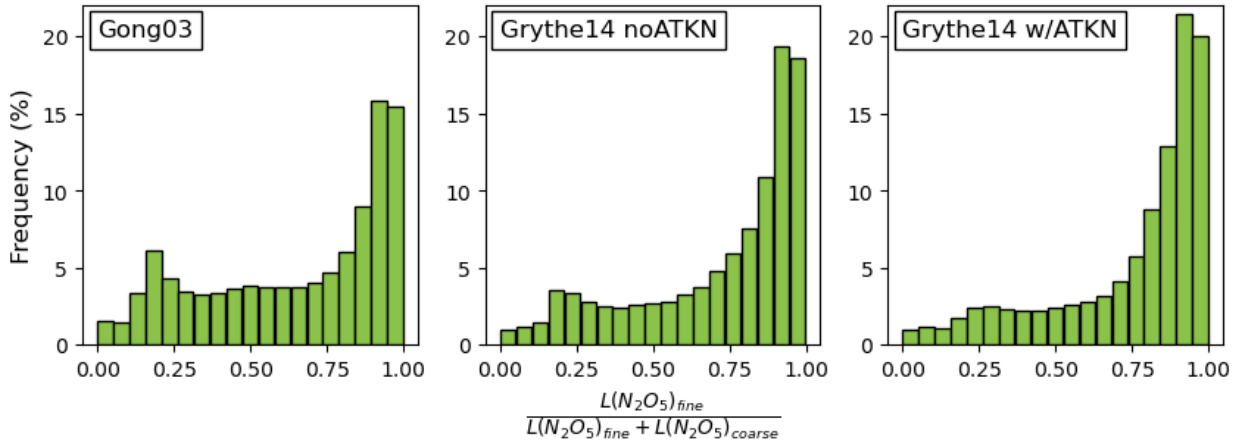

Figure 4. Frequency distribution of the ratio of fine mode versus total N_2O_5 loss to particles. The fine mode is a combination of Aitken and accumulation modes.

5.4 Discussion

5.4.1 Impact of particle composition

The morphology and composition of SSA particles has been shown to vary as a function of biological activity and size of the particles (Ault et al., 2013; Kaluarachchi et al., 2022; Lee et al., 2020). The size-dependent morphologies and composition impact the hygroscopicity of the particles, meaning there is an influence on the water and ice nucleation capacity, and therefore radiative forcing, of the emitted SSA (Cochran et al., 2017; Kaluarachchi et al., 2022; Quinn et al., 2015; Schill et al., 2015). Composition also determines the ability of particles to undergo heterogeneous reactions that affect air quality (Bertram et al., 2018). Despite these complexities, chemical transport models often assume that SSA have a consistent composition across sizes, and that all species in the SSA particles are uniformly distributed throughout the particle volume (i.e., internally mixed). Only recently have SSA source functions sought to include the effects of biology on changing particle composition (Burrows et al., 2014; Quinn et al., 2015). In CMAQ, sea spray particles are assumed to have a constant composition in fine and coarse modes, although

the labeling of the particle species varies in the coarse mode due to differences in species tracking.

There are two main avenues through which particle composition is included in SSA formation in CMAQ: hygroscopic growth of particles at some RH, and conversion from volume flux to mass flux using particle density. I will first assess the impact of hygroscopic growth factor on $D_g(RH)$. Currently, D_g at each RH is calculated using correction factors that assume particle composition is like bulk seawater. However, real sea spray particles do not have a composition identical to bulk seawater, and the hygroscopic growth of SSA depends on the ratio and type of organic and inorganic components (Bertram et al., 2018; Cochran et al., 2017).

I performed a sensitivity analysis for the calculation of D_g look-up tables using a variety of hygroscopic growth factors to account for differences in particle composition. I calculated a reference D_g at 80% RH using three different hygroscopic growth factors (HGFs) assuming the wave channel D_g values were dry ($RH << 45\%$). Then, I calculated D_g at each RH using the 80% RH reference diameter correction factor in Eq. 1 and 2. Although this correction factor again makes assumptions about particle composition, I can use the differences in HGF to evaluate how organic versus inorganic composition can affect particle size distributions in the RH range used in CMAQ. It should be noted that I did not use the growth factors that are derived for the wave channel particles because these growth factors were for 75, 85, and 92% RH rather than 80% (Prather et al., 2013).

$$HGF = {d_{wet}}/{d_{dry}} \qquad \text{Eq. 6}$$

Table 3 lists the percent differences between the baseline $D_g(RH)$ that was calculated from the wave channel particle sizes assuming $RH = 45\%$ and the $D_g(RH)$ assuming $RH <<$

45% for a variety of HGFs. Reef salt, although most similar to bulk seawater composition, had the highest difference compared to the baseline while the glucose HGF had the smallest absolute value of difference but decreased $D_g(RH)$ compared to baseline. Reef salt created larger particles while glucose decreased particle size relative to the baseline by inhibiting growth.

Table 3. Impact of hygroscopic growth factors on particle geometric mean diameter

HGF value, representative composition	Mean percent difference (standard deviation)
1.8, reef salt	33.0% (2.03%)
1.62, NaCl/glucose (2:1) mixture	21.5% (2.07%)
1.2, glucose	-7.23% (2.09%)

The second way in which composition is included in SSA formation in CMAQ is the conversion from volume to mass flux using density. CMAQ assumes density of 2162.7 kg/m^3 in each mode. However, smaller particles have a larger organic fraction and smaller inorganic fraction (Ault et al., 2013; Kaluarachchi et al., 2022). The ratio of different cations and anions in the inorganic phase also changes as a function of particle size (Jayarathne et al., 2016; Keene et al., 2007; Salter et al., 2014). These factors would alter density so that Aitken mode particles would have a lower density than coarse mode particles, thus affecting the conversion from volume to mass flux.

Following SSA formation, CMAQ also uses particle composition to calculate the contribution of freshly emitted SSA to each aerosol species. The list of aerosol species in sea spray includes 16 species, even though there are 110 total aerosol species included in CMAQ. This list

includes only inorganic species, no organic species, which may contribute to the general underestimate in organic aerosol within CMAQ. This means that Aitken mode SSA particles in this work have an outsized impact on heterogeneous chemistry, given that they have no organic fraction to reduce or inhibit uptake of species such as N_2O_5. Future modifications to CMAQ SSA should include updating sea spray composition so that it is mode-specific and includes organic components. This will also result in new mode-specific sea spray particle densities.

5.4.2 Further modifications to SSA source functions

The Grythe14 source function depends on sea surface temperature and 10 m wind speed (Grythe et al., 2014). The Gong03 source function also depends on 10 m wind speed (Gong, 2003; Monahan et al., 1983), and the CMAQ implementation of this source function includes the effects of sea surface temperature (Gantt et al., 2015; Jaeglé et al., 2011). The sea spray emission for Gong03 in CMAQ is also modulated by the open ocean versus surf zone fraction (Kelly et al., 2010). Here, I discuss possible changes to the CMAQ inclusion of these factors in calculating sea spray emissions.

In both source functions, wind speed is limited to a maximum speed of 20 m/s. If wind speed in CMAQ exceeds this value, the model uses 20 m/s instead. Higher wind speeds can result in spume droplets (Smith & Harrison, 1998; Spada et al., 2013), which could contribute to coarse mode particles. Analysis of the impact of wind speed on SSA over remote marine environments found a larger influence of wind speed on supermicron particles compared to submicron (Liu et al., 2021). Over the month of July, 0.014% of 10 m wind speed values in sea spray emission grid cells (non-zero open ocean or surf zone fraction) was greater than 20 m/s. This fraction varies by

month, and in January 2019 was 0.25%. In both months, high 10 m wind speeds are infrequent, but could contribute to a new supermicron regime of particle formation. Future work could assess the sensitivity of the CMAQ model to inclusion of spume droplet formation at high wind speeds.

CMAQ assumes a monotonic increase in SSA with increasing temperature to modulate SSA formation at high wind speeds. However, studies have found a suppression of SSA emission with temperature through various processes such as reduction in air entrainment at low temperatures (Christiansen et al., 2019; Salter et al., 2014), and that this suppression is size-dependent (Zábori et al., 2012). Lui et al (2021) found that SSA formation does vary monotonically with sea surface temperature, but that this influence varies by wind speed and is most influential at higher wind speeds. The wind speed dependence is not included in the current linearized sea surface temperature scaling in CMAQ (Ovadnevaite et al., 2014) and future work could assess the impact of wind-speed dependent sea surface temperature scaling on the emission of SSA particles in each mode.

Both the Grythe14 and Gong03 source functions are based on open ocean measurements of sea spray. Neither source function is optimized for surf zone formation, which has been shown to have different sea spray formation mechanisms than the open ocean (De Leeuw et al., 2000). For the Gong03 case, CMAQ addresses differences in surf zone formation by weighting flux by half of the surf zone coverage and the whitecap coverage in that zone (Clarke et al., 2006; Kelly et al., 2010). While Kelly et al. (2010) found that including the surf zone weighting improved CMAQ predictions of SSA over Florida, Neumann et al. (2016) found that there was not a significant difference when including surf zone weighting in CMAQ over the Baltic Sea. This may

be due to the coarse resolution (12 km) of the CMAQ surf zone grid, which is unable to resolve fine-scale features of the Baltic Sea coastline (Neumann et al., 2016). This weighting of the surf zone was not included in the Grythe14 cases, and future work should assess how surf zone weighting might change coastal sea spray emissions with this source function.

Neither source function includes the effects of salinity, which has been proposed in other sea spray source functions (Neumann et al., 2016; Zábori et al., 2012), as salinity impacts particle size and may alter formation mechanism (Mårtensson et al., 2003). Salinity is not a current input variable to CMAQ but could be added as a static variable in the ocean and surf zone mask. By including a scaling factor in CMAQ to account for lower salinity in the Baltic Sea, Neumann et al. (2016) found that sea spray emissions and concentrations of sea spray species decreased slightly. This has implications for the SSA emission composition in the different marine environments that affect CONUS: Pacific and Atlantic oceans and the Gulf of Mexico.

5.5 Conclusions

I tested the sensitivity of particle sizes in the CMAQ model to different sea spray aerosol emission functions. While the average number of emitted sea spray particles decreased relative to the default Gong03 case, there were size-specific impacts to particle number and surface area concentration that has implications for heterogeneous chemistry. Total number concentration in the Aitken mode more than doubled when emission of Aitken mode sea spray particles was included. Accumulation and coarse mode particle number concentrations decreased, as did particle surface area in these modes. Aitken mode surface area increased for both Grythe14

updated cases. The increase in Aitken mode particles when no Aitken mode emission was added is likely due to decreased coagulation with accumulation mode particles.

The changes to sea spray aerosol emission had impacts on N_2O_5 loss to the particle phase by changing both available surface area for uptake and the average particle composition. In the fine mode, both factors were favorable: increasing particle surface area in the Aitken mode and increasing particle sulfate in both Aitken and accumulation modes. However, the accumulation mode showed a decrease in surface area concentration, which modulated the effect of increasing particle sulfate in this mode. In the coarse mode, the decrease in particle surface area and the decrease of particle chloride resulted in lower N_2O_5 loss in the coarse mode relative to the Gong03 default case.

I did not modify sea spray aerosol composition to reflect the dependence on size. Because smaller SSA generally have a larger organic fraction and smaller inorganic fraction, inclusion of size-specific particle composition may reduce heterogeneous uptake to these particles. Future work should assess how size-dependent particle composition affects sea spray aerosol in terms of both emissions and chemistry.

References

Abbatt, J. P. D., Lee, A. K. Y., & Thornton, J. A. (2012). Quantifying trace gas uptake to tropospheric aerosol: recent advances and remaining challenges. *Chemical Society Reviews*, *41*(19), 6555–6581. https://doi.org/10.1039/C2CS35052A

Andreas, E. L. (1992). Sea Spray and the Turbulent Air-Sea Heat Fluxes. *Journal of Geophysical Research*, *97*(C7), 11429–11441. https://doi.org/10.1029/92JC00876

Appel, K. W., Bash, J. O., Fahey, K. M., Foley, K. M., Gilliam, R. C., Hogrefe, C., et al. (2021). The Community Multiscale Air Quality (CMAQ) model versions 5.3 and 5.3.1: system updates and evaluation. *Geoscientific Model Development*, *14*(5), 2867–2897. https://doi.org/10.5194/gmd-14-2867-2021

Ault, A. P., Moffet, R. C., Baltrusaitis, J., Collins, D. B., Ruppel, M. J., Cuadra-Rodriguez, L. A., et al. (2013). Size-Dependent Changes in Sea Spray Aerosol Composition and Properties

with Different Seawater Conditions. *Environmental Science & Technology*, *47*(11), 5603–5612. https://doi.org/10.1021/es400416g

Bertram, T. H., & Thornton, J. A. (2009). Toward a general parameterization of N2O5 reactivity on aqueous particles: the competing effects of particle liquid water, nitrate and chloride. *Atmospheric Chemistry and Physics*, *9*, 8351–8363.

Bertram, T. H., Cochran, R. E., Grassian, V. H., & Stone, E. A. (2018). Sea spray aerosol chemical composition: Elemental and molecular mimics for laboratory studies of heterogeneous and multiphase reactions. *Chemical Society Reviews*, *47*(7). https://doi.org/10.1039/c7cs00008a

Binkowski, F. S., & Roselle, S. J. (2003). Models-3 Community Multiscale Air Quality (CMAQ) model aerosol component 1. Model description. *Journal of Geophysical Research D: Atmospheres*, *108*(6). https://doi.org/10.1029/2001jd001409

Blanchard, D. C. (1963). The electrification of the atmosphere by particles from bubbles in the sea. *Progress in Oceanography*, *1*, 73–202. https://doi.org/10.1016/0079-6611(63)90004-1

Bondy, A. L., Wang, B., Laskin, A., Craig, R. L., Nhliziyo, M. V., Bertman, S. B., et al. (2017). Inland Sea Spray Aerosol Transport and Incomplete Chloride Depletion: Varying Degrees of Reactive Processing Observed during SOAS. *Environmental Science & Technology*, *51*(17), 9533–9542. https://doi.org/10.1021/acs.est.7b02085

Burrows, S. M., Ogunro, O., Frossard, A. A., Russell, L. M., Rasch, P. J., & Elliott, S. (2014). *A physically-based framework for modelling the organic fractionation of sea spray aerosol from bubble film Langmuir equilibria* (preprint). Aerosols/Atmospheric Modelling/Troposphere/Chemistry (chemical composition and reactions). https://doi.org/10.5194/acpd-14-5375-2014

Byun, D., & Schere, K. L. (2006). Review of the Governing Equations, Computational Algorithms, and Other Components of the Models-3 Community Multiscale Air Quality (CMAQ) Modeling System. *Applied Mechanics Reviews*, *59*(2). https://doi.org/10.1115/1.2128636

Christiansen, S., Salter, M. E., Gorokhova, E., Nguyen, Q. T., & Bilde, M. (2019). Sea Spray Aerosol Formation: Laboratory Results on the Role of Air Entrainment, Water Temperature, and Phytoplankton Biomass. *Environmental Science & Technology*, *53*(22), 13107–13116. https://doi.org/10.1021/acs.est.9b04078

Clarke, A. D., Owens, S. R., & Zhou, J. (2006). An ultrafine sea-salt flux from breaking waves: Implications for cloud condensation nuclei in the remote marine atmosphere. *Journal of Geophysical Research: Atmospheres*, *111*(D6), 6202. https://doi.org/10.1029/2005JD006565

Cochran, R. E., Laskina, O., Trueblood, J. V., Estillore, A. D., Morris, H. S., Jayarathne, T., et al. (2017). Molecular Diversity of Sea Spray Aerosol Particles: Impact of Ocean Biology on Particle Composition and Hygroscopicity. *Chem*, *2*(5), 655–667. https://doi.org/10.1016/j.chempr.2017.03.007

Davis, J. M., Bhave, P. V., & Foley, K. M. (2008). Parameterization of N2O5 reaction probabilities on the surface of particles containing ammonium, sulfate, and nitrate. *Atmos. Chem. Phys*, *8*, 5295–5311.

De Leeuw, G., Neele, F. P., Hill, M., Smith, M. H., & Vignati, E. (2000). Production of sea spray aerosol in the surf zone. *Journal of Geophysical Research: Atmospheres*, *105*(D24), 29397–29409. https://doi.org/10.1029/2000JD900549

De Leeuw, G., Andreas, E. L., Anguelova, M. D., Fairall, C. W., Lewis, E. R., O'Dowd, C., et al. (2011). Production flux of sea spray aerosol. *Reviews of Geophysics*, *49*(2), 2001. https://doi.org/10.1029/2010RG000349

DeMott, P. J., Hill, T. C. J., McCluskey, C. S., Prather, K. A., Collins, D. B., Sullivan, R. C., et al. (2016). Sea spray aerosol as a unique source of ice nucleating particles. *Proceedings of the National Academy of Sciences*, *113*(21), 5797–5803. https://doi.org/10.1073/pnas.1514034112

Emery, C., Jung, J., Koo, B., & Yarwood, G. (2015). *Improvements to CAMx Snow Cover Treatments and Carbon Bond Chemical Mechanism for Winter Ozone. Final Report*. Salt Lake City, UT: Ramboll Environ. Retrieved from http://www.deq.utah.gov/locations/U/uintahbasin/docs/2014/03Mar

Finlayson-Pitts, B. J. (2003). The Tropospheric Chemistry of Sea Salt: A Molecular-Level View of the Chemistry of NaCl and NaBr. *Chemical Reviews*, *103*(12), 4801–4822. https://doi.org/10.1021/cr020653t

Foley, K. M., Pouliot, G. A., Eyth, A., Aldridge, M. F., Allen, C., Appel, K. W., et al. (2023). 2002–2017 anthropogenic emissions data for air quality modeling over the United States. *Data in Brief*, *47*, 109022. https://doi.org/10.1016/j.dib.2023.109022

Gantt, B., Kelly, J. T., & Bash, J. O. (2015). Updating sea spray aerosol emissions in the Community Multiscale Air Quality (CMAQ) model version 5.0.2. *Geoscientific Model Development*, *8*(11), 3733–3746. https://doi.org/10.5194/GMD-8-3733-2015

Gong, S. L. (2003). A parameterization of sea-salt aerosol source function for sub- and super-micron particles. *Global Biogeochemical Cycles*, *17*(4), 1097. https://doi.org/10.1029/2003GB002079

Grythe, H., Ström, J., Krejci, R., Quinn, P., & Stohl, A. (2014). A review of sea-spray aerosol source functions using a large global set of sea salt aerosol concentration measurements. *Atmospheric Chemistry and Physics*, *14*(3), 1277–1297. https://doi.org/10.5194/acp-14-1277-2014

Jaeglé, L., Quinn, P. K., Bates, T. S., Alexander, B., & Lin, J. T. (2011). Global distribution of sea salt aerosols: New constraints from in situ and remote sensing observations. *Atmospheric Chemistry and Physics*, *11*(7), 3137–3157. https://doi.org/10.5194/ACP-11-3137-2011

Jayarathne, T., Sultana, C. M., Lee, C., Malfatti, F., Cox, J. L., Pendergraft, M. A., et al. (2016). Enrichment of Saccharides and Divalent Cations in Sea Spray Aerosol During Two Phytoplankton Blooms. *Environmental Science & Technology*, *50*(21), 11511–11520. https://doi.org/10.1021/acs.est.6b02988

Kaluarachchi, C. P., Or, V. W., Lan, Y., Madawala, C. K., Hasenecz, E. S., Crocker, D. R., et al. (2022). Size-Dependent Morphology, Composition, Phase State, and Water Uptake of Nascent Submicrometer Sea Spray Aerosols during a Phytoplankton Bloom. *ACS Earth and Space Chemistry*, *6*(1), 116–130. https://doi.org/10.1021/ACSEARTHSPACECHEM.1C00306/ASSET/IMAGES/LARGE/SP1C00306_0010.JPEG

Keene, W. C., Maring, H., Maben, J. R., Kieber, D. J., Pszenny, A. A. P., Dahl, E. E., et al. (2007). Chemical and physical characteristics of nascent aerosols produced by bursting bubbles at a model air-sea interface. *Journal of Geophysical Research*, *112*(D21), D21202. https://doi.org/10.1029/2007JD008464

Kelly, J. T., Bhave, P. V., Nolte, C. G., Shankar, U., & Foley, K. M. (2010). Simulating emission and chemical evolution of coarse sea-salt particles in the Community Multiscale Air Quality (CMAQ) model. *Geoscientific Model Development*, *3*(1), 257–273. https://doi.org/10.5194/GMD-3-257-2010

Lee, H. D., Wigley, S., Lee, C., Or, V. W., Hasenecz, E. S., Stone, E. A., et al. (2020). Physicochemical Mixing State of Sea Spray Aerosols: Morphologies Exhibit Size Dependence. *ACS Earth and Space Chemistry*, *4*(9), 1604–1611. https://doi.org/10.1021/ACSEARTHSPACECHEM.0C00153/ASSET/IMAGES/LARGE/SP0C00153_0005.JPEG

Lewis, E. R., & Schwartz, S. E. (2004). *Sea Salt Aerosol Production: Mechanisms, Methods, Measurements and Models*. Place of publication not identified: American Geophysical Union.

Lewis, E. R., & Schwartz, S. E. (2006). Comment on "size distribution of sea-salt emissions as a function of relative humidity." *Atmospheric Environment*, *40*(3), 588–590. https://doi.org/10.1016/J.ATMOSENV.2005.08.043

Liu, S., Liu, C.-C., Froyd, K. D., Schill, G. P., Murphy, D. M., Bui, T. P., et al. (2021). Sea spray aerosol concentration modulated by sea surface temperature. *Proceedings of the National Academy of Sciences*, *118*(9), e2020583118. https://doi.org/10.1073/pnas.2020583118

Luecken, D. J., Yarwood, G., & Hutzell, W. T. (2019). Multipollutant modeling of ozone, reactive nitrogen and HAPs across the continental US with CMAQ-CB6. *Atmospheric Environment*, *201*, 62–72. https://doi.org/10.1016/J.ATMOSENV.2018.11.060

Mårtensson, E. M., Nilsson, E. D., De Leeuw, G., Cohen, L. H., & Hansson, H. -C. (2003). Laboratory simulations and parameterization of the primary marine aerosol production. *Journal of Geophysical Research: Atmospheres*, *108*(D9), 2002JD002263. https://doi.org/10.1029/2002JD002263

Meskhidze, N., Petters, M. D., Tsigaridis, K., Bates, T., O'Dowd, C., Reid, J., et al. (2013). Production mechanisms, number concentration, size distribution, chemical composition, and optical properties of sea spray aerosols. *Atmospheric Science Letters*, *14*(4), 207–213. https://doi.org/10.1002/asl2.441

Monahan, E. C., & Spillane, M. C. (1986). The Role of Oceanic Whitecaps in Air-Sea Gas Exchange. In W. Brutsaert & G. H. Jirka (Eds.), *Gas Transfer at Water Surfaces* (pp. 495–503). Dordrecht: Springer Netherlands. https://doi.org/10.1007/978-94-017-1660-4_45

Monahan, E. C., Fairall, C. W., Davidson, K. L., & Boyle, P. J. (1983). Observed inter-relations between 10m winds, ocean whitecaps and marine aerosols. *Quarterly Journal of the Royal Meteorological Society*, *109*(460), 379–392. https://doi.org/10.1002/qj.49710946010

Murphy, D. M., Anderson, J. R., Quinn, P. K., McInnes, L. M., Brechtel, F. J., Kreidenweis, S. M., et al. (1998). Influence of sea-salt on aerosol radiative properties in the Southern Ocean marine boundary layer. *Nature*, *392*(6671), 62–65. https://doi.org/10.1038/32138

Neumann, D., Matthias, V., Bieser, J., Aulinger, A., & Quante, M. (2016). Sensitivity of modeled atmospheric nitrogen species and nitrogen deposition to variations in sea salt emissions in the North Sea and Baltic Sea regions. *Atmospheric Chemistry and Physics*, *16*(5), 2921–2942. https://doi.org/10.5194/acp-16-2921-2016

Nolte, C. G., Bhave, P. V., Arnold, J. R., Dennis, R. L., Zhang, K. M., & Wexler, A. S. (2008). Modeling urban and regional aerosols-Application of the CMAQ-UCD Aerosol Model to Tampa, a coastal urban site. *Atmospheric Environment*, *42*, 3179–3191. https://doi.org/10.1016/j.atmosenv.2007.12.059

Nolte, C. G., Appel, K. W., Kelly, J. T., Bhave, P. V., Fahey, K. M., Collett, J. L., et al. (2015). Evaluation of the Community Multiscale Air Quality (CMAQ) model v5.0 against size-resolved measurements of inorganic particle composition across sites in North America. *Geoscientific Model Development*, *8*(9), 2877–2892. https://doi.org/10.5194/gmd-8-2877-2015

Ovadnevaite, J., Manders, A., De Leeuw, G., Ceburnis, D., Monahan, C., Partanen, A. I., et al. (2014). A sea spray aerosol flux parameterization encapsulating wave state. *Atmospheric Chemistry and Physics*, *14*(4), 1837–1852. https://doi.org/10.5194/ACP-14-1837-2014

Park, S.-K., Marmur, A., Kim, S. B., Tian, D., Hu, Y., McMurry, P. H., & Russell, A. G. (2006). Evaluation of Fine Particle Number Concentrations in CMAQ. *Aerosol Science and Technology*, *40*(11), 985–996. https://doi.org/10.1080/02786820600907353

Partanen, A.-I., Dunne, E. M., Bergman, T., Laakso, A., Kokkola, H., Ovadnevaite, J., et al. (2014). Global modelling of direct and indirect effects of sea spray aerosol using a source function encapsulating wave state. *Atmospheric Chemistry and Physics*, *14*(21), 11731–11752. https://doi.org/10.5194/acp-14-11731-2014

Prather, K. A., Bertram, T. H., Grassian, V. H., Deane, G. B., Stokes, M. D., DeMott, P. J., et al. (2013). Bringing the ocean into the laboratory to probe the chemical complexity of sea spray aerosol. *Proceedings of the National Academy of Sciences of the United States of America*, *110*(19). https://doi.org/10.1073/pnas.1300262110

Quinn, P. K., Collins, D. B., Grassian, V. H., Prather, K. A., & Bates, T. S. (2015). Chemistry and Related Properties of Freshly Emitted Sea Spray Aerosol. *Chemical Reviews*, *115*(10), 4383–4399. https://doi.org/10.1021/cr500713g

Quinn, P. K., Coffman, D. J., Johnson, J. E., Upchurch, L. M., & Bates, T. S. (2017). Small fraction of marine cloud condensation nuclei made up of sea spray aerosol. *Nature Geoscience*, *10*(9), 674–679. https://doi.org/10.1038/ngeo3003

Salter, M. E., Nilsson, E. D., Butcher, A., & Bilde, M. (2014). On the seawater temperature dependence of the sea spray aerosol generated by a continuous plunging jet. *Journal of Geophysical Research: Atmospheres*, *119*(14), 9052–9072. https://doi.org/10.1002/2013JD021376

Sarwar, G., & Bhave, P. V. (2007). Modeling the Effect of Chlorine Emissions on Ozone Levels over the Eastern United States. *Journal of Applied Meteorology and Climatology*, *46*(7), 1009–1019. https://doi.org/10.1175/JAM2519.1

Sarwar, G., Simon, H., Bhave, P., & Yarwood, G. (2012). Examining the impact of heterogeneous nitryl chloride production on air quality across the United States. *Atmos. Chem. Phys*, *12*, 6455–6473. https://doi.org/10.5194/acp-12-6455-2012

Schill, S. R., Collins, D. B., Lee, C., Morris, H. S., Novak, G. A., Prather, K. A., et al. (2015). The Impact of Aerosol Particle Mixing State on the Hygroscopicity of Sea Spray Aerosol. *ACS Central Science*, *1*(3), 132–141. https://doi.org/10.1021/acscentsci.5b00174

Simpson, W. R., Brown, S. S., Saiz-Lopez, A., Thornton, J. A., & Von Glasow, R. (2015). Tropospheric Halogen Chemistry: Sources, Cycling, and Impacts. *Chemical Reviews*, *115*(10), 4035–4062. https://doi.org/10.1021/cr5006638

Smith, B. E., & Adamski, W. J. (1998). Eight-Hour Ozone Trends at Sites in Lake Michigan Ozone Nonattainment Areas. *Journal of the Air & Waste Management Association*, *48*(12), 1204–1206. https://doi.org/10.1080/10473289.1998.10463756

Smith, M. H., & Harrison, N. M. (1998). The sea spray generation function. *Journal of Aerosol Science*, *29*, S189–S190. https://doi.org/10.1016/S0021-8502(98)00280-8

Spada, M., Jorba, O., Pérez García-Pando, C., Janjic, Z., & Baldasano, J. M. (2013). Modeling and evaluation of the global sea-salt aerosol distribution: sensitivity to size-resolved and sea-surface temperature dependent emission schemes. *Atmospheric Chemistry and Physics*, *13*(23), 11735–11755. https://doi.org/10.5194/acp-13-11735-2013

Spiel, D. E. (1998). On the births of film drops from bubbles bursting on seawater surfaces. *Journal of Geophysical Research: Oceans*, *103*(C11), 24907–24918. https://doi.org/10.1029/98JC02233

Textor, C., Schulz, M., Guibert, S., Kinne, S., Balkanski, Y., Bauer, S., et al. (2006). Analysis and quantification of the diversities of aerosol life cycles within AeroCom. *Atmospheric Chemistry and Physics*, *6*(7), 1777–1813. https://doi.org/10.5194/acp-6-1777-2006

Tsai, I., Chen, J., Lin, Y., Chou, C. C., & Chen, W. (2015). Numerical investigation of the coagulation mixing between dust and hygroscopic aerosol particles and its impacts. *Journal of Geophysical Research: Atmospheres*, *120*(9), 4213–4233. https://doi.org/10.1002/2014JD022899

US EPA. (2021). EQUATESv1.0: Emissions, WRF/MCIP, CMAQv5.3.2 Data -- 2002-2019 US_12km and NHEMI_108km (Version V5) [Data set]. UNC Dataverse. https://doi.org/10.15139/S3/F2KJSK

Wang, X., Sultana, C. M., Trueblood, J., Hill, T. C. J., Malfatti, F., Lee, C., et al. (2015). Microbial Control of Sea Spray Aerosol Composition: A Tale of Two Blooms. *ACS Central Science*, *1*(3), 124–131. https://doi.org/10.1021/acscentsci.5b00148

Wang, X., Deane, G. B., Moore, K. A., Ryder, O. S., Stokes, M. D., Beall, C. M., et al. (2017). The role of jet and film drops in controlling the mixing state of submicron sea spray aerosol particles. *Proceedings of the National Academy of Sciences*, *114*(27), 6978–6983. https://doi.org/10.1073/pnas.1702420114

Xu, W., Ovadnevaite, J., Fossum, K. N., Lin, C., Huang, R.-J., Ceburnis, D., & O'Dowd, C. (2022). Sea spray as an obscured source for marine cloud nuclei. *Nature Geoscience*, *15*(4), 282–286. https://doi.org/10.1038/s41561-022-00917-2

Zábori, J., Matisāns, M., Krejci, R., Nilsson, E. D., & Ström, J. (2012). Artificial primary marine aerosol production: a laboratory study with varying water temperature, salinity, and succinic acid concentration. *Atmospheric Chemistry and Physics*, *12*(22), 10709–10724. https://doi.org/10.5194/acp-12-10709-2012

Zhang, K. M., Knipping, E. M., Wexler, A. S., Bhave, P. V., & Tonnesen, G. S. (2005). Size distribution of sea-salt emissions as a function of relative humidity. *Atmospheric Environment*, *39*(18), 3373–3379. https://doi.org/10.1016/J.ATMOSENV.2005.02.032

Zhang, K. M., Knipping, E. M., Wexler, A. S., Bhave, P. V., & Tonnesen, G. S. (2006). Reply to comment on “Size distribution of sea-salt emissions as a function of relative humidity.” *Atmospheric Environment*, *40*(3), 591–592. https://doi.org/10.1016/J.ATMOSENV.2005.08.044

Chapter 6 Conclusions

In my dissertation, I have attempted to answer three questions relevant to heterogeneous NO_x chemistry in the CMAQ model. There are advantages and disadvantages to using CMAQ to understand the chemistry that impacts NO_x air quality. One limitation of the models is that they are representations of the physical world based on assumptions and the best scientific understanding of physical and chemical processes. These assumptions mean that model outputs may not be accurate, and throughout my dissertation I assess several model parametrizations that simplify the processes affecting heterogeneous NO_x chemistry. In this chapter, I will summarize my findings and address limitations to the work as well as future directions for study.

6.1 Summary of findings

Question 1: How do parameterizations of nocturnal heterogeneous chemistry affect model predictions of the NO_x reservoir species N_2O_5 and $ClNO_2$?

In Chapter 3, I showed that existing CMAQ parameterizations of $\gamma(N_2O_5)$ do not account for the organic component of particles, resulting in an overestimation of $\gamma(N_2O_5)$. The existing CMAQ parameterization of $\Phi(ClNO_2)$ is also a simplification and does not account for reactions that compete with chlorination and hydrolysis of N_2O_5. **I implemented two chemically representative model parameterizations of $\boldsymbol{\gamma(N_2O_5)}$ and $\boldsymbol{\Phi(ClNO_2)}$ in CMAQ and showed that these parameterizations increased ambient concentrations of $\boldsymbol{N_2O_5}$ and decreased $\boldsymbol{ClNO_2}$ concentrations**.

The added Gaston parameterization for $\gamma(N_2O_5)$ includes the effects of an organic coating on particles which inhibits N_2O_5 uptake. The Gaston parameterization performed best at predicting measured N_2O_5 concentrations, but none of the three CMAQ parameterizations were able to capture the full range of flight values. The added Staudt parameterization for $\Phi(ClNO_2)$ includes the catalytic role for sulfate in the hydrolysis of N_2O_5 that effectively limits the chlorination reaction leading to $ClNO_2$ production. Because of the low concentration of chloride predicted in the CMAQ fine mode, I found that the Staudt parameterization tends to underpredict $\Phi(ClNO_2)$. Both yield parameterizations produced erroneous $ClNO_2$ concentrations: the default CMAQ method overpredicted $ClNO_2$ concentration relative to the flight data and updated method tended to underpredict. Improving model performance of fine mode particle chloride is necessary to address the discrepancies between the model yield and flight-derived values.

I also found that the coarse mode contributed to total N_2O_5 loss and $ClNO_2$ production, affecting ambient concentrations. The small surface area in the coarse mode limited the impact on $L(N_2O_5)$, as the coarse mode accounted for only 17.2% of total loss. However, the coarse mode was responsible for 60.3% of the total $P(ClNO_2)$ despite contributing very little to the total particle surface area available for reactions. When assessing model performance of heterogeneous NO_x chemistry, it is important to consider how the coarse mode particle composition differs from fine mode.

Question 2: What is the spatial and seasonal impact of the updated parameterizations on the NO_x budget and air quality?

One limitation to the results in Chapter 3 is the focus on nocturnal reservoir species rather than pollutants relevant to daytime air quality such as NO_2. In Chapter 4, I address this limitation by exploring how nocturnal loss affects the NO_x budget and therefore daytime NO_2 concentrations. I used the CMAQ model to calculate nocturnal NO_x loss pathways in January and July across the United States. **Loss through NO_3 reactions is on average greater than loss by N_2O_5 and is greatest in areas with high BVOC emissions such as the southeast US. Loss by N_2O_5 uptake is highest in more polluted regions such as over major cities.** Although nocturnal pathways are important, daytime loss, specifically NO_2 + OH, dominates total NO_x loss across CONUS.

Local meteorology and chemistry play a role in determining dominant loss pathway. In Salt Lake City and over Lake Michigan, local meteorology is important for determining nocturnal loss. In Atlanta, local meteorology did not explain much of the variability in NO_3 or N_2O_5 loss, implying that other factors, such as BVOC concentration, NO_2 concentrations, or particle surface area and composition, that are more important for determining loss. By comparing different representations of N_2O_5 uptake, I was able to assess the impact of heterogeneous chemistry on nocturnal NO_x loss. Uptake is increased when particles are modeled without an organic coating. This increase in N_2O_5 uptake has a corresponding decrease in loss by NO_3 reactions, as NO_3 will react with NO_2 to maintain equilibrium with the lost N_2O_5. Not all regions are equally impacted by the differences in heterogenous chemistry. The effect is greatest over Lake Michigan and smallest in Salt Lake City.

The differences in nocturnal loss between the two parameterization cases results in higher daytime NO_2 concentrations for coated particles. Because the NO_x loss is small with organic coatings on particles, ambient NO_2 concentrations are higher than the model case

without the organic particle coating. **The difference in NO_2 concentration is greatest in January and small in July, emphasizing how nocturnal heterogeneous chemistry is an important loss term in the NO_x budget during the winter.**

Question 3: How do representations of sea spray aerosol emissions affect particle size distributions and the loss of N_2O_5?

In Chapter 5, I tested the sensitivity of particle sizes in the CMAQ model to different sea spray aerosol emission functions. While the average number of emitted sea spray particles decreased relative to the default emission scenario, there were size-specific impacts to particle number and surface area concentration that has implications for heterogeneous chemistry. **Total surface area concentration of the smallest particle size more than doubled (+286%) while surface area concentrations of larger particle sizes decreased (-5% for accumulation mode and -30% for coarse mode).** The changes in sea spray emissions impacted heterogeneous loss of N_2O_5 because the uptake of N_2O_5 depends on particle surface area and particle composition. **In the fine mode, increasing particle surface area in the Aitken mode and increasing particle sulfate in both Aitken and accumulation modes resulted in greater loss of N_2O_5.** In the coarse mode, the decrease in particle surface area and the decrease of particle chloride resulted in lower N_2O_5 loss in the coarse mode relative to the default sea spray emission scenario.

6.2 Limitations and future work

Throughout my dissertation, I have attempted to address limiting assumptions within the CMAQ model that impact predictions of nocturnal NO_x chemistry. However, the work presented here has additional limitations and considerations that present avenues for further study.

In Chapter 3, I showed that the Gaston parameterization of $\gamma(N_2O_5)$ was limited by the parameterization dependence on relative humidity and organic-phase composition. The stepwise dependence of k_{org}, D_{org}, and H_{org} on RH and organic-phase composition are based on one laboratory study, so more research should aim better understand these relationships (Gaston et al., 2014). The CMAQ model predictions of uptake using the Gaston parameterization may also be improved by including more POA in the calculation of O:C, an category of organic aerosol which is currently underestimated in CMAQ (Murphy et al., 2017; Qin et al., 2021). Finally, I did not assess the sensitivity of the Gaston parameterization to assumptions about other variables in the resistor model, such as mass accommodation. Mass accommodation determines the probability of gas-particle interactions and depend on temperature, volatility, and particle composition (Shiraiwa & Pöschl, 2021; Zaveri et al., 2014). Mass accommodation can have a large impact on uptake when organic coatings are thin (Anttila et al., 2006). Future work should explore the sensitivity of CMAQ to mass accommodation as a function of organic coating composition.

One limitation of my implementation of a new $\Phi(ClNO_2)$ parameterization is the model underestimates of particle chloride concentration. The coarse mode parameterization predicted large yield values because of the higher concentrations of particle chloride in the coarse mode compared to the fine mode. Because chloride content in the fine mode is so low, the yield is also biased low. If the Staudt yield were to be adjusted up to account for this bias without first adjusting particle chloride, then the yield parameterization would likely overpredict yield in cases where particle chloride is accurate. One area of future work that may address the underestimate is adding road salt as an emission source in CMAQ. Road salt may be a large, unquantified source of inland particle chloride in the winter (McNamara et al., 2020). Even if road salt does not

contribute to aerosol emissions, road salt in snow pack has been shown to increase $ClNO_2$ production following N_2O_5 uptake to the snow (Jeong et al., 2023; McNamara et al., 2021). $ClNO_2$ can be produced from other aerosol sources as well, such as Cl-containing dust (Mitroo et al., 2019), but dust in the CMAQ model does not emit Aitken mode particles and thus the fine mode emissions of dust are underestimated. Dust and road salt are areas of emission in CMAQ that could be added to improve representations of both particle chloride and fine mode particle number concentrations.

In Chapter 4, I assessed the seasonal and spatial differences in nocturnal NO_x loss and the impact on daytime air quality. One limitation of this study is the short time range. I assessed loss for two months, representing winter and summer, for one year. There may be interannual variability in dominant loss pathways, and there may be trends across years as emissions have changed. NO_x emissions have decreased across the US (U.S. EPA, 2021), and this will impact nighttime NO_3 and N_2O_5 concentrations. In addition, changes in particulate matter concentrations, especially during wildfire seasons, may also impact N_2O_5 loss by changing the available particle surface area and composition (Burke et al., 2023; Goldberger et al., 2019). Future work should consider how changes in emissions over time have impacted dominant nocturnal loss pathways. Future work should also consider the contribute of other loss and production pathways to the NO_x budget. For example, HONO can be produced from particles containing nitrogen, and this will increase total NO_x production (Alicke et al., 2002; Dyson et al., 2021).

In Chapter 5, I tested different sea spray emission scenarios in CMAQ and found that adding Aitken mode particles changed the particle size distributions. However, I did not modify

sea spray aerosol composition to reflect the dependence on size. Because smaller SSA generally have a larger organic fraction and smaller inorganic fraction, inclusion of size-specific particle composition may reduce heterogeneous uptake to these particles (Jayarathne et al., 2016; Keene et al., 2007; Salter et al., 2014; Wang et al., 2017). Particle composition also affects hygroscopic growth of particles (Cochran et al., 2017), and the RH-dependent look-up tables of particle size in the sea spray calculation should be modified to represent particle composition in each mode. Future work should assess how size-dependent particle composition affects sea spray aerosol in terms of both emissions and chemistry.

By modifying mechanisms affecting NO_x chemistry and air quality in the CMAQ model, I have assessed the accuracy of the CMAQ default parameterizations and the sensitivity of NO_x predictions to representations of heterogeneous chemistry. Future work can continue to improve both model performance and our understanding of the nocturnal chemistry that influences daytime air quality.

References

Alicke, B., Platt, U., & Stutz, J. (2002). Impact of nitrous acid photolysis on the total hydroxyl radical budget during the Limitation of Oxidant Production/Pianura Padana Produzione di Ozono study in Milan. *Journal of Geophysical Research: Atmospheres*, *107*(D22). https://doi.org/10.1029/2000JD000075

Anttila, T., Kiendler-Scharr, A., Tillmann, R., & Mentel, T. F. (2006). On the Reactive Uptake of Gaseous Compounds by Organic-Coated Aqueous Aerosols: Theoretical Analysis and Application to the Heterogeneous Hydrolysis of N2O5. *Journal of Physical Chemistry A*, *110*(35), 10435–10443. https://doi.org/10.1021/JP062403C

Burke, M., Childs, M. L., De La Cuesta, B., Qiu, M., Li, J., Gould, C. F., et al. (2023). The contribution of wildfire to PM2.5 trends in the USA. *Nature*, *622*(7984), 761–766. https://doi.org/10.1038/s41586-023-06522-6

Cochran, R. E., Laskina, O., Trueblood, J. V., Estillore, A. D., Morris, H. S., Jayarathne, T., et al. (2017). Molecular Diversity of Sea Spray Aerosol Particles: Impact of Ocean Biology on Particle Composition and Hygroscopicity. *Chem*, *2*(5), 655–667. https://doi.org/10.1016/j.chempr.2017.03.007

Dyson, J. E., Boustead, G. A., Fleming, L. T., Blitz, M., Stone, D., Arnold, S. R., et al. (2021). Production of HONO from NO₂ uptake on illuminated TiO₂ aerosol particles and following the illumination of mixed TiO₂/ammonium nitrate particles. *Atmospheric Chemistry and Physics*, *21*(7), 5755–5775. https://doi.org/10.5194/acp-21-5755-2021

Gaston, C. J., Thornton, J. A., & Ng, N. L. (2014). Reactive uptake of N2O5 to internally mixed inorganic and organic particles: The role of organic carbon oxidation state and inferred organic phase separations. *Atmospheric Chemistry and Physics*, *14*(11), 5693–5707. https://doi.org/10.5194/ACP-14-5693-2014

Goldberger, L. A., Jahl, L. G., Thornton, J. A., & Sullivan, R. C. (2019). N_2O_5 reactive uptake kinetics and chlorine activation on authentic biomass-burning aerosol. *Environmental Science: Processes & Impacts*, *21*(10), 1684–1698. https://doi.org/10.1039/C9EM00330D

Jayarathne, T., Sultana, C. M., Lee, C., Malfatti, F., Cox, J. L., Pendergraft, M. A., et al. (2016). Enrichment of Saccharides and Divalent Cations in Sea Spray Aerosol During Two Phytoplankton Blooms. *Environmental Science & Technology*, *50*(21), 11511–11520. https://doi.org/10.1021/acs.est.6b02988

Jeong, D., McNamara, S. M., Chen, Q., Mirrielees, J., Edebeli, J., Kulju, K. D., et al. (2023). Quantifying the Contributions of Aerosol- and Snow-Produced $ClNO_2$ through Observations and 1D Modeling. *ACS Earth and Space Chemistry*, *7*(12), 2548–2561. https://doi.org/10.1021/acsearthspacechem.3c00237

Keene, W. C., Maring, H., Maben, J. R., Kieber, D. J., Pszenny, A. A. P., Dahl, E. E., et al. (2007). Chemical and physical characteristics of nascent aerosols produced by bursting bubbles at a model air-sea interface. *Journal of Geophysical Research*, *112*(D21), D21202. https://doi.org/10.1029/2007JD008464

McNamara, S. M., Kolesar, K. R., Wang, S., Kirpes, R. M., May, N. W., Gunsch, M. J., et al. (2020). Observation of Road Salt Aerosol Driving Inland Wintertime Atmospheric Chlorine Chemistry. *ACS Central Science*, *6*, 684–694. https://doi.org/10.1021/acscentsci.9b00994

McNamara, S. M., Chen, Q., Edebeli, J., Kulju, K. D., Mumpfield, J., Fuentes, J. D., et al. (2021). Observation of N_2O_5 Deposition and $ClNO_2$ Production on the Saline Snowpack. *ACS Earth and Space Chemistry*, *5*(5), 1020–1031. https://doi.org/10.1021/acsearthspacechem.0c00317

Mitroo, D., Gill, T. E., Haas, S., Pratt, K. A., & Gaston, C. J. (2019). $ClNO_2$ Production from N_2O_5 Uptake on Saline Playa Dusts: New Insights into Potential Inland Sources of $ClNO_2$. *Environmental Science & Technology*, *53*(13), 7442–7452. https://doi.org/10.1021/acs.est.9b01112

Murphy, B. N., Woody, M. C., Jimenez, J. L., Carlton, A. M. G., Hayes, P. L., Liu, S., et al. (2017). Semivolatile POA and parameterized total combustion SOA in CMAQv5.2: Impacts on source strength and partitioning. *Atmospheric Chemistry and Physics*, *17*(18), 11107–11133. https://doi.org/10.5194/ACP-17-11107-2017

Qin, M., Murphy, B. N., Isaacs, K. K., McDonald, B. C., Lu, Q., McKeen, S. A., et al. (2021). Criteria pollutant impacts of volatile chemical products informed by near-field modelling. *Nature Sustainability 2020 4:2*, *4*(2), 129–137. https://doi.org/10.1038/s41893-020-00614-1

Salter, M. E., Nilsson, E. D., Butcher, A., & Bilde, M. (2014). On the seawater temperature dependence of the sea spray aerosol generated by a continuous plunging jet. *Journal of Geophysical Research: Atmospheres*, *119*(14), 9052–9072. https://doi.org/10.1002/2013JD021376

Shiraiwa, M., & Pöschl, U. (2021). Mass accommodation and gas–particle partitioning in secondary organic aerosols: dependence on diffusivity, volatility, particle-phase reactions, and penetration depth. *Atmospheric Chemistry and Physics*, *21*(3), 1565–1580. https://doi.org/10.5194/acp-21-1565-2021

U.S. EPA. (2021). Our Nation's Air: Trends through 2021. Retrieved from https://gispub.epa.gov/air/trendsreport/2022/

Wang, X., Deane, G. B., Moore, K. A., Ryder, O. S., Stokes, M. D., Beall, C. M., et al. (2017). The role of jet and film drops in controlling the mixing state of submicron sea spray aerosol particles. *Proceedings of the National Academy of Sciences*, *114*(27), 6978–6983. https://doi.org/10.1073/pnas.1702420114

Zaveri, R. A., Easter, R. C., Shilling, J. E., & Seinfeld, J. H. (2014). Modeling kinetic partitioning of secondary organic aerosol and size distribution dynamics: representing effects of volatility, phase state, and particle-phase reaction. *Atmospheric Chemistry and Physics*, *14*(10), 5153–5181. https://doi.org/10.5194/acp-14-5153-2014

Appendix

Text A1 Development of the Gaston parameterization

To implement the Gaston parameterization in CMAQ v5.3.2, a calculation of oxygen to carbon ratio (O:C) and calculation of the organic particle volume relative to the total particle volume needed to be added to the model source code in the AEROSOL_CHEMISTRY.F module. For calculation of the organic volume ratio, I coded species as either organic, inorganic, or other. Only organic and inorganic were included in the total particle volume. I excluded select species as other because they did not fit within the organic or inorganic categories; were combinations of other components as soil or dust; or would not contribute significantly to uptake. Table A1 lists the species I excluded from the calculation of particle volume.

Table A1: Species excluded from the calculation of total particle volume

Species name	Long name
AEC	Elemental (black) carbon
AOTHR	
ASOIL	Soil, includes AAL, ASI, ACA, AFE, and ATI
ACORS	Coarse PM
ANI	Nickel, associated with the Multi-Pollutant code
ACR_VI	Chromium 6, associated with the Multi-Pollutant code
ACR_III	Chromium 3, associated with the Multi-Pollutant code
ABE	Beryllium, associated with the Multi-Pollutant code
APB	Lead, associated with the Multi-Pollutant code
ADE_OTHR	Diesel fine PM, associated with the Multi-Pollutant code
ADE_EC	Diesel black carbon, associated with the Multi-Pollutant code
ADE_OC	Diesel organic carbon, associated with the Multi-Pollutant code
ADE_NO3	Diesel nitrate, associated with the Multi-Pollutant code
ADE_SO4	Diesel sulfate, associated with the Multi-Pollutant code
ADE_CORS	Diesel coarse PM, associated with the Multi-Pollutant code
ACD	Cadmium, associated with the Multi-Pollutant code
AMN_HAPS	Manganese, associated with the Multi-Pollutant code
APHG	Mercury, associated with the Multi-Pollutant code
AAS	Arsenic, associated with the Multi-Pollutant code

For the calculation of O:C, I used organic-phase species included in version 5.3.2 that have a calculated individual O:C value based on the literature (Pye et al., 2017; Xu et al., 2018; Murphy et al., 2017; Li et al., 2021; Qin et al., 2021). Not all these organic-phase species are used in all chemical mechanism options in CMAQ, so the values of O:C would change based on the mechanism selected. For this set of CMAQ runs, I used the Carbon Bond 6 (cb6r3) chemical mechanisms. Starred species in Table A2 are not in the cb6r3 mechanism version that I ran. Although I used CMAQ v5.3.2, these species names and individual O:C can also be referenced in the v5.4 documentation and SOA_DEFN.F list of organic aerosol components. For the lumped anthropogenic SOA species that replaced the ALK, XYL, TOL, BNZ, TOL, and PAH in later versions of CMAQ (see supplement of Qin et al. 2021), I calculated the number of carbons using eq. 2 and 3 of Pye et al. (2017) (here, Eq. S1 and S2) and the C* values from Supplementary Table 5 of Qin et al. (2021).

$$\log_{10} C^* = 0.475(25 - n_c) - 2.3n_o + \frac{0.6 n_c n_o}{n_c + n_o} \quad \text{(S1)}$$

$$n_o = n_c(O{:}C) \quad \text{(S2)}$$

Table A2: Organic species included in O:C calculation

Species name	Individual O:C	Number of carbons $\boldsymbol{n_c}$	Long name
ALK1	0.315	12	Alkane SOA 1
ALK2	0.203	12	Alkane SOA 2
XYL1	1.003	6	Xylene SOA 1
XYL2	0.611	8	Xylene SOA 2
XYL3	0.907	8	Xylene SOA 3
TOL1	0.875	6	Toluene SOA 1
TOL2	0.523	8	Toluene SOA 2
TOL3	1.227	6	Toluene SOA 3
BNZ1	1.211	5	Benzene SOA 1
BNZ2	0.851	5	Benzene SOA 2
BNZ3	1.467	5	Benzene SOA 3
TRP1	0.539	8	Terpene SOA 1
TRP2	0.531	9	Terpene SOA 2

ISO1	0.827	5	Isoprene SOA 1
ISO2	0.851	5	Isoprene SOA 2
ISO3	1.307	5	Isoprene SOA 3
SQT	0.283	15	Sesquiterpene SOA
PAH1	0.371	10	PAH SOA 1
PAH2	0.259	10	PAH SOA 2
PAH3	0.483	10	PAH SOA 3
OLGA	1.067	7	Anth. Oligomer SOA
OLGB	0.747	10	Biogenic Oligomer SOA
ORGC	0.667	7	Cloud-Processed SOA
DIM*	0.723	10	IEPOX-derived dimers
GLY	0.771	3	glyoxal + methylglyoxal SOA
IEOS*	1.947	5	IEPOX-derived organosulfate
IETET*	0.883	5	2-methyltetrols
IMGA*	1.067	4	2-methylglyceric acid
IMOS*	2.403	4	MPAN-derived organosulfate
ISOPNN*	2.107	5	isoprene dinitrate
MTHYD*	0.299	10	organic nitrate hydrolysis product
MTNO3*	0.587	10	monoterpene nitrate
MT1	0.400	15	Lowest volatility monoterpene SOA
MT2	0.400	10	
MT3	0.444	9	
MT4	0.300	10	
MT5	0.333	9	
MT6	0.200	10	
MT7	0.222	9	Highest volatility monoterpene SOA
LVPO1	0.185	13	Low volatility POA
SVPO1	0.123	14.5	Semi-volatile POA 1
SVPO2	0.073	16	Semi-volatile POA 2
SVPO3	0.032	17.5	Semi-volatile POA 3
IVPO1	0.000	19	Intermediate volatility POA
LVOO1	0.886	5	Low volatility SOA 1
LVOO2	0.711	5.5	Low volatility SOA 2
SVOO1	0.567	6	Semi-volatile SOA 1
SVOO2	0.447	6.5	Semi-volatile SOA 2
SVOO3	0.345	7	Semi-volatile SOA 3
AVB1	1.227	4.5	
AVB2	0.947	5	
AVB3	0.803	5.5	
AVB4	0.659	5.5	

As outlined in Anttila et al. (2006), the numerator and denominator of F in the calculation of $\gamma(N_2O_5)$ approach zero at large particle radii (Eq. S3). This is because $\coth(q_{org})$ approaches 1 while $h(q_{aq}, q^*_{org})$ approaches -1. The point at which these terms approach their respective limits depends on the particle size and the diffuso-reactive parameters determined by k_{org}, D_{org}, and H_{org}. These organic phase diffusion and reaction coefficients depend are set by ranges of RH and O:C. In addition, F depends on the particle organic-phase volume ratio β and the aqueous-phase reaction rate k_{aq}. I therefore set particle radius limits when calculating F to prevent a convergence error. I determined these radius cut-offs by the local minima in F (dashed lines shown in Figure A1). This was done to avoid the increases in F as the denominator goes to zero faster than the numerator. Beyond the particle radius limit, $F = 1$. The radius limits are listed in Table A3 are for ranges of RH, O:C, β, and k_{aq}.

$$F = \frac{\coth(q_{org}) + h(q_{aq}, q^*_{org})}{1 + \coth(q_{aq})h(q_{aq}, q^*_{org})} \quad \text{(S3)}$$

Table A3: Radius limits to prevent convergence error of diffuso-reactive parameters

RH	O:C	Volume ratio (β)	Aqueous-phase reaction rate (k_{aq}) (/s)	Particle radius limit (nm)
$RH \leq 0.3$	$O:C < 0.7$	$\beta \leq 0.1$	--	50
		$\beta \leq 0.2$	$k_{aq} < 1.1x10^6$	30
			$k_{aq} \geq 1.1x10^6$	40
		$\beta \leq 0.3$	--	30
		$\beta \leq 0.4$	$k_{aq} < 1.1x10^6$	20
			$k_{aq} \geq 1.1x10^6$	30
		$\beta \leq 0.5$	$k_{aq} < 1.1x10^6$	20
			$k_{aq} \geq 1.1x10^6$	25
		$\beta \leq 0.8$	--	20
		$\beta \leq 1.0$	$k_{aq} < 1.1x10^6$	10
			$k_{aq} \geq 1.1x10^6$	15
	$O:C \geq 0.7$	$\beta \leq 0.1$	$k_{aq} < 1.1x10^6$	70
			$k_{aq} \geq 1.1x10^6$	80
		$\beta \leq 0.2$	--	60
		$\beta \leq 0.3$	$k_{aq} < 1.1x10^6$	50
			$k_{aq} \geq 1.1x10^6$	60
		$\beta \leq 0.4$	$k_{aq} < 1.1x10^6$	50

				$k_{aq} \geq 1.1x10^6$	70
		$\beta \leq 0.7$		$k_{aq} < 1.1x10^6$	40
				$k_{aq} \geq 1.1x10^6$	60
		$\beta \leq 0.9$		$k_{aq} < 1.1x10^6$	40
				$k_{aq} \geq 1.1x10^6$	50
		$\beta \leq 1.0$		$k_{aq} < 1.1x10^6$	30
				$k_{aq} \geq 1.1x10^6$	50
$0.3 < RH \leq 0.7$	$O:C < 0.7$	$\beta \leq 0.1$		$k_{aq} < 1.1x10^6$	90
				$k_{aq} \geq 1.1x10^6$	100
		$\beta \leq 0.4$	--		70
		$\beta \leq 0.5$		$k_{aq} < 1.1x10^6$	60
				$k_{aq} \geq 1.1x10^6$	70
		$\beta \leq 0.6$		$k_{aq} < 1.1x10^6$	50
				$k_{aq} \geq 1.1x10^6$	70
		$\beta \leq 0.8$		$k_{aq} < 1.1x10^6$	50
				$k_{aq} \geq 1.1x10^6$	60
		$\beta \leq 1.0$	--		50
	$O:C \geq 0.7$	$\beta \leq 0.1$	--		200
		$\beta \leq 0.4$	--		100
		$\beta \leq 0.5$		$k_{aq} < 1.1x10^6$	90
				$k_{aq} \geq 1.1x10^6$	100
		$\beta \leq 0.8$		$k_{aq} < 1.1x10^6$	80
				$k_{aq} \geq 1.1x10^6$	100
		$\beta \leq 1.0$		$k_{aq} < 1.1x10^6$	70
				$k_{aq} \geq 1.1x10^6$	100
$RH > 0.7$	$O:C < 0.7$	$\beta \leq 0.1$		$k_{aq} < 1.1x10^6$	300
				$k_{aq} \geq 1.1x10^6$	400
		$\beta \leq 0.3$	--		300
		$\beta \leq 0.6$		$k_{aq} < 1.1x10^6$	200
				$k_{aq} \geq 1.1x10^6$	300
		$\beta \leq 0.8$		$k_{aq} < 1.1x10^6$	200
				$k_{aq} \geq 1.1x10^6$	250
		$\beta \leq 1.0$	--		200
	$O:C \geq 0.7$	$\beta \leq 0.2$	--		200
		$\beta \leq 0.4$		$k_{aq} < 1.1x10^6$	150
				$k_{aq} \geq 1.1x10^6$	100
		$\beta \leq 0.6$	--		100
		$\beta \leq 0.8$		$k_{aq} < 1.1x10^6$	100
				$k_{aq} \geq 1.1x10^6$	90
		$\beta \leq 0.8$		$k_{aq} < 1.1x10^6$	100
				$k_{aq} \geq 1.1x10^6$	80

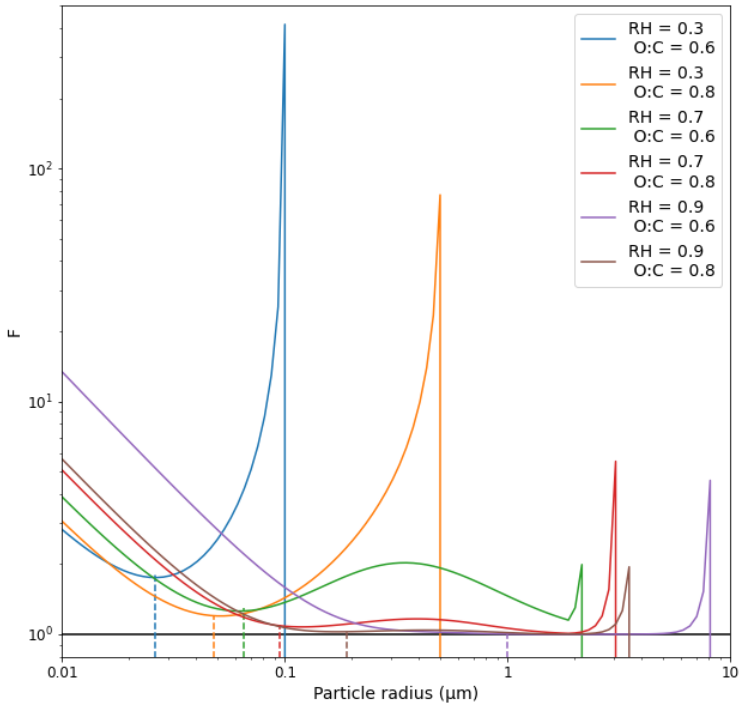

Figure A1. Behavior of diffuso-reactive parameter F at large radii. The volume ratio β and the aqueous-phase reaction rate k_{aq} are arbitrarily set to 0.3 and 1.0x10^6/s as an example. Each solid line represents the behavior of F based on organic-phase parameters determined by the ambient relative humidity (RH) and oxygen to carbon ratio (O:C). A maximum radius (vertical dashed lines) for combinations of β, k_{aq}, RH, and O:C were set so F would be 1 above this radius.

Text A2 CMAQ modal size distributions

The CMAQ model calculates surface area within three modes: Aitken, accumulation, and coarse. It is assumed that the number concentration, and therefore surface area concentration, are lognormally distributed in each mode with a geometric mean diameter and standard deviation (D_g and σ_g) (Bergin et al., 2022; Binkowski and Roselle, 2003).

Figure **A1** shows the average modal wet surface area distributions from CMAQ for the WINTER 2015 campaign period. On average during the WINTER period, the coarse mode contributed 7% to the total particle surface area. The fine mode, the sum of Aitken and accumulation modes in the CMAQ model, dominated total particle surface area. Particle surface area is related to the

total amount of N_2O_5 that can enter the particle. The rate coefficient of uptake, k_{het}, is a function of the uptake coefficient $\left(\gamma(N_2O_5)\right)$, mean molecular speed of N_2O_5 (c), and the particle surface area (SA).

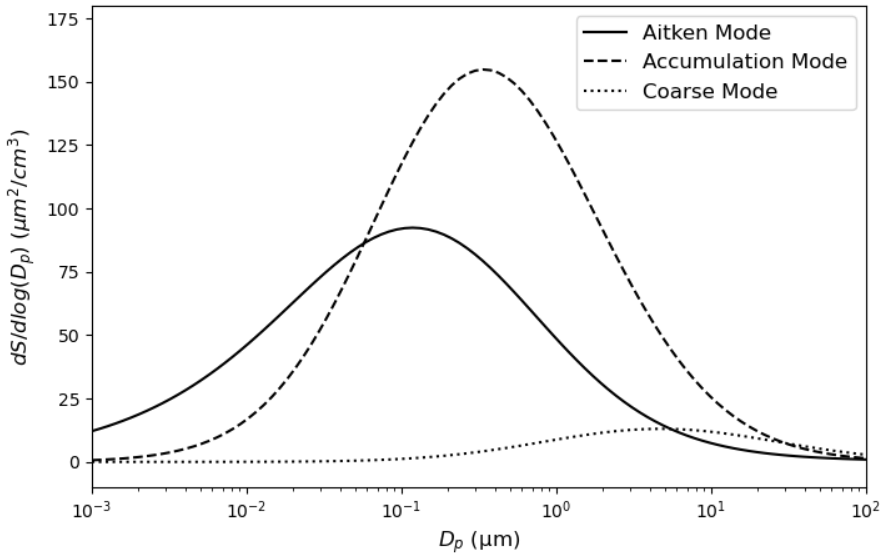

Figure A1. Average lognormal wet surface area distributions for each particle mode in CMAQ during the WINTER campaign period.

Text A3 Comparison of N_2O_5 uptake to flight data

Figure 3 of the text shows that all parameterizations overpredicted a subset of the flight data. Figure A3 shows that these overpredicted flight values occur at different locations and during different research flights throughout the WINTER 2015 campaign. Table A4 lists the correlation metrics of these flight $\gamma(N_2O_5)$ with various meteorological and chemical data. There is no strong correlation with any of the metrics.

The lack of statistical significance with RH, temperature, and surface is consistent with the box model design. The box model used to derive uptake from WINTER data held temperature and RH constant and assumed a constant wet surface area density for each box model simulation. The box model did use measurements of N_2O_5 concentration and particle nitrate at each time

step to calculate uptake, so it is interesting that there is no statistical significance in the correlations between low uptake values and these measurements. Most of the low flight $\gamma(N_2O_5)$ values in these tails occur around the Atlanta area during RF 10 or off the coast of Long Island in RF 6. Only one low value occurred during RF 3, where $\gamma(N_2O_5) = 1.09 \times 10^{-4}$. Interestingly, all three parameterizations overestimated this single data point. This flight value occurred when the plane was at a low altitude (285 m) and cold temperature (-1.5 ˚C) but high RH (85%). The measured N_2O_5 concentration for this single point was 0.13 ppb.

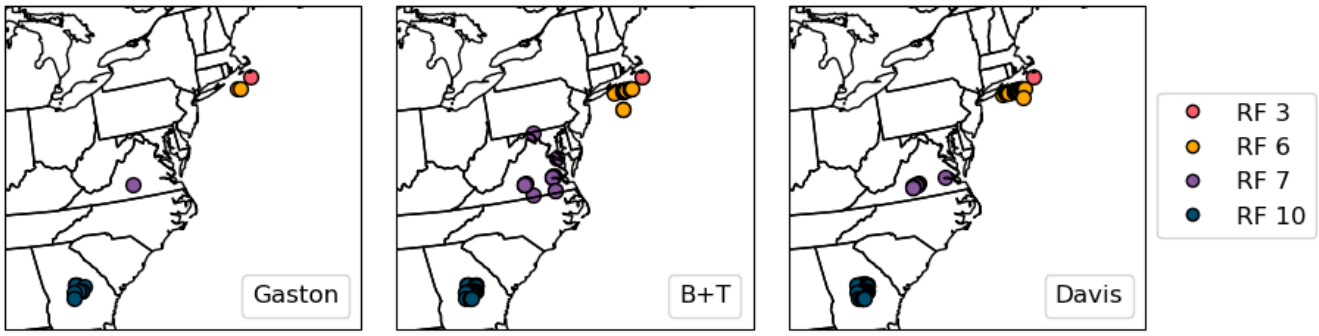

Figure A3. Locations of low flight $\gamma(N_2O_5)$ values along the research flight tracks. Each flight $\gamma(N_2O_5)$ value that is outside the -x10 dashed line (tails to the left) in Figure 3 is plotted here along the flight track. Research flights are color-coded, and the number of low $\gamma(N_2O_5)$ flight values in each research flight are listed in the legend. Numbers vary between parameterization methods because some parameterizations capture the lower $\gamma(N_2O_5)$ values better and therefore move the $\gamma(N_2O_5)$ in Figure 3 further down and within the -x10 line.

Table A4: Correlation of low flight $\gamma(N_2O_5)$ with measurements

Variable	Slope	R^2 $(p-value)$
Humidity (%)	5.68×10^3 /%	$R^2 = 0.00$ $(p = 0.96)$
Temperature (˚C)	1.46×10^4 /˚C	$R^2 = 0.13$ $(p = 0.76)$
Altitude (m)	6.17×10^4 /m	$R^2 = 0.03$ $(p = 0.29)$
N_2O_5 concentration (ppb)	-4.85×10^1 /ppb	$R^2 = 0.00$ $(p = 0.96)$
Particle NO_3 (µg/m³)	4.19×10^7 /µg/m³	$R^2 = 0.05$ $(p = 0.14)$
HNO_3 concentration (ppt)	-2.30×10^6 /ppt	$R^2 = 0.00$ $(p = 0.85)$
Wet surface area density (µm²/cm³)	-2.24×10^4 /µm²/cm³	$R^2 = 0.01$ $(p = 0.47)$

Text A4 Particle chloride in CMAQ

Within CMAQ, I found that assumptions were placed on the calculation of $ClNO_2$ yield based on particle water and chloride concentrations. If the concentrations of either of these

species were not high enough, the model would assume that yield was zero. There were additional cases of $\Phi(ClNO_2) = 0$ even when the concentration conditions were met (Figure A4).

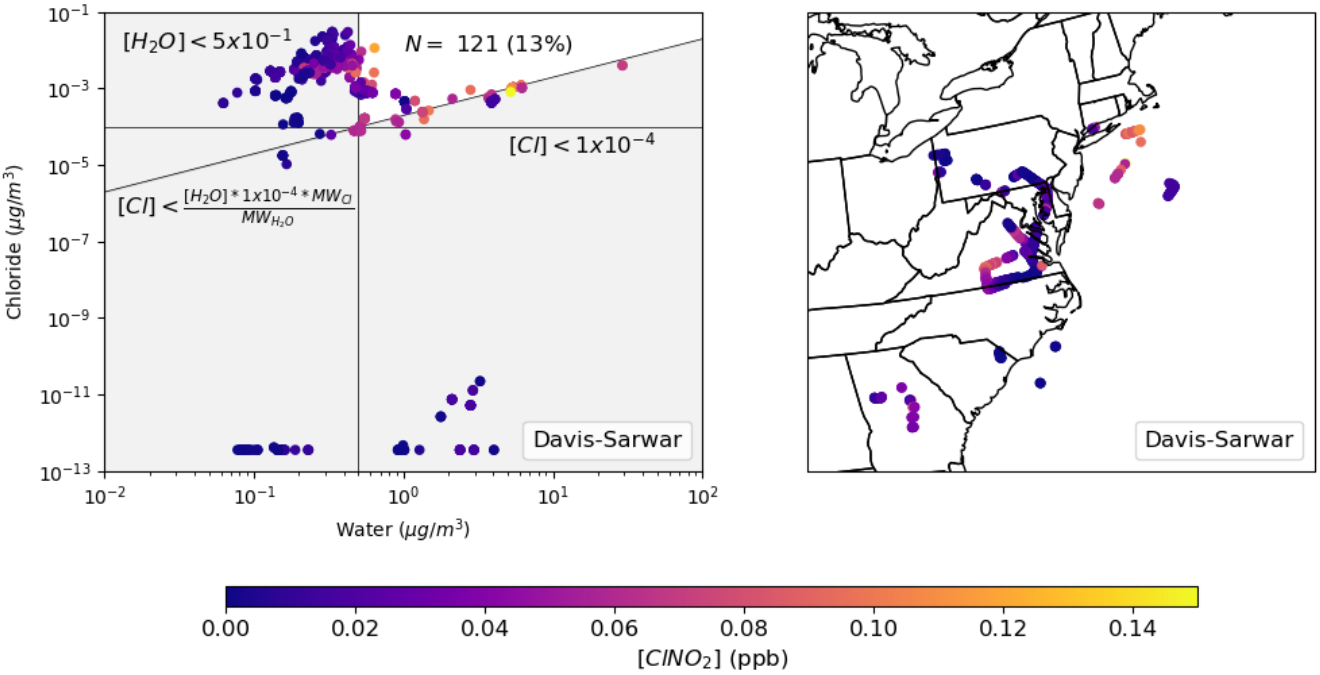

Figure A4. Instances of $\Phi(ClNO_2) = 0$ for the Davis-Sarwar (default) case. Left panel shows a scatterplot of particle chloride versus water mixing ratios. Shaded areas represent regions where CMAQ conditions are not met for calculation of $\Phi(ClNO_2)$, therefore yield is assumed to be zero. The number of $\Phi(ClNO_2) = 0$ instances where the CMAQ conditions are met, and calculated yield still equaled zero are listed in the unshaded region in the top right. Right panel shows the locations of each $\Phi(ClNO_2) = 0$ instance along the WINTER flight track for the default case. In both panels, dots are colored by model $ClNO_2$ concentration.

The left panel in Figure A4 shows the chloride versus water mixing ratios for each instance of $\Phi(ClNO_2) = 0$ in the Davis-Sarwar case (default case), with grey shaded regions representing areas where the conditions are not met. The majority of $\Phi(ClNO_2) = 0$ instances do not meet the CMAQ conditions, but 8-15% do meet the conditions and should have a calculated yield value, depending on the parameterization combination. The right panel of Figure A4 shows the locations of each of these $\Phi(ClNO_2) = 0$ values along the WINTER flight

track for the Davis-Sarwar case. The $\Phi(ClNO_2) = 0$ instances occur throughout the WINTER campaign with a higher frequency in the mid-Atlantic region.